2016

Structural And Functional Analysis Of Engineered Cardiac Tissues In Response To Hypertrophic Growth Factors

Rosa Maria Alvarez Lopez
University of Pennsylvania, rosaa@seas.upenn.edu

Structural And Functional Analysis Of Engineered Cardiac Tissues In Response To Hypertrophic Growth Factors

Abstract
The development of myocardial hypertrophy and fibrosis are central pathological processes that are common features resulting from many types of cardiac diseases. Moreover, a wide variety of inputs and interactions contribute to pathological hypertrophy and fibrosis. For example, changes in biomechanical stress on the myocardium, as occur during chronic pressure or volume overload, is a fundamental trigger for hypertrophy and fibrosis. In addition, crosstalk between myocytes and fibroblasts contributes to the structural, mechanical, and electrical remodeling in the pathogenesis of various heart conditions that lead to heart failure. During the development of pathological hypertrophy and fibrosis, many agonists such as endothelin (ET)-1, angiotensin (Ang) II, and transforming growth factor (TGF)-β are activated in parallel, obscuring attribution of their individual, synergistic or subordinate effects. Finally, the development of hypertrophy and fibrosis themselves contribute to load changes in the heart, further complicating mechanistic interpretation. One impediment to further progress has been the lack of model systems that allow the experimental control required to draw definitive mechanistic conclusions of each of its components, yet retain the essential features of the in vivo environment.

Accordingly, a major focus of this thesis is to examine the ability of a myocardial tissue engineering platform to decouple the effects of biochemical, mechanical and cell-specific inputs on microtissue auxotonic contractility. The model employed is based on microfabricated polydimethylsiloxane (PDMS) templates that generate arrays of 3D cardiac microtissues (CMT). Cantilevers within templates provide physiologically relevant auxotonic loading to the CMTs, promote the appropriate 3D organization of neonatal rat cardiac myocytes and fibroblasts, and report resting and twitch force generation in real time. Additionally, we evaluated the correlation between sarcomere length and microtissue length, and developed twitch forces of these microtissues in an auxotonic preparation.

While the role of known hypertrophic factors has been extensively studied using conventional cell culture and integrated in vivo models, few studies have used engineered cardiac tissues to examine how key hypertrophic agonists, alone or in combination, affect contractile parameters, including resting and twitch force as well as rates of force generation and relaxation. We found that the pathological mediators, endothelin (ET)-1, angiotensin (Ang) II, and transforming growth factor (TGF)-β, altered contractility with different magnitudes. Differences in contractile responses led us to further investigate the length-tension relationship in the microtissues. We further investigated how sarcomere length related to tissue length and contractile properties. Interestingly, we identified differential sarcomere lengths upon stimulation with different hypertrophic factors. ET-1 in particular, led to the largest changes in contractile properties. These results are described in greater detail in Chapter 2.

Recognizing that biomechanical load acts in concert with pathological mediators in the development if cardiac hypertrophy, we utilized this cardiac microtissue model to generate templates with cantilevers with increased stiffness (Legant et al. 2009). The cantilever stiffness represent the resistance against which the engineered CMTs needs to contract, and mimics increased afterload as might occur during hypertension. We also studied the effect of increased afterload in combination with ET-1, Ang II, TGF-β upon force generation, and cell and tissue morphology. Interestingly, our data shows that cell area is altered only in the presence of increased afterload combined with hypertrophic factors, but not with the hypertrophic factors alone. These results are described in greater detail in Chapter 3.

While many studies have focused on the interactions of nonmyocytes and myocytes, few studies have looked at the role of nonmyocytes in engineered tissue contractile function. Our studies focus on the role of nonmyocytes in contractile function. Our results suggest that myocyte enrichment (nonmyocyte depletion) leads to decreased contractile function, suggesting that nonmyocytes are required for proper contractile function. We also evaluated how nonmyocytes within engineered tissues contribute to the ET-1-induced changes in contractility. These results are described in greater detail in Chapter 4.

Collectively, these studies have provided insights as to how cardiac microtissues can be employed to both isolate and integrate the biochemical and mechanical signals that contribute to changes in contractile function in the context of myocardial hypertrophy and disease. Continued work and future directions is discussed in Chapter 5.

Degree Type
Dissertation

Degree Name
Doctor of Philosophy (PhD)

Graduate Group
Bioengineering

First Advisor
Kenneth B. Margulies

Subject Categories
Biomedical

STRUCTURAL AND FUNCTIONAL ANALYSIS OF ENGINEERED CARDIAC TISSUES IN RESPONSE TO HYPERTROPHIC GROWTH FACTORS

Rosa María Álvarez López

A DISSERTATION

in

Bioengineering

Presented to the Faculties of the University of Pennsylvania

in

Partial Fulfillment of the Requirements for the

Degree of Doctor of Philosophy

2017

Supervisor of Dissertation

_____

Kenneth B. Margulies, Professor of Medicine

Graduate Group Chairperson

_____

Jason A. Burdick, Professor of Bioengineering

Dissertation Committee

Paul A. Janmey, Professor of Physiology

Christopher S. Chen, Professor of Biomedical Engineering (Boston University)

John D. Gearhart, Professor of Cellular and Molecular Biology

I dedicate this thesis to my husband for his love and support throughout my PhD

and the many years of long distance.

I also dedicate this thesis to my brother and parents, for their unconditional love and support.

ACKNOWLEDGEMENT

Thank you to the following people:

Family

Thank you for always pushing me to do better, and always providing unconditional love and support. David: Thank you for being my rock, my love and my inspiration throughout the years. I would not have been able to do this without you. Jesús: Thank you for your support and being the best brother. Thank you for Mom and Dad: Thank you also for all the sacrifices you have made to provide me with the best education possible, and everything you have done to push me to be the very best version of myself.

Scientific Mentors

Kenneth Margulies: Thank you for your patience, guidance and mentorship over the years, and guiding my development as a scientist. The work represented here would not have been possible without the support. Christopher Chen, Paul Janmey and John Gearhart: Thank you for your thesis mentorship and providing thoughtful critiques to encourage me to go further in my research.

Lab

Rachel: Thank you for sharing long days in lab, great times “building fires” in the microscope room, and the love for the uTUGS. Anbin, Xiaoyin: Thank you for your scientific support throughout the years.

Friends

Thank you for the unforgettable memories at Penn. I am grateful for the great dinners, wonderful conversations as well as your support and sound advice. My time at Penn would not have been the same without you.

ABSTRACT

STRUCTURAL AND FUNCTIONAL ANALYSIS OF ENGINEERED CARDIAC TISSUES IN RESPONSE TO HYPERTROPHIC GROWTH FACTORS

Rosa M. Álvarez

Kenneth B. Margulies

The development of myocardial hypertrophy and fibrosis are central pathological processes that are common features resulting from many types of cardiac diseases. Moreover, a wide variety of inputs and interactions contribute to pathological hypertrophy and fibrosis. For example, changes in biomechanical stress on the myocardium, as occur during chronic pressure or volume overload, is a fundamental trigger for hypertrophy and fibrosis. In addition, crosstalk between myocytes and fibroblasts contributes to the structural, mechanical, and electrical remodeling in the pathogenesis of various heart conditions that lead to heart failure. During the development of pathological hypertrophy and fibrosis, many agonists such as endothelin (ET)-1, angiotensin (Ang) II, and transforming growth factor (TGF)-β are activated in parallel, obscuring attribution of their individual, synergistic or subordinate effects. Finally, the development of hypertrophy and fibrosis themselves contribute to load changes in the heart, further complicating mechanistic interpretation. One impediment to further progress has been the lack of model systems that allow the experimental control required to draw definitive mechanistic conclusions of each of its components, yet retain the essential features of the *in vivo* environment.

Accordingly, a major focus of this thesis is to examine the ability of a

myocardial tissue engineering platform to decouple the effects of biochemical, mechanical and cell-specific inputs on microtissue auxotonic contractility. The model employed is based on microfabricated polydimethylsiloxane (PDMS) templates that generate arrays of 3D cardiac microtissues (CMT). Cantilevers within templates provide physiologically relevant auxotonic loading to the CMTs, promote the appropriate 3D organization of neonatal rat cardiac myocytes and fibroblasts, and report resting and twitch force generation in real time. Additionally, we evaluated the correlation between sarcomere length and microtissue length, and developed twitch forces of these microtissues in an auxotonic preparation.

While the role of known hypertrophic factors has been extensively studied using conventional cell culture and integrated *in vivo* models, few studies have used engineered cardiac tissues to examine how key hypertrophic agonists, alone or in combination, affect contractile parameters, including resting and twitch force as well as rates of force generation and relaxation. We found that the pathological mediators, endothelin (ET)-1, angiotensin (Ang) II, and transforming growth factor (TGF)-β, altered contractility with different magnitudes. Differences in contractile responses led us to further investigate the length-tension relationship in the microtissues. We further investigated how sarcomere length related to tissue length and contractile properties. Interestingly, we identified differential sarcomere lengths upon stimulation with different hypertrophic factors. ET-1 in particular, led to the largest changes in contractile properties. These results are described in greater detail in **Chapter 2**.

Recognizing that biomechanical load acts in concert with pathological mediators in the development if cardiac hypertrophy, we utilized this cardiac microtissue model to generate templates with cantilevers with increased stiffness (Legant et al. 2009). The cantilever stiffness represent the resistance against which the engineered CMTs needs to contract, and mimics increased afterload as might occur during hypertension. We also studied the effect of increased afterload in combination with ET-1, Ang II, TGF-β upon force generation, and cell and tissue morphology. Interestingly, our data shows that cell area is altered only in the presence of increased afterload combined with hypertrophic factors, but not with the hypertrophic factors alone. These results are described in greater detail in **Chapter 3.**

While many studies have focused on the interactions of nonmyocytes and myocytes, few studies have looked at the role of nonmyocytes in engineered tissue contractile function. Our studies focus on the role of nonmyocytes in contractile function. Our results suggest that myocyte enrichment (nonmyocyte depletion) leads to decreased contractile function, suggesting that nonmyocytes are required for proper contractile function. We also evaluated how nonmyocytes within engineered tissues contribute to the ET-1-induced changes in contractility. These results are described in greater detail in **Chapter 4.**

Collectively, these studies have provided insights as to how cardiac microtissues can be employed to both isolate and integrate the biochemical and mechanical signals that contribute to changes in contractile function in the context of myocardial hypertrophy and disease. Continued work and future

directions is discussed in **Chapter 5**.

TABLE OF CONTENTS

LIST OF ILLUSTRATIONS

CHAPTER 1: INTRODUCTION AND BACKGROUND

1.1 Background

1.1.1 Cardiac cycle and loading

The primary function of the heart is to pump blood through the circulation. In this chapter, cardiac function is discussed in the context of the mechanics of the ventricle, which is the most important component for the mechanical function of the heart and relevant to cardiac tissue engineering. The contraction cycle of the heart is typically presented as a pressure–volume loop with distinct phases of isotonic and isometric contraction during systole and relaxation during diastole. Briefly, the ventricles are relaxed during diastole, and blood fills them. Ventricular systole occurs in stages. First, an isometric contraction occurs, where the ventricle remains the same volume with the inflow and outflow valves closed. Once pressure rises sufficiently, the semilunar (outflow) valves open and the ventricles begin to eject the blood out and ventricular volume decreases. This interval ends when the ventricles begin to relax, and the semilunar valves close. It is important to note that while the cardiac cycle is described as a sequence of isotonic and isometric states, simultaneous and coupled changes in force and length occur. Therefore the contraction and relaxation of the heart is more precisely auxotonic.

The mechanical forces acting on the heart are called preload and afterload. Preload is the initial distension of the ventricle by filling of the chamber with blood prior to contraction. The degree of filling modulates the force produced during contraction. At the cellular level, increases in the length of rod-shaped cardiac myocytes and their sarcomeres are likewise a major factor regulating the force generation (ter keurs HE et al. 2008). The Frank-Starling law of the heart states that the larger the volume of blood, the further the ventricle is stretched (with larger sarcomere length), leading to stronger

forces of the contraction, and thus, larger quantity of blood that is pumped into the aorta during systole (Konhilas JP et al. 2002). The sarcomere itself is comprised of thick myofilaments that contain myosin and thin myofilaments that contain actin. As seen in Figure 1, the part of the sarcomere that contains Titin and thin myofilaments is called the I band, and the part that contains the overlap of thick and thin myofilaments is called the A band. The Z band attaches the thin myofilaments to each end of the sarcomere, while the thick filaments reside in the middle of the sarcomere. When a sarcomere contracts, myosin heads within the thick filament attach to actin to form cross-bridges. This step is called the power-stroke. Then, the thin filaments slide over the thick filaments as the heads pull the actin. When a new ATP binds with myosin, actin is released. Myosin then reaches forward again to bind actin in a new cycle with the high energy ADP + P configuration. This process is known as myosin-actin crossbridge cycling. During this cycling, the thick filaments composed of myosin do not change in length. It is the I band, which is rich in thin myofilaments and Titin that change length. By convention, the sarcomere length or the distance between two adjacent Z bands. The resulting sarcomere shortening leads to the generation of tension during the muscle contraction. Titin's primary functions are to stabilize the thick filament, center it between the thin filaments, prevent overstretching of the sarcomere, and to help the sarcomere re-establish baseline length, like a spring, after it is stretched. If a sarcomere is stretched too far, there will be insufficient overlap or cross-bridge of the myofilaments and the less force will be produced (Figure 1B). In contrast, if the muscle is over-contracted, the potential for further contraction is reduced, which in turn reduces the amount of force produced (Figure 1C).

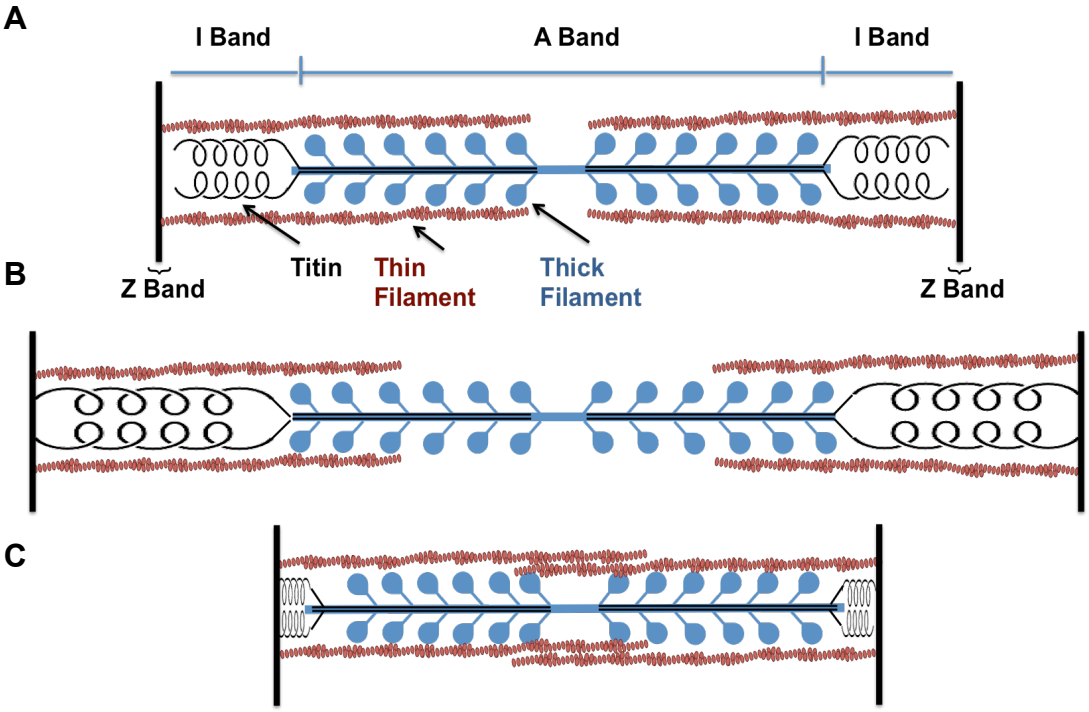

Figure 1. Illustration of a sarcomere structure. An illustration of a sarcomere structure in resting state is depicted in A. Thin filaments attached to Z discs are depicted in red. Interdigitating with the actin filaments are the thick filaments depicted in blue. The motor heads in the thick filaments can bind to the actin in the thin filament. Together with the titin molecules, which are represented as springs that go through the hollow thick filaments and attach to the Z-discs, providing structural integrity to sarcomeres. When overstretched, the cross bridges between thin and thick filaments are reduced (B). Upon activation they move towards the thin filaments and contract the structure (C).

Two key aspects of the regulation of myosin-actin cycling are the energy made available by the hydrolysis of ATP, and the calcium that makes the myosin-binding site available for myosin binding. Calcium is required by two proteins, troponin and tropomyosin, that regulate muscle contraction by blocking the binding of myosin to filamentous actin. In a resting sarcomere, tropomyosin covers the myosin binding sites of the actin molecules. Calcium ions need to bind with troponin-C molecules (within the tropomyosin protein) to alter the structure of the tropomyosin, forcing it to reveal the myosin-binding sites on the actin.

Afterload, on the other hand, describes the end load or "resistance" against which the heart contracts to eject blood. Factors that affect afterload include the pressure within the vessels into which blood is ejected (e.g. this increases in hypertension), the elasticity of the vessels that receive blood ejected by the ventricles (e.g. this decreases with aging), and the chamber geometry of the ventricles themselves (chamber dilation and/or wall thinning increase wall tension in the ventricular myocardium).

1.1.2 Pathological development of the heart

Abnormal increases in afterload and neurohumoral regulatory systems are frequently observed contributors to the progression of ventricular dysfunction to clinical heart failure. Upon initial increase in pressure or load, the heart responds with compensatory or adaptive responses by increasing force of contraction and increasing in mass (hypertrophy). These adaptations initially augment the work capacity of the myocardium (Xu J et al. 2007, Souders CA et al. 2012, Emdad L et al. 2001, Bujak M and Frangogiannis NG 2007). However, over time, sustained activation and interaction between mechanical forces and pathology-associated mediators leads to cardiac dysfunction. There are numerous circulating factors that have been implicated in the development of pathologic hypertrophy of the heart, including endothelin 1 (ET-1), angiotensin II (Ang II), and transforming growth factor β (TGF-β), which regulate contractility, rates of contraction and relaxation, gene transcription, protein translation, and cellular metabolism during hypertrophic remodeling. Prior studies have shown functional crosstalk between these factors (Gray MO et al. 1998, Rosenkranz S et al. 2002, Iwanaga Y et al. 2001). For example, exogenous administration of Ang II results in the development of myocyte hypertrophy, coupled with the release of ET-1 and TGF-β in

vitro (Castanares C et al. 2007). However, it has been suggested that ET-1 plays a central role in mediating the actions of other hypertrophic factors (Weng X et al. 2015, Castanares C et al. 2007). Additionally, Ang II, ET-1, and their receptors (AT_1 and ET_A) compose a mutually reciprocal signal network in the myocardium (Piuhola J et al. 2003, Iwanaga Y et al. 2001, Drawnel FM et al. 2013). However, their redundancy is not complete, as the dual blockade of Ang II and ET-1 inhibition has resulted in enhanced anti-hypertensive benefits (Iwanaga Y et al. 2001). Furthermore, TGF-β has been shown to act downstream of Ang II and mediate Ang II-related hypertrophic and fibrotic changes (Schultz J et al. 2002). Further complexity arises because these hypertrophic factors are locally and systemically regulated, making it difficult to distinguish the effects from local activation and effects of mechanical loading. These local feedback loops and signal redundancy have made it difficult to isolate their individual and specific roles in pathological hypertrophy and the progression of heart failure

1.1.3 Nonmyocytes in the development of cardiac hypertrophy

Additionally, pathological myocardial hypertrophy involves at least two cell types undergoing distinct and interacting processes: cardiac myocyte (CM) enlargement or hypertrophy and cardiac fibroblast (CF) activation and proliferation. Approximately 70% of the cells in the human heart are nonmyocytes, primarily cardiac endothelial cells and cardiac fibroblasts, which is the predominant cell type (Chlopcíková S et al. 2001, Martin ML et al. 2012). The crosstalk between the two cell types contributes to the structural, mechanical and electrical remodeling involved in the pathogenesis of various conditions that lead to heart failure. A large body of research indicates that this crosstalk is mediated by paracrine signals and direct cell-cell interactions (Ottaviano FG et al. 2011, Ongstad et al. 2016, Zhang P et al. 2012). Studying CF-to-CM crosstalk *in vivo* and

determining how each cell type contributes to myocardial remodeling has proven difficult. One impediment to further progress is the lack of model systems that allow the experimental control required to draw definitive mechanistic conclusions, yet retain the essential features of the *in vivo* environment. *In vivo*, CFs are buried within densely packed CMs making a direct investigation of the function of each cell type *in situ* extremely difficult. For example, in a study using chimeric mice that had both angiotensin type 1a receptor null- and intact cells, infusion of Ang II induced hypertrophy and fibrosis (Rivard K et al. 2008). Because the majority of the proliferating fibroblasts were found to be surrounding CMs carrying the wild-type AT1aR gene, this report suggests that fibroblast activation by Ang II is CM-dependent. However, due to the small size of the fibroblasts and their location within densely packed CMs, the genetic background of the proliferating fibroblasts was not determined. To address the converse role of CF in modulating CM hypertrophy, one would want to selectively manipulate fibroblasts *in vivo*. Unfortunately, CF-specific promoters do not exist, so *in vivo* studies examining the CF-dependence of CM hypertrophy are not currently possible.

1.1.4 Gene expression associated with hypertrophy and fibrosis

On a molecular level, cardiomyocyte hypertrophy is accompanied by re-activation of many genes ordinarily prominent during fetal development. The most characterized genes are β-myosin heavy chain (β-MHC), α-skeletal actin (α-SKA), α-smooth muscle actin (α-SMA), and atrial natriuretic factor (ANF) may be observed concomitant with a downregulation of α-myosin heavy chain and the Ca^{2+} pump of sarcoplasmic reticulum. In normal myocardium, α-SKA and α-SMA, are co-expressed and the amount of their transcripts has been shown to vary with species, developmental stage, aging, and during pathological situations (Suurmeijer AJH et al. 2003, Schwartz K et al. 1986), while

skeletal actin mRNA accumulation is observed during hemodynamic overload of rat hearts (Souders CA et al. 2012), passive stretch (Sadoshima J et al. 1993), and after administration of hypertrophic factors such as TGF-β or fibroblast growth factor 2 (FGF-2), to cultured neonatal rat cardiomyocytes. Hypertrophic ventricular myocytes are also characterized by significant up-regulation of ANF (Izumo et al., 1988), which is scarcely expressed in normal adult ventricular myocytes. Myocardial hypertrophy leads to a replacement αMHC by the fetal βMHC isoform. It has been previously shown that predominance of the βMHC isoform tends to reduce cardiac power output compared to hearts in which the αMHC isoform predominates. Changes in gene expression related to myocyte hypertrophy occur alongside changes in gene expression related to fibroblast activation to the proliferative and secretory state that promotes fibrosis (scar formation). Furthermore, Ang II, ET-1 and TGF-β have been implicated in increased gene expression of collagen type I and type III, as well as expression of α-SMA (Sadoshima J et al. 1993) by cardiac fibroblasts.

1.1.5 Isolated muscle strip system in vitro model

A commonly used model system to measure cardiac hypertrophic effects in contractility is papillary muscle or isolated muscle strip system. This model system has provided a way to study mature tissue contractile properties, however there are some limitations. Only short-term experiments (few hours) can be done due to short-term survival of explanted macroscopic tissue. Moreover, cell type distribution in the tissue cannot be controlled, and different proportions of myocytes and fibroblasts can lead to differences in resting and twitch force. Additionally, the experimental loading conditions of isolated tissue strip systems have mainly been limited to isometric (constant length) or isotonic (constant force) controls, whereas in physiological conditions cardiac muscle

contracts against auxotonic loads (simultaneous change in load and length). These differences in loading conditions can lead to differences in contractile responses. Force generation as well as kinetics of myocardial tissues, are dependent on many factors including muscle length and associated sarcomere length, and myofilament calcium sensitivity, among others. Model system differences in the loading conditions, and associated differences in myofilament properties such as sarcomere length lead to varying inotropic (force-altering) responses (Palomeque J et al. 2006, Guccione JM et al. 1997, MacGowan GA and Koretsky AP 2000, ter Keurs HE et al. 2008, Li P et al. 1994). In a pioneering study, Layland et al. demonstrated that cardiac troponin I (cTnI) has a pivotal role in the positive inotropic response of the murine heart to beta-adrenergic stimulation (isoprenaline), however this effect is highly dependent on loading conditions, as dependence of cTnI in inotropic responses was most evident in the auxotonic, not the isotonic hearts nor in externally unloaded isolated cardiomyocytes. In another study, Li et al determined that the inotropic effects of Ang II are dependent on resting sarcomere length of the muscle tissue in an isometric preparation. While the untreated tissues exerted the maximal twitch force at the sarcomere length at the peak of the Frank Starling curve (~2.2um), the tissues treated with Ang II exhibited a different response. At the same maximal sarcomere length, Ang II exerted a negative inotropic response; while at shorter lengths, Ang II exhibited a positive inotropic response. Therefore, the inotropic actions of hypertrophic agonists such as ET-1, Ang II and TGF-β are dependent on the resting sarcomere length. While sarcomere length is usually set in isometric preparations, in auxotonic preparations tissues are allowed simultaneously change load and length, and thus, sarcomere length is not typically measured.

1.2.6 In vitro 2D models of cardiac hypertrophy

In vitro 2D models of cardiac hypertrophy have allowed rigorous mechanistic studies of cardiac cell-specific responses (avoiding systemic effects) to hypertrophy, however, there are still some limitations. Cardiac cells adapted to typical flat cell culture models lack 3-dimensional (3D) architecture and differ substantially from those of the intact heart. For example, in a rigid 2D culture substrate, cardiac myocyte hypertrophy is amplified due to the stiffness of the culture substrates, while fibroblasts expand and differentiate to myofibroblasts, the activated hypersecretory phenotype seen in pathological fibrosis (Rohr S. 2011, Wang J et al. 2003). In flat CF monocultures, it has been shown that Ang II directly stimulates CF proliferation, expression of collagens and other extracellular matrix proteins via AT1a receptors (Sadoshima J et al. 1993). Also, *in vitro* studies have shown that stimulation of CFs by Ang II induces the secretion of prohypertrophic and profibrotic factors such as TGF-β, ET-1, FGF-2, IL-6 and others, all of which function in an autocrine and paracrine manner (Fredj S et al. 2005, Fredj SP et al. 2005, Pedrotty DM et al. 2009). Thus, discerning between the effects of substrate stiffness and soluble factor-mediated responses is difficult to achieve. Culturing cells in silicon membranes that can be exposed to static stretch has overcome some of these limitations, however static stretch more closely mimics increase in preload rather than afterload, which is more relevant to the development of cardiac hypertrophy that occurs in many clinical conditions, such as hypertension and aortic stenosis.

Therefore developing an *in vitro* culture method that recapitulates the 3D in vivo organization of the CMs, CFs, and extracellular matrix (ECM) is needed in order to identify mechanisms by which cell-cell interactions influence myocardial structure and function in vivo.

1.2.7 Engineered cardiac tissues as model systems to answer mechanistic questions in myocardial biology

Engineered 3D tissues offer unique opportunities to study mechanistic questions in myocardial biology. A particularly desirable feature of an engineered tissue is the ability to control cell population and hence, cell-type specific gene expression while maintaining physiologically relevant tissue architecture. Despite recent progress, relatively few studies have used engineered cardiac tissue for mechanistic studies (Hinson JT et al. 2015). A key feature of the 3D engineered tissues is that they are able to display more physiological characteristics of intact heart tissue than monolayer cultures. Cells in 3D tissues can make contact with surrounding cells in all directions in contrast to cells in a standard monolayer that sit on a rigid plastic surface and only make side-to-side contacts with other cells. These variations in the spatial distribution of adhesions has been shown to influence cell morphology, responses to soluble factors and forces generated (Baker BM and Chen CS 2012). The 3D microenvironment provides necessary cues to reconstitute the physiological phenotype of the isolated cells.

Multiple studies have shown that the inclusion of nonmyocytes in engineered tissue constructs enhances neonatal rat cardiomyocyte survival and spreading (Naito H et al. 2006, Radisic M et al. 2008, Asnes et al. 2010). Narmoneva et al. showed that co-culture of neonatal rat cardiomyocytes with nonmyocytes from the heart within a hydrogel promoted spreading and reorganization of neonatal cardiomyocytes contractions and enhanced expression of gap junction protein connexin-43. In contrast, cardiomyocytes cultured alone aggregated into sparse clusters and underwent significant apoptosis and necrosis. Naito et al. showed that collagen gels containing cardiomyocyte-enriched heart cell populations developed inferior contractile performance compared to Native heart cell population. Another group showed that

neonatal rat fibroblast and CMs co-cultured in agarose hydrogels resulted in prolonged action potential duration compared to cardiomyocyte cultures alone (Desroches et al., 2012). Additionally, another group showed that spheroid microtissues derived from nonmyocytes showed remarkably enhanced contractile function, as well as enhanced response to inotropic drugs, which the authors suggest it is due a greater degree of cardiomyocyte maturity using a scaffold-free co-culture of myocytes and nonmyocytes express ECM and Ca^{2+}-handling proteins, form functional cell-cell connections (as evidenced by spontaneous action potentials (APs), contractions, and connexin-43 expression), and are amenable to cell type-selective gene transfer (Figure 2A). While the authors observed greater elongation of cells, sarcomere length was not measured, and could have impacted the force generation of these preparations.

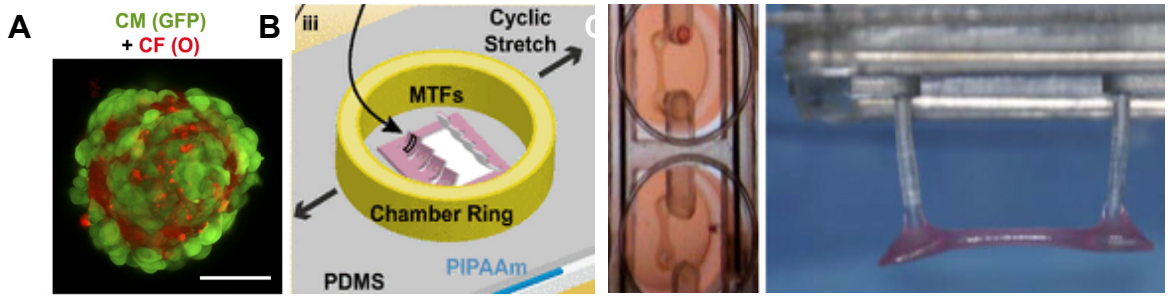

Figure 2: Cardiac tissue engineering methods to study physiological and pathological functionality of the heart. Scaffold-free engineered tissues composed of fibroblasts and myocytes is useful to study cell-cell interaction without cell-ECM interaction (Desroches BR et al. 2012) (A). Muscular thin film 2D engineered tissue model allows cyclic stretch that leads to hypertrophic phenotype (McCain ML et al. 2013) (B) Increased afterload model achieved by changing the spring constant of the resisting material after tissues have been formed, resulting in cardiac dysfunction (Hirt MN et al. 2012) (C).

1.2.8 Cardiac tissue engineering to study pathological remodeling

In one early application, engineered heart tissues derived from chicken embryonic cardiac cells were infected with adenovirus expressing β-adrenergic receptors to evaluate the effect on isometric force generation (Eschenhagen T et al. 1997). Recently, de Lange WJ et al. developed engineered cardiac tissue fusing isolated neonatal mouse cardiac cells derived from both wild-type and myosin-binding protein C (cMyBP-C)-null mouse hearts. They were able to detect contractile abnormalities similar to those seen in intact hearts from cMyBP-C-/- mice. While these studies demonstrate the use of engineered cardiac tissue to model myocardial tissue function, the primary output was isometric force generation as opposed to a more relevant auxotonic contraction. Additionally, the relatively small numbers of cells that can be extracted from mouse hearts and concerns about species differences between mouse cells/hearts beating at 8-12 Hz vs. human cells/hearts beating at 1-3 Hz, represent additional shortcomings of this approach (de Lange et al. 2011). Moreover, the tissues had to be transferred from a culture dish to an intact fiber apparatus to perform mechanical and electrical measurements. Another group developed a 2D muscular thin film (MTF) model (Figure 2B) to recapitulate expression of genes associated with pathological cardiac hypertrophy as well as contractile impairment upon stimulation with cyclic stretch (McCain ML et al. 2013) and AngII (Horton et al. 2016). However, a key limitation to this study is the relative absence of biomechanical loading that is a critical factor regulating myocardial structure and function. Additionally, the sarcomere length of cell sheet has not been described, and this is an important shortcoming in the context of a negative inotropic response to Ang II. A recent study modeled the increased afterload by creating 3D millimeter-scale tissues tethered around silicone tubes with a low spring constant (Hirt MN et al. 2012). The addition of metal rods into the silicon tubes generated a 12x increase in afterload. Interestingly, adding ET-1 and afterload increase resulted in

similar hypertrophic responses, including alterations in gene expression, and increased fibrosis and decreased contractile forces and relaxation velocities (Hirt MN et al. 2012). One of the limitations of this study was that the increase in afterload is not physiologically relevant. Also, the tissues engineered in these studies were large, which can lead to inadequate oxygen and nutrient diffusion, that is particular limiting under conditions associated with increased contractile demands. Interestingly, this group also published studies where addition of ET-1 resulted in a positive inotropic response in engineered tissues in an isometric preparation. Furthermore, the myocyte sarcomere length was not measured in these studies, so it is possible that differences in sarcomere length contributed to the differences in force generation observed in the two studies.

Developing engineered tissues to answer mechanistic questions requires the use of a smaller, more reproducible platform, organized and evenly distributed cells throughout the construct with the ability to directly measure functional outputs without having to transfer them to a different apparatus.

1.2.9 Cardiac microtissue model utilized in the present studies

In this work, we utilized an approach to generate cardiac microtissues (CMTs) that contract against flexible cantilevers and allow measurements of contractility in real time. Using photolithography, pairs of flexible cantilevers are molded into microwells (Figure 2A) where a cell-collagen mix is added.

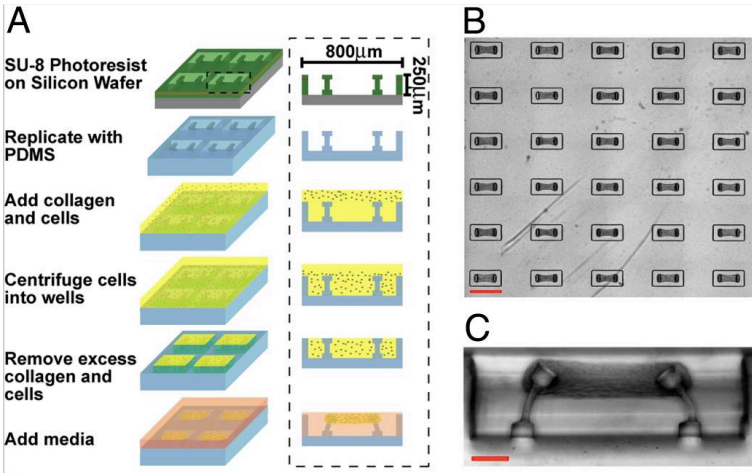

Figure 3. Fabrication of microtissues. Process flow diagram for creating tissue arrays and tissue formation(A) Large arrays of microtissues are simultaneously generated on a substrate. (*B*) Cross section view of a single well (C). (adapted from (Legant WR et al. 2009))

This system also generates over 100 tissues in a micro scale (Figure 3B), allowing concentration gradients in microtissues (thickness ≈100 µm) to equilibrate 100 times faster than those in bulk gels (thickness ≈1 mm), improving the ability of gradients to take full effect (Legant WR et al. 2009). The cantilevers guide the contraction of the cell-matrix mix allowing the formation of CMTs (Figure 3B). After 3 days, the band of tissue draws the cantilevers closer together, and the syncytium of cardiac cells produces synchronized contractions (Figure 3C). Fluorescent beads embedded in the flexible cantilevers allow tracking of their deflection. Because the stiffness of cantilevers is calibrated, their deflection allows real-time measurement of force by taking advantage of the Euler-Bernoulli beam theory (Legant WR et al. 2009) to measure resting and twitch forces of tissues attached to the cantilevers. Generating tissues that are tethered to cantilevers allows for direct auxotonic (shortening) contractile measurements, as opposed to isometric contractions or cyclic stretch that are not reflective of *in vivo* myocardial biology. These cantilevers have measurable and customizable stiffness that

mimics the *in vivo* biomechanical load experienced by myocardium. Because the cantilevers represent the force or resistance that the cardiac tissue needs to surpass, the stiffness of the cantilever mimics afterload. Another advantage is the ability to change the stiffness of the cantilevers by a factor of (2.25x) by varying their geometry and material properties. The ability of changing the stiffness of the cantilevers allows us to decouple and combine the effect of load with other parameters. The CMTs provide a homogeneous, reproducible test bed for studies of myocardial biology.

1.2.10 Cardiac microtissue function vs. other physiological models of cardiac contraction

While great strides have been made in advancing cardiac engineered tissue models, there are differences between engineered and native cardiac tissues that must be kept in mind when extrapolating results from in vitro models to the clinical setting. A key design element of the μTUG engineered tissue system is the use of elastic cantilevers, which enhance the force development of cardiomyocytes within the tissue, resulting in higher tissue/cell tension, compacted extracellular matrix, increased alignment of the cells, and a better development of the sarcomeric structure. However, cardiac microtissues engineered with neonatal rat ventricular myocytes in this system generate twitch forces that range between 3μN and 5μN, if tethered to soft pillars or stiff pillars, respectively. Resting forces range between 10μN and 18μN depending on whether the tissues are tethered to soft or stiff pillars, respectively. These engineered tissues are on average between 0.2mm^2 and 0.08 mm^2 in cross sectional area, yielding stresses of 0.2 mN/mm^2 to 0.3mN/mm^2 for twitch cross-sectional stresses, and 0.6mN/mm^2 to 1.1mN/mm^2 for resting cross-sectional stresses (depending if tethered to soft or stiff pillars). Previous work using mouse trabeculae demonstrated force generation between 18mN/mm^2 – 70mN/mm^2 (under preload resulting in a sarcomere

length of 2.2um) depending on the cross sectional areas of the trabeculae, which ranged between 0.05mm and 0.3mm (Raman S et al. 2005). An even greater difference is observed when engineered cardiac tissues are compared to adult human cardiac cells. Intact human trabeculae in an organ bath usually develop between 16.7mN/mm^2 (Freq = .5hz) - 30.3mN/mm^2 (Freq = 2.5hz) (Rossman EI et al. 2003).

Many things should be taken into consideration when studying functional differences between these muscle preparations. The loading system used to measure the force generated by the tissues can affect the force generated by the isolated tissues, as mentioned in section 1.2.4. While auxotonic preparations resemble more closely native cardiac loading, they do not allow preload adjustments to achieve maximal force generation. For example, increases in resting tissue tension, would tend to produce decreased in resting tissue length. These changes in resting tissue length can lead to potential differences in active force generation within the engineered tissues (as described in section 1.1.1). The use of more immature neonatal myocytes in engineered tissues likely also contributes to lower force development. Another factor to consider is that the fraction of the engineered cardiac construct populated by cells and compact muscle strands is generally much smaller than in normal hearts. The rest of the engineered tissue is cell-free extracellular matrix, which can lead to inhomogeneous cell distribution decreases in force generation (Wang H et al. 20. Therefore, all these factors should be taken into consideration when interpreting results from engineered cardiac tissues.

CHAPTER 2: MEASUREMENT AND ANALYSIS OF FORCES IN RESPONSE TO HYPERTROPHIC AGONISTS

2.1 Rationale

Hypertrophic remodeling occurs in response to hemodynamic load and neurohormonal activation, leading to contractile dysfunction that progresses to heart failure, a common endpoint that carries a high mortality risk. Despite great progress in understanding key pathological processes, many fundamental questions remain unanswered. Numerous soluble substances are involved in cardiac function through their effects on cytoskeletal organization and contractility. There are numerous neurohormonal hypertrophic factors involved in the pathological development of the heart, such as endothelin (ET)-1, angiotensin (Ang) II, and transforming growth factor (TGF)-β, which regulate contractility, kinetics, gene transcription, protein translation, and cellular metabolism during hypertrophic remodeling. Prior studies have shown functional crosstalk between these factors (Schultz et al. 2002, Rosenkranz S et al. 2002). For example, exogenous administration of Ang II results in the development of myocyte hypertrophy, coupled with the release of ET-1 and TGF-β in vitro (Sadoshima J et al. 1993). However, it has been suggested that ET-1 plays a central role in mediating the actions of other hypertrophic factors (Wang X et al. 2015, Castanares C et al. 2007). Additionally, Ang II, ET-1, and their receptors (AT_1 and ET_A) compose a mutual reciprocal signal network in the myocardium (Piuhola J et al. 2003). However, their redundancy is not complete, as the dual blockade of Ang II and ET-1 inhibition has resulted in enhanced anti-hypertensive benefits (Iwanaga Y et al. 2001). These local feedback loops and signal redundancy have made their individual and specific roles in hypertrophy and the progression of heart failure difficult to isolate.

A limitation of these studies has been the model systems utilized to parse

out the roles of different hypertrophic agonists. For example, in a rigid 2D culture substrate, cardiac myocyte hypertrophy is amplified due to the stiffness of the culture substrates, while fibroblasts expand, differentiate to myofibroblasts and release TGF-β, ET-1, and Ang II, all of which function in an autocrine and paracrine manner (8). Thus, discerning between the effects of substrate stiffness and soluble factor-mediated responses is difficult to achieve. Additionally, while 2D substrates allow for rigorous mechanistic studies, contractility measurements are hard to achieve. Another model system used to measure cardiac hypertrophic effects in contractility is papillary muscle or isolated muscle strip systems. This model system has provided a way to study mature tissue contractile properties, however there are some limitations. Only short-term experiments (few hours) can be done due to short-term survival of explanted macroscopic tissue. Moreover, cell type distribution in the tissue cannot be controlled, and different proportions of myocytes and fibroblasts can lead to differences in resting and twitch force. Additionally, the experimental loading conditions of isolated tissue strip systems have mainly been limited to isometric (constant length) or isotonic (constant force) controls, whereas in physiological conditions cardiac muscle contracts against auxotonic loads (simultaneous change in load and length). These differences in loading conditions can lead to differences in contractile responses. A model system is needed that allows the experimental control necessary to draw definitive mechanistic conclusions and retains the essential *in vivo* features with the ability to measure contractile function. We describe the implementation of a microfluidic device that allows us measure auxotonic contractility in real-time after generating cardiac microtissues (CMTs) that contract against flexible cantilevers. We used the CMT model to measure the contractile effects hypertrophic factors and determine whether their co-application had a synergistic effect on contractility. Additionally, due to the evidence of ET-1

mediating the actions of other hypertrophic factors we hypothesized that ET-1 would result in an enhanced hypertrophic response, leading to greater changes in contractility.

Force generation as well as kinetics of myocardial tissues, are dependent on many factors including muscle length and associated sarcomere length, myofilament calcium sensitivity, among others. Model system differences in the loading conditions, and associated differences in myofilament properties such as sarcomere length lead to varying inotropic (force-altering) responses (Palomenque J et al. 2006, Guccione JM et al. 1997, MacGowan JM et al. 1997, ter Keurs HE et al. 2008, Li P et al. 1994). In a pioneering study, Layland J et al. demonstrated that cardiac troponin I (cTnI) has a pivotal role in the positive inotropic response of the murine heart to beta-adrenergic stimulation (isoprenaline), however this effect is highly dependent on loading conditions, as dependence of cTnI in inotropic responses was most evident in the auxotonic, not the isovolumic hearts nor in externally unloaded isolated cardiomyocytes. In another study, Li et al determined that the inotropic effects of Ang II are dependent on resting sarcomere length of the muscle tissue in an isometric preparation. While the untreated tissues exerted the maximal twitch force at the sarcomere length at the peak of the Frank Starling curve (~2.2um), the tissues treated with Ang II exhibited a different response. At the same maximal sarcomere length, Ang II exerted a negative inotropic response; while at shorter lengths, Ang II exhibited a positive inotropic response. Therefore, the inotropic actions of hypertrophic agonists such as ET-1, Ang II and TGF-β are dependent on the resting sarcomere length. While sarcomere length is usually set in isometric preparations, in auxotonic preparations tissues are allowed simultaneously change load and length, and thus, sarcomere length is not typically measured. We aimed to determine the inotropic and kinetic effects of these hypertrophic agonists in auxotonic loading conditions and subsequently determine how the sarcomere length is

associated with these responses.

2.2 Materials and Methods

2.2.1 *Neonatal Rat Ventricular Myocyte (NRVM) isolation*

Cardiomyocytes were isolated from 1 to 2-day old neonatal Sprague-Dawley rats using a trypsin-based dissociation method as previously described (Radisic M et al. 2003). The cells were pre-plated onto multiple T-75 flasks for 1 hour to allow fibroblasts to attach to the dishes. Cardiomyocytes still suspended in the media were retained and seeded onto a T-75 flask coated with fibronectin. Growth media was changed the next day. Three hours after media change, cells were dissociated with a 0.05% trypsin digestion for 3 minutes. The resulting cell population was subjected CMT generation. CMTs were cultured in high-glucose DMEM (Mediatech, Inc.) containing 10% horse serum (Invitrogen), 2% chick embryo extract (Charles River Laboratories International, Inc.), and Antibiotic-Antimycotic (Invitrogen). Cell culture medium was changed daily.

2.2.2 *Device fabrication and microtissue seeding*

Polydimethylsiloxane (PDMS) micro-fabricated tissue gauges (μTUG) were molded from the SU-8 masters as described previously (Legant et al. 2009). Fluorescent microbeads were embedded (Fluoresbrite 17147; Polysciences, Inc.) into the cantilevers to permit cantilever deflection tracking as previously described (Boudou T et al. 2012) PDMS molds were then cast onto the stamps to produce the final μTUG substrates. A PDMS to cross-linker ratio of 1:20 was used, to yield nominal spring constants of 0.20μN/μm. Cantilever spring constants were computed utilizing a capacitive MEMS force sensor mounted on a micromanipulator as described previously (Legant et al. 2009). CMT substrates were treated with 0.02% Pluronic F127 for 30 minutes to

prevent cell-extracellular matrix interactions.

A suspension of ~1.1x10^6 NRVMs within a reconstitution mixture, consisting of 1mg/mL liquid neutralized collagen I (BD Biosciences) and 0.5mg/mL human fibrinogen (Sigma-Aldrich), was added to the substrate. The device was centrifuged to drive the cells into the micro-patterned wells. Cells contract around the cantilevers forming a synchronous tissue 2 days after seeding**.**

2.2.3 *Mechanical and kinetic measurements*

Once the tissue is fully formed and synchronously beating, contractility measurements are taken. To quantify microtissue forces, brightfield and fluorescence images (Figure 2A) were taken at 30Hz using the EXi Blue Fluorescence Microscopy Camera (Q Imaging), and an Fl-Plan 10X objective on a Nikon Eclipse TE200-U (Nikon Instruments, Inc.) microscope, which was equipped with a live cell incubator. Only tissues that were uniformly anchored to the tips of the cantilevers were included in the analysis. Electrical field stimulation of biphasic square pulses of 1 ms was given by placing two carbon electrodes (1/4 in diameter; Ladd Research laboratories) separated by 2 cm on the sides of the samples connected through platinum wires to a stimulator (Radisic et al. 2008).

To calculate resting force, brightfield images were used to calculated the difference in the position of the base of the cantilever and the deflected cantilever cap (Figure 4B) at that particular instance in time and force is calculated using F= kδ*,* Where *F* is the force generated by the microtissue, *k* is the bending stiffness of the post (0.20 μN/μm), and δ is its deflection. To measure twitch force, the displacement of fluorescent microbeads at the top of the cantilevers was then tracked using the SpotTracker plug-in in ImageJ (NIH) and the average peak force measured during each twitch event (Figure

4A) was recorded. The velocity of a cantilever at a given time point is calculated from $V_i=\delta_{i+1}-\delta_{i-1}/t_{i+1}-t_{i-1}$ where t represents the time elapsed from the start of the video. Values of maximum twitch velocity reported in this work were determined by comparing the maximum contraction and relaxation velocities measured at each post, and then averaging these values across multiple beats (Figure 4D). In turn, twitch force and twitch velocity at a given time point can be multiplied together to obtain the twitch power, $P_i=F_iV_i$ (Figure 4E).

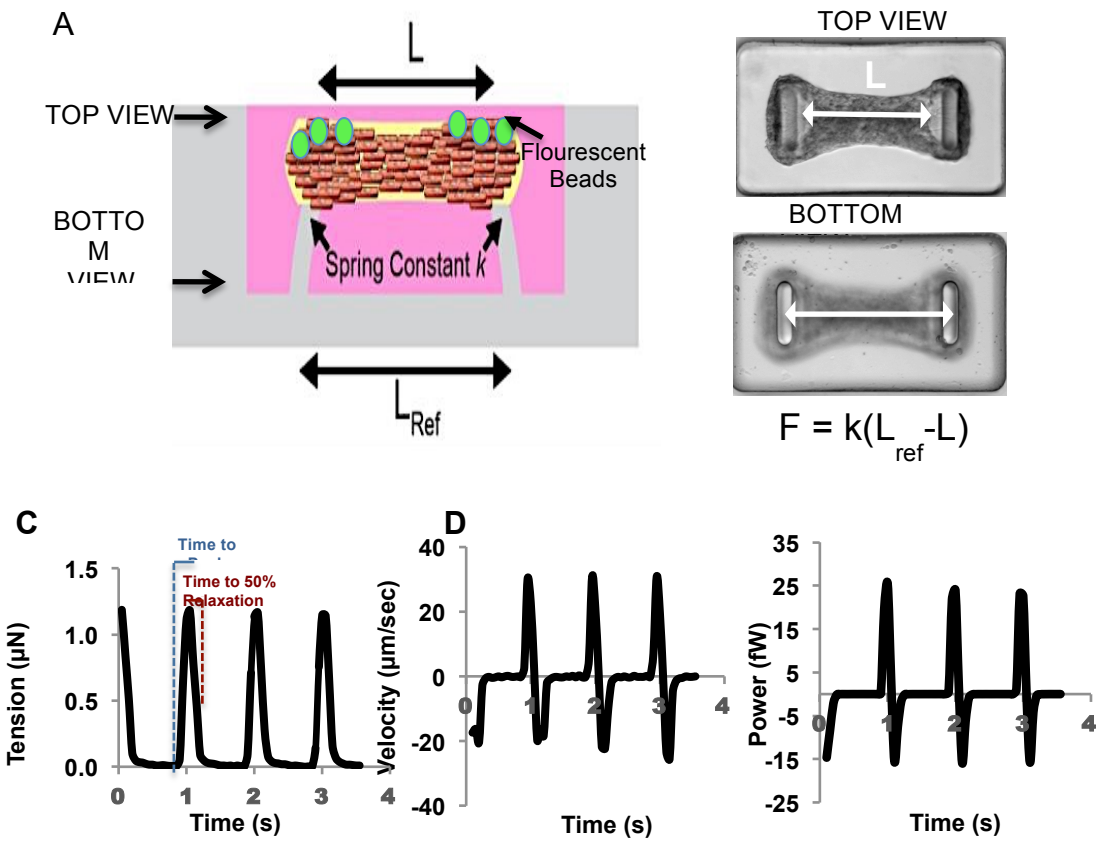

Figure 4. Measurement CMT twitch force, velocity, and power. Twitch force is calculated by measuring the displacement of fluorescent microbeads at the top of the cantilevers, which are tracked using a high-speed camera (Figure by Thomas Boudou) (A). To calculate resting force, brightfield images were used to calculate the difference in the position of the base of the cantilever and the deflected cantilever cap at that particular instance in time (B). The videos allows us to track the fluorescent beads over multiple twitch events at 1hz, which can be multiplied by the post stiffness to yield the twitch force (*C*). From this trace, the displacement data from the fluorescent beads can then be used to determine the twitch velocity (D) and power (E).

2.2.4 Hypertrophic agonist stimulation

Hypertrophic factor treatment was started once the tissues formed a syncytium, generated synchronous twitches, which occurred 2 days after seeding the cells on the uTUG (3 days after cell isolation). Data were collected before hypertrophic factor addition and after 24 hours and 48 hours of growth factor stimulation (see Figure2 below). To determine the optimal concentration for the hypertrophic factors, we treated tissues with increasing concentrations of factors until there was no further increase in resting or twitch force amplitude. The range of concentrations were chosen based on the previously reported concentration ranges that induced inotropic and other hypertrophy-related responses in NRVMs. For each hypertrophic factor we tested the following concentrations (in 1ml of media): TGF-β (5 ng, 10 ng, 20 ng), Ang II (500 ng, 750 ng, 1 μg, 2 μg), and ET-1 (250 ng, 375 ng, 500 ng, 1 μg) (Olson ER et al. 2008, Malhotra R et al. 1999, Schaub MC et al. 1997, Castanares C et al. 2007). 10 ng of TGF-β, 1 ug of AngII, and 500ng of ET-1 were chosen based on maximum resting and twitch force generation. To evaluate additive contractile responses to these growth factors, a cocktail using the final concentration of each factor was utilized.

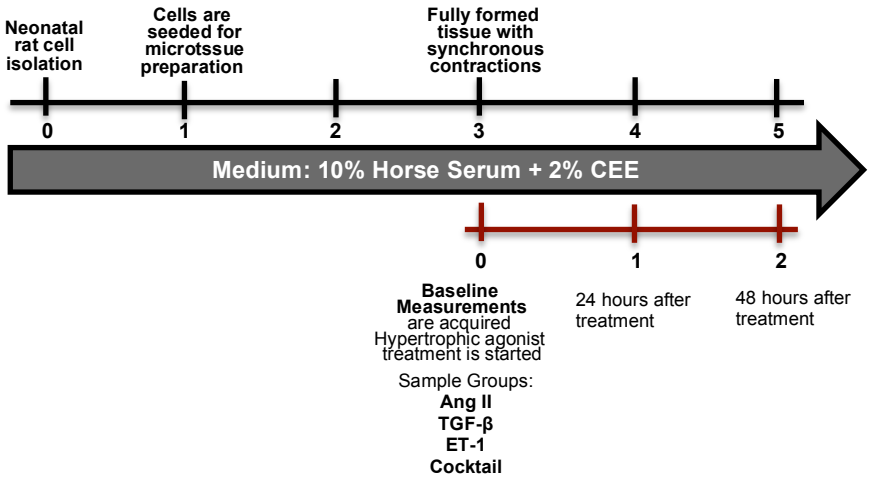

Figure 5. Experimental Timeline. After the neonatal cardiac cell isolation, cells were pre-plated onto multiple T-75 flasks for 1 hour to allow fibroblasts to attach to the dishes. Cardiomyocytes still suspended in the media were retained and seeded onto a T-75 flask coated with fibronectin. Growth media was changed the next day to eliminate dead cells. Three hours after media changes cells are seeded into the microtissue array. After 2 days in culture (with media changes every day), tissues form and generate synchronous contractions, and videos and brighfield images are acquired for baseline measurements before beginning the hypertrophic agonist treatment. Measurements are acquired again after 24 and 48 hours of treatment.

2.2.5 *Sarcomere length measurements*

Microtissues were fixed with 4% paraformaldehyde in PBS for 15 minutes and permeabilized with 0.1% Triton X-100 in in 1xPBS+1%BSA+5% Goat serum. The tissues were incubated with antibodies against α-actinin (Abcam) in 1xPBS+2%GS+1%BSA for 48 hours, and thereafter incubated with the secondary antibody in 1xPBS+2%GS+1%BSA overnight. Counterstaining was done with DAPI (Invitrogen). Images were processed by a custom routine in ImageJ (NIH) and MATLAB (Mathworks). The 2D Fourier transforms of images were determined as described

previously (AG Rodriguez et al. 2011) Only sarcomere length measurements with variance less 0.2 were included in the study, which excluded ~5-10% of the measurements per sample

2.2.6 *Statistics*

Results are expressed as mean ± standard error of the mean (SEM). Statistical significance was defined as a *p-value < 0.05 or **p-value < 0.005 for at least three independent experiments. Student's t-test was performed with Microsoft Excel® for sarcomere length measurements. A two-way ANOVA analysis with post hoc Tukey tests was performed with Stata (to determine statistical significance relative to control tissues for hypertrophic factor treatments).

2.3 Results

2.3.1 *Effect of hypertrophic factors on auxotonic contractility of microtissues exposed to hypertrophic factors for 24 hours and 48 hours*

To determine early contractile responses of different hypertrophic agonists on engineered tissues, we treated tissues for 24 hours and 48 hours with 10ng TGF-β, 1μg AngII, and 500ng ET-1 in arrays of cantilevers with a nominal spring constant of k=0.20 μN/μm. Additionally, we tested whether co-application of hypertrophic factors resulted in a synergistic effect on mechanical response. Single hypertrophic factor treatment as well as the cocktail of hypertrophic factors induced increases in resting force (Figure 6A). We measured the change in force produced by each tissue, to correct for differences in baseline measurements. After 24 hours of treatment, change in resting force ($\Delta F_R = F_R$ d1- F_R d0) for the ET-1 treatment resulted in 13-fold higher change in resting force than the Untreated (Untreated: ΔF_R = 0.32±0.15 μN vs. ET-1 ΔF_R = 4.26±0.36 μN), while Ang II and TGF-β resulted lower changes in resting force (Ang II: ΔF_R=

2.48±0.47 μN, TGF-β: Δ F_R= 0.76±0.08 μN) (Fig. 2B). Interestingly, the cocktail of the 3 hypertrophic factors generated a change in resting force similar to ET-1 sample (Cocktail: Δ F_R 4.71±0.28 μN). We also measured the change exerted by the tissues after the first day and the change from the day 1 to day 2, However, no statistically significant differences were observed for the changes from day 1 to day 2 of treatment. A one-way between subjects ANOVA was conducted to compare the effect of hypertrophic factor treatment on the contractility of CMTs in TGF-β, AngII, ET-1 and cocktail treatments. There were significant effects of hypertrophic factor treatment on CMT contractility at the $p < 0.05$ level for the 4 treatments [$F(4,4) = 43.33$, $p < 0.00005$]. Post hoc comparisons using the Tukey HSD test indicated that the resting force mean for the ET-1 ($F_{R\ day1}$ 4.26±1.36 μN) was significantly different than the Untreated ($F_{R\ day1}$ 0.32±0.15 μN). Ang II ($F_{R\ day1}$ 2.48±0.47 μN) demonstrated significant, but more moderate difference to the Untreated sample. Additionally AngII was statistically significantly different to each of the other groups, and the Untreated ($F_{R\ day1}$ 0.32±0.15 μN) did not significantly differ from TGF-β ($F_{R\ day1}$ 0.76±0.08 μN), likewise ET-1 did not significantly differ from Cocktail treatment ($F_{R\ day1}$ 4.71±0.28 μN).

Additionally we measured twitch force generated after 24 hours and 48 hours of hypertrophic factor treatment (Figure 6C). Twitch force was recorded while microtissues were being electrically paced at 1hz using field electrodes. As was done for resting force measurements, we measured the change in force produced by each tissue, to correct for differences in baseline measurements. The cocktail of hypertrophic factors resulted in a 23-fold increase in twitch force while ET-1 resulted in an 18-fold fold increase in twitch force compared to the Untreated sample. (Cocktail ΔF_T=1.17±0.01 μN vs. ET-1: ΔF_T=0.89±0.04 μN vs. Untreated: Δ F_T =0.05±0.03 μN, $p<0.001$) (Figure 6D). TGF-β was the only hypertrophic factor that resulted in a decrease in twitch force (Δ F_T =-0.21±0.06

μN, p<0.0001) (Figure 6D). AngII had a more moderate increase in twitch force (Δ F_T =0.30±0.16 μN). While the co-application of hypertrophic factors resulted in higher resting and twitch force, it did not result in a synergistic effect in the contractility. Based on these results, we showed that ET-1 has a larger increase in both resting force and twitch force generation in microtissues A one-way between subjects ANOVA was conducted to compare the effect of hypertrophic factor treatment on contractility of CMTs in TGF-β, AngII, ET-1 and cocktail conditions. There was a significant effect of hypertrophic factor treatment on CMT contractility at the p<. 05 level for the 4 conditions [F(4, 4) = 41.53, p <0.00005]. Post hoc comparisons using the Tukey HSD test indicated that the mean twitch force for the ET-1 ($F_{R\ day1}$ 4.26±1.36 μN) was significantly different than the Untreated sample ($F_{R\ day1}$ 0.32±0.15 μN, p<0.001) and Ang II ($F_{R\ day1}$ 0.30±0.16 μN, p<0.001). However, the Untreated did not significantly differ from TGF-β ($F_{R\ day1}$ 0.76±0.08 μN). Likewise, the Cocktail ($F_{R\ day1}$ 4.71±1.22 μN) did not significantly differ from ET-1.

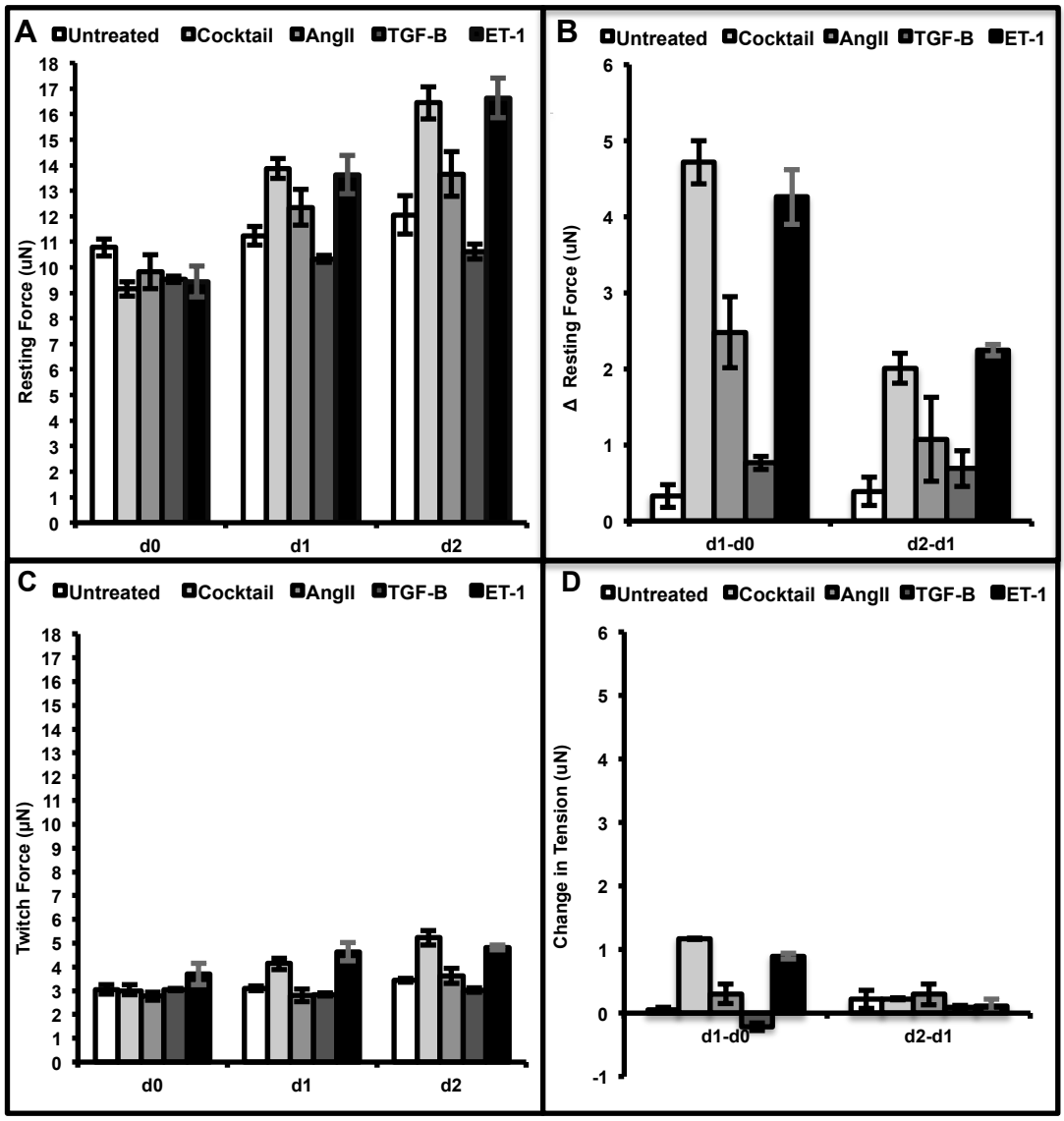

Figure 6. Resting and Twitch force generation in CMTs after 24 and 48 hours of hypertrophic agonist treatment. After CMTs were formed and synchronously beating, baseline force measurements at day 0 were acquired. Brightfield images were used to calculate the resting force (A). To account for baseline force differences, we computed the change in resting force per tissue after 24 and 48 hours of treatment, and the average across multiple tissues (N=25) is represented by the bar graph above (B). Using a high-speed camera, we collected data of the displacement of the cantilevers over multiple contractions. The bar graph above represents the average peak force for 3-5 contractions across multiple tissues (N=25) (C). Similarly to resting force, we computed the change in twitch force after 24 and 48 hours (D).

2.3.2 *Correlation between microtissue length and twitch force generation after 24 hours of hypertrophic factor exposure*

The mechanical properties of isolated cardiac muscle in isometric preparations (constant length) have been widely studied. Under isometric conditions, if the muscle is set at a short resting length, the resulting twitch force is relatively small, while if it is set at a longer resting length, the resulting twitch force is higher. However, the effect of resting length in an auxotonic preparation of engineered cardiac muscle is poorly understood. Because we observed the greatest magnitude of change in force in the first 24 hours, we sought out to evaluate how the change in resting force affected the change in twitch force for individual tissues after 24 hours of treatment. Based on the previous work on isometric tissue experiments, we predicted that the larger the increase in resting force per tissue, the shorter the resting length, and consequently the lower the twitch force generated.

However, our data showed that Ang II, ET-1 and the Cocktail treatment resulted in significant increases in resting force as well as twitch force as compared to the untreated sample, with ET-1 and the Cocktail exerting a larger increase than Ang II. Based on this data, we asked whether there was any relationship between the change in length from day 0 to day 1 to the change in twitch force on the same time span. Interestingly the change in resting force, which is directly related to, the decrease in microtissue length, did not correlate with the change in twitch force generated in untreated (Figure 7A) and treated samples (7B-E). Consequently, we assessed how the length of the tissue at day 1, after 1 day of hypertrophic agonist treatment correlated with the twitch force on that same day. For individual growth factors, Ang II (Figure 8C), TGF-β (Figure 8D), and ET-1 (Figure 8E), there was a statistically significant moderate negative correlation between resting length and generated twitch force (Ang II: R^2=0.31

p=0.001, TGF-β R^2=0.25 p=0.002, ET-1 R^2=0.47 p=0.00001), however there was no significant correlation for the Untreated (Figure 8A) and Cocktail groups (Figure 8B). These data tells us that while the change in resting force does not affect the change in twitch force, the final resting length does moderately affects the final twitch force generated.

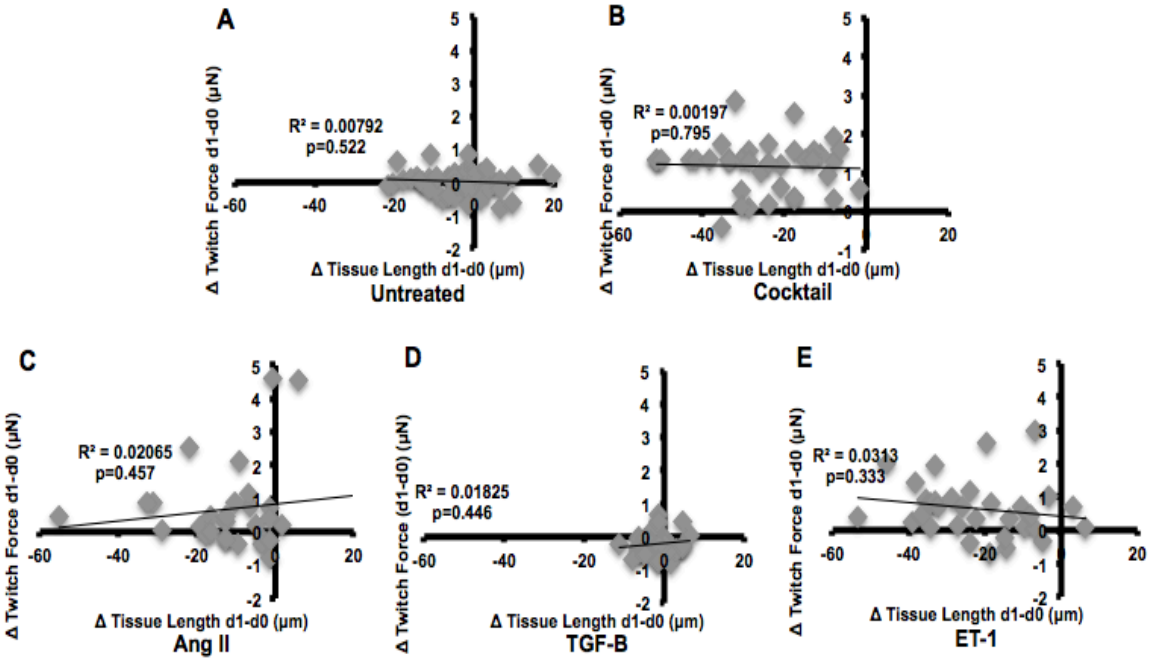

Figure 7. Correlation of the change in tissue length and the change in twitch force after 24 hours of hypertrophic factor treatment. Change in twitch force was plotted against change in tissue length. A linear regression analysis and a correlation coefficient R^2 were determined. All samples, Untreated (A), Cocktail (B), Ang II (C), TGF-β (D) and ET-1 (E), showed no correlation between the change in tissue length and the twitch force generated.

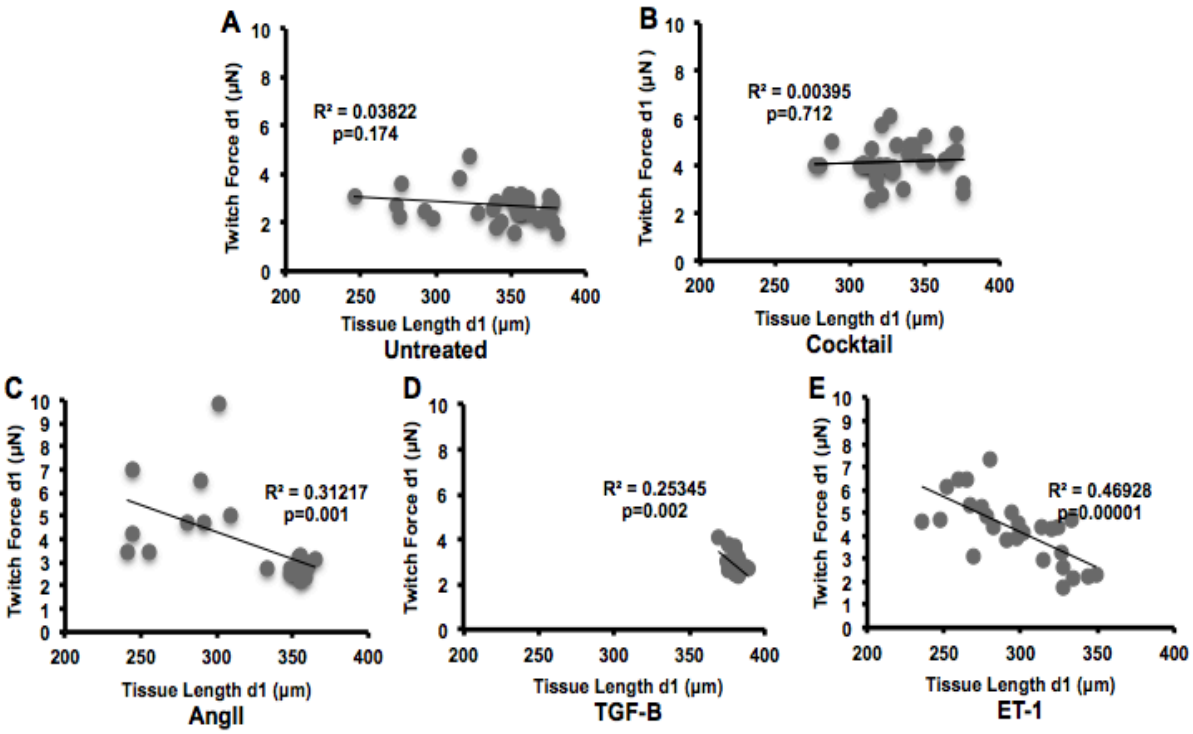

Figure 8. Correlation of the tissue length and twitch force at 1 day after hypertrophic agonist treatment. The twitch force and tissue length after 24 hours of hypertrophic agonist treatment were plotted against Each other. A linear regression analysis and a correlation coefficient R^2 were determined. No correlation was identified in Untreated (A) and Cocktail (B). For AngII (C), TGF-β (D) and ET-1 (E), showed that 31%, 25% and 47% respectively of the variance in Twitch Force was related to the tissue length at day 1.

2.3.3 Tissue length and tissue breakage upon hypertrophic agonist treatment

In addition to increases in resting force that paralleled increases in twitch force for ET-1 and the Cocktail, we observed that those treatments also led to higher rate of tissue rupture occurred after hypertrophic factor stimulation. We observed the highest failure rate for the Cocktail group (61%), and ET-1 (54%), while Ang II (43%), TGF-β (21%), and Untreated group (10%) had more moderate tissue breakage (Figure 9A). We evaluated whether the resting force (or tissue length) before hypertrophic factor treatment had an effect on the probability of breakage after hypertrophic treatment was added to the samples. For the Cocktail, Ang II, and ET-1 groups, we found that higher resting forces before treatment led to a higher likelihood of tissue rupture in the first 24 hours of hypertrophic factor treatment (Figure 9B). There was no significant difference between the twitch force before the addition of hypertrophic factor of tissues that ruptured and those that did not rupture (data not shown). Collectively, these findings indicate that, after 24 hours of hypertrophic growth factor stimulation, shorter tissue lengths, with higher resting forces, are associated with a higher probability of tissue breakage in our auxotonic microtissue model, primarily for ET-1, Ang II and the Cocktail. However, while hypertrophic factors are correlated with twitch force generated, twitch force itself is not correlated with rate of rupture.

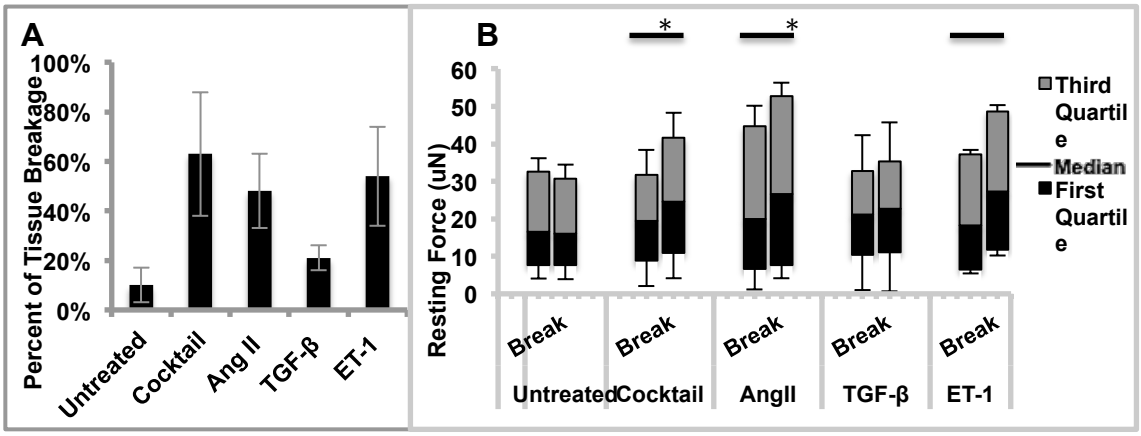

Figure 9. Effect of resting force on tissue breakage. We measured the average percentage of tissue breakage for each for each of the hypertrophic agonist treatments (A). We evaluated differences in resting force from the tissues that broke and remained attached (B). Student's t-test was used to compare between the agonist treatments and the Untreated, (A) and between Attached and Broken populations (B); * denotes $p<0.05$ and ** denotes $p<0.005$.

2.3.4 Characterization of resting sarcomere length and relationship to tissue length and twitch force generation after 24 hours of hypertrophic agonist treatment

Sarcomere measurements have been traditionally done in isometric preparations where the sarcomeres are measured for a specific tissue length. Tissue length is typically positively correlated with sarcomere length. In other words, the longer the tissue, the longer the sarcomeres. The increased length of these sarcomeres may imply an elevated probability of actin-myosin cross-bridge formation, which contributes to higher actomyosin forces and leads to an enhanced force-generating capacity. To understand how sarcomere length correlated with microtissue length in our auxotonic preparation, we fixed the samples after 24 hours of stimulation and stained with α-actinin (ABCAM) (Figure10A). A line was drawn across the center of five or more consecutive sarcomeres, resulting in a Plot Profile function that reports the intensity profile along the line. The data from this plot was analyzed using MATLAB, the distance between the brightest points or peaks of the plot results in sarcomere length. We only included sarcomere lengths with variance less than 0.2 μm.

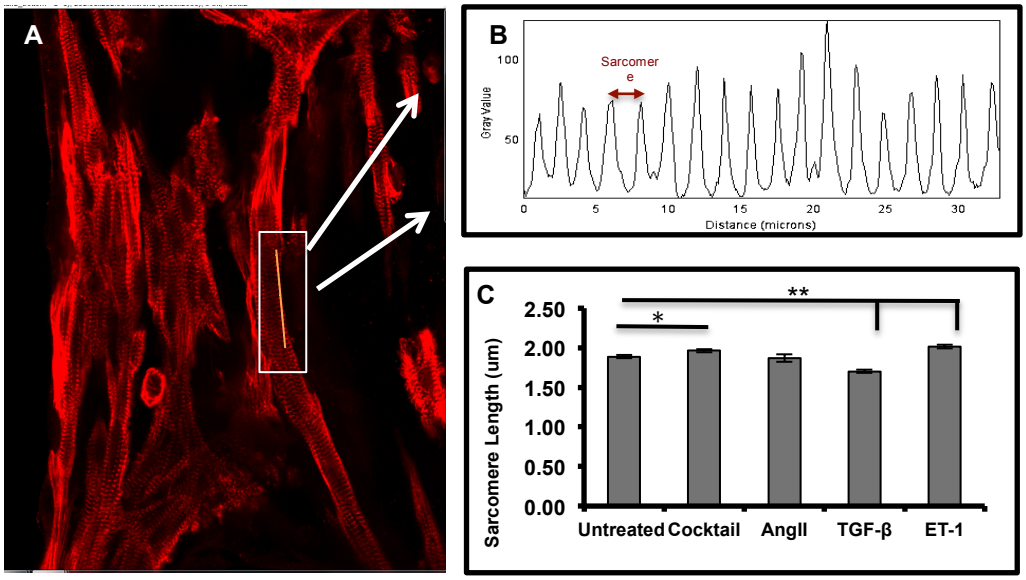

Figure 10. Resting sarcomere length in different hypertrophic agonist treatments. Immunofluorescent image shows Microtissues attached to cantilevers stained with a-actinin to detect sarcomeres (red). A linescan (shown in yellow) is drawn across at least 5 sarcomeres, and the distance between the peaks is averaged to determine sarcomere length. Scale bar. Student's t-test was used to compare between an agonist treatment and the Untreated sample; * denotes $p<0.05$ and ** denotes $p<0.005$

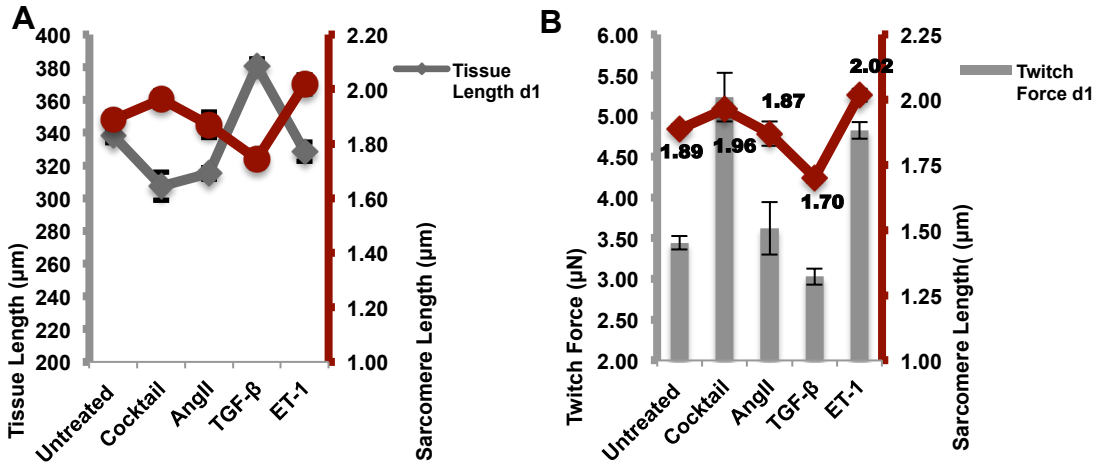

Figure 11. Relationship between sarcomere length, tissue length and twitch force after 24-hour hypertrophic factor treatment. Tissue length is plotted alongside sarcomere length to visualize the association with resting sarcomere length (A) to show_that sarcomere length is inversely correlated to tissue length. Additionally, Twitch force generation after hypertrophic agonist treatment was plotted alongside sarcomere length to show that higher resting sarcomere length is associated with higher twitch force generation (B).

We found that the Cocktail, and ET-1 treatments resulted in significant increases in resting sarcomere length 1.96 ± 0.02 µm, $p<0.05$ and 2.07 ± 0.02µm $p<.0005$ respectively, compared to 1.89 ± 0.02 µm in the untreated sample. The TGF-β treatment resulted in a decrease in sarcomere length, resulting in sarcomere length of 1.70 ± 0.02µm $p <.005$. Ang II did exhibit significant differences as compared to the Untreated (1.87 ± 0.02µm vs. 1.89 ± 0.02 µm). Interestingly, the sarcomere length was negatively correlated to tissue length (Fig. 11A), in other words, the longer the tissue length, or the lower the resting force, the shorter the sarcomere length.

To further understand how this relationship affected twitch force generation, we

plotted sarcomere length against twitch force generation and found that the longer the sarcomere length of the tissue, the higher the twitch force generated after 24 hours of treatment (Fig. 11B). Myocardial length-dependent effects characterized in isometric preparations in twitch force generation have been well characterized. However, it is the first time that we observe a change in resting sarcomere length in an auxotonic preparation upon hypertrophic agonist stimulation.

2.3.5 Characterization of contraction velocity and relaxation after 24 hours of hypertrophic agonist treatment

While the strength contraction of cardiac tissue is important, the kinetics of the contraction and relaxation are also an essential determinant of cardiac performance. The regulation of myocardial contraction and relaxation kinetics is currently incompletely understood in auxotonic-loaded microtissues. From the start of the contraction phase, the contraction velocity of the CMT speeds up, reaches a maximum value, and then decreases back down to zero when the peak twitch force is reached. Here, the maximum value in the velocity is identified as V_{max} Contraction and the average of the velocities up to the peak twitch force is identified as V_{avg} Contraction. Similarly, during relaxation, the CMT contraction speed starts at zero, decreases to some negative maximal value, and then returns to zero until the next twitch contraction commences. The greatest negative velocity reached during this phase is henceforth referred to as V_{max} Relaxation and the average velocity, V_{avg} Relaxation. Because, the velocities are identified as V_{max} Contraction vs. V_{max} Relaxation, no negative values are used.

As we observed the greater changes in force in the 24 hours of hypertrophic agonist treatment, we further evaluated the kinetic contractile profile in these first 24 hours. We observed that the V_{max} Contraction of the Ang II ($V_{max\ day0}$= 58.18±2.51μm/s

vs. $V_{maxday1}$= 76.992±3.68 μm/s, p<0.005), ET-1($V_{max\ day0}$= 60.21±4.38 μm/s vs. $V_{max\ day1}$= 86.21±8.11μm/s, p<0.005) and Cocktail ($V_{max\ day0}$= 55.36±3.64μm/s vs. $V_{maxday1}$ = 93.85±2.43μm/s, p<0.005) treatments were significantly increased after 24 hours (Figure 10A). However, for the Untreated ($V_{max\ day0}$ = 63.05±6.50 μm/s vs. $V_{max\ day1}$= 48.72± 8.12μm/s) and TGF-β ($V_{maxday0}$ = 65.82±5.11μm/s vs. $V_{maxday1}$= 42.76±3.32μm/s) the V_{max}Contraction decreased, but was not statistically significant (Figure 10A). Similarly, for V_{max} Relaxtion of the Ang II ($V_{max\ day0}$ 54.01±2.58 μm/s vs. $V_{max\ day1}$ = 71.29±3.56 μm/s p<0.005), ET-1 ($V_{max\ day0}$ 51.51±3.75 μm/s vs. $V_{max\ day1}$ = 73.58±7.34 μm/s p<0.005), and Cocktail ($V_{max\ day0}$ 54.83±3.48μm/s vs. $V_{max\ day1}$ = 80.20±2.04 μm/s p<0.005) treatments were significantly increased, while Untreated ($V_{max\ day0}$ 49.03±5.02 μm/s vs. $V_{maxday1}$ = 40.30±6.58μm/s) and TGF-β ($V_{maxday0}$ 61.75±4.11μm/s vs. $V_{max\ day1}$ = 60.92±2.99μm/s) did not show statistical significant differences when comparing to the values before hypertrophic agonist treatment.

Moreover, we examined the ratio of V_{max}Relaxation /V_{max} Contraction. In a previous study using tissues in an isometric preparation of isolated muscle strip systems, the author showed that while the magnitudes of the velocities of contraction and relaxation can change vastly, the ratio of the Vmax of relaxation over Vmax of Contraction was not significantly different in 16 different conditions, which included different rodent strains, lengths, frequencies, isoproterenol concentrations, etc. Only when the tissues were not mechanically loaded, exposed not normal frequencies nor under physiological temperature this ration was out of balance (Janssen PML, 2010). In our studies we observed no statistically significant changes between the ratio of V_{max}Relaxation /V_{max} Contraction in the Untreated sample and in samples that were treated with hypertrophic agonists for 24 hours. Furthermore, the ratios of V_{max}Relaxation /V_{max} Contraction were similar across all samples. The ratios between all

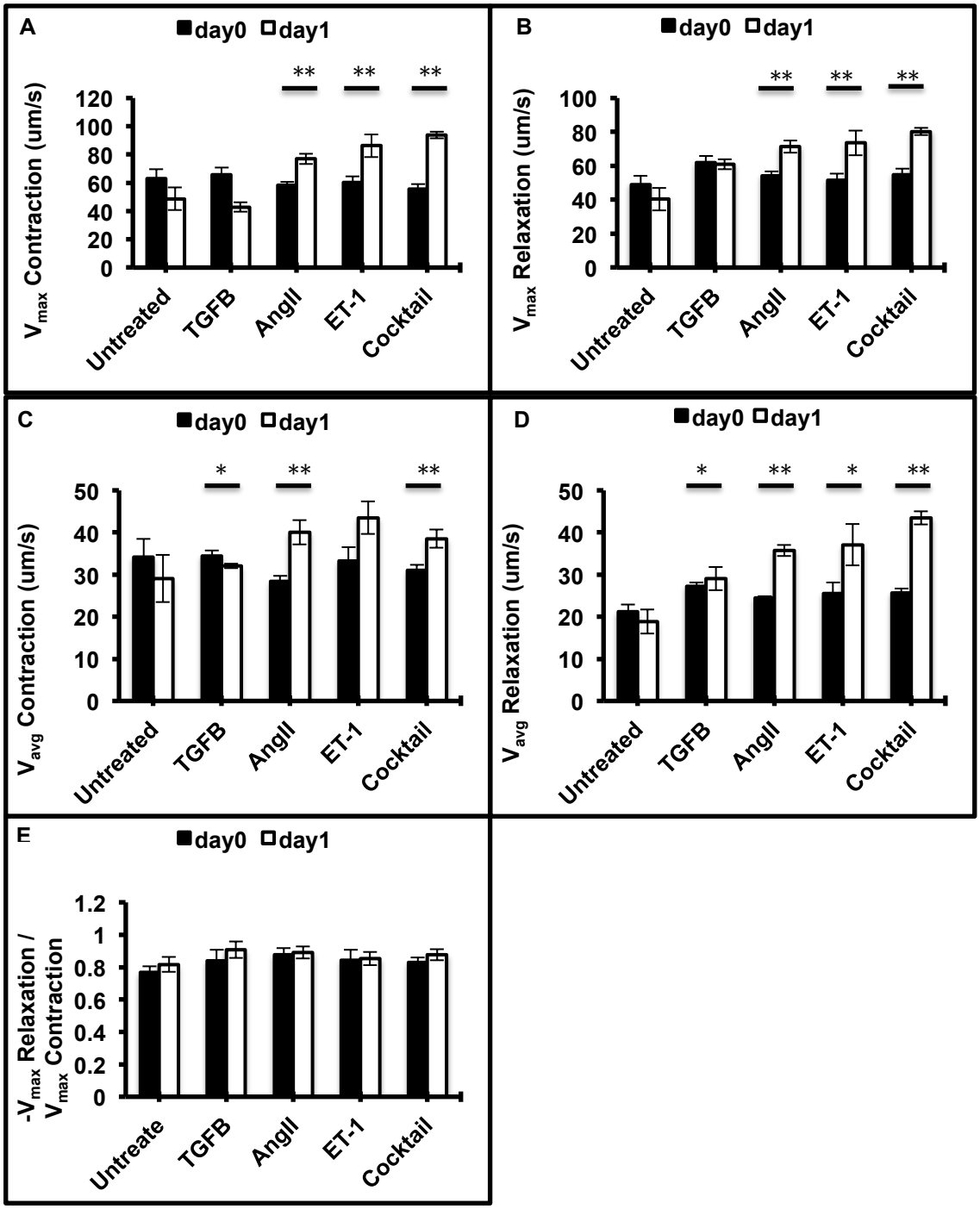

Figure 12. Contractile kinetics profile in CMTs after 24 hours of hypertrophic agonist treatments. Using a high-speed camera, we tracked the displacement of fluorescent beads atop of CMTs, and calculated kinetics of contractility. Bars represent the average of individual tissues velocities over 3-5 twitches. Maximum velocity of contraction (Vmax Contraction) (A),Vmax Relaxation (B), Vavg Contraction (C), Vavg Relaxation (D), V_{max}Relaxation /V_{max} Contraction (E) were calculated from the data. Student's t-test was used to compare between day0 and day1; * denotes $p<0.05$ and ** denotes $p<0.005$.

samples were fairly similar and ranged between 0.77-0.91.

2.3.6 *Contraction, peak force and 50% relaxation time measurements after 24 hours of hypertrophic agonist treatment*

In addition to the speed of contraction and relaxation we measured the time it took to reach peak force, 50% relaxation, and to complete a contraction. We observed that time to reach peak force, 50% relaxation, and complete a contraction was reduced for the untreated sample after 24 hours, but it was not statistically significant. Tissues exposed to TGF-β had decreased contraction and relaxation velocities upon treatment, and consequently had a longer time to reach peak force, 50% relaxation, and complete a contraction (Figure 13A-C). For the Cocktail, however, we observed an increase in speed of contraction and relaxation, but found that despite the increase in velocities, it took a longer time to reach peak force (increased force generation), 50% relaxation, and complete a contraction (Figure 13A-C). Moreover, ET-1 reached peak force at a shorter time, but took a longer time to reach 50% relaxation, and no statistically significant change in contraction time(Figure 13 A-C). On the hand, Ang II exhibited a statistically significant decrease in time to reach peak force, and a decrease in time to reach 50% relaxation and contraction, however these were not statistically significant(Figure A-C). Lastly, we looked at the ratio of time to peak and time to reach 50% relaxation. We did not observe any statistically significant change in this ratio, indicating, that the equilibrium between contraction and relaxation are maintained (Figure 11D).

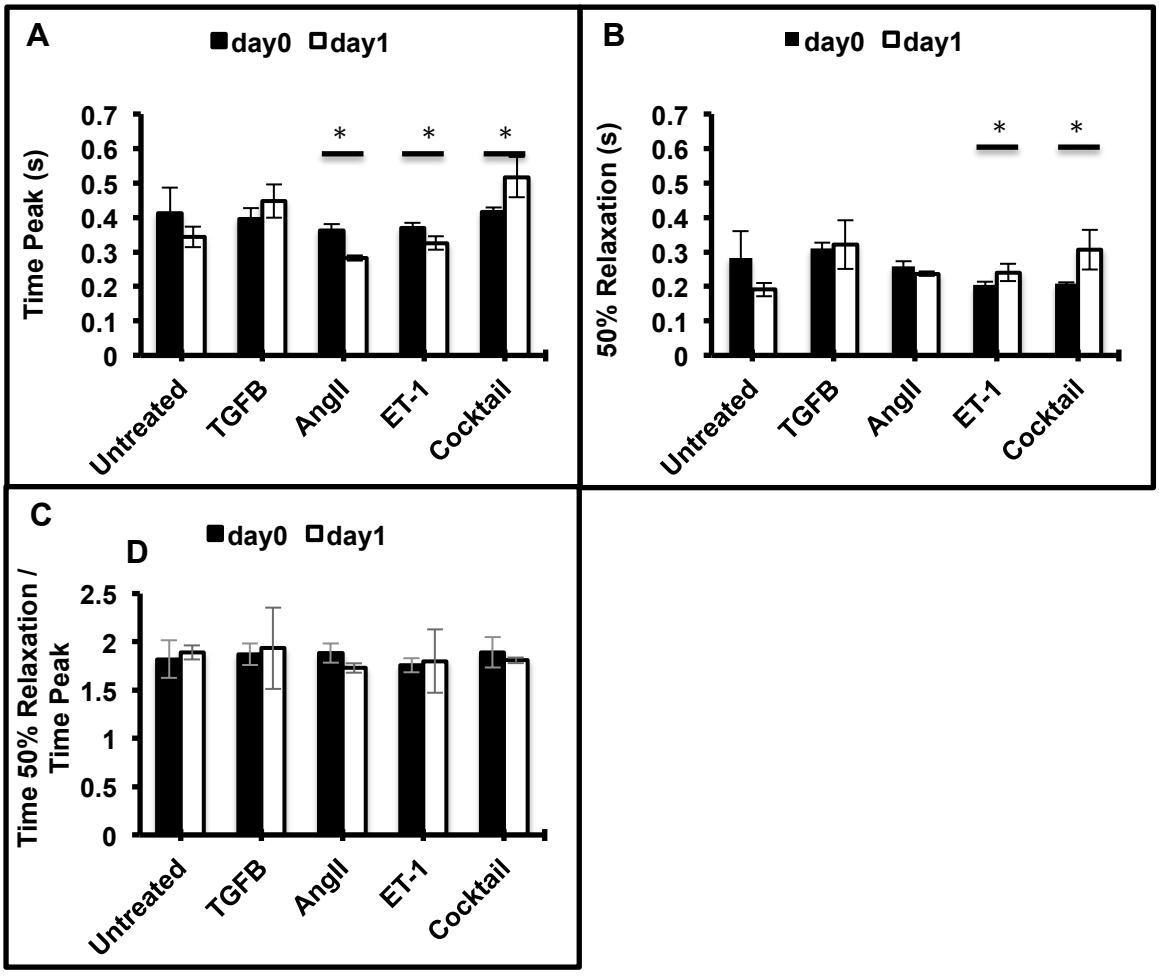

Figure 13. Contraction, peak force and 50% relaxation time measurements after 24 hours of hypertrophic agonist treatment. From the displacement data obtained from the fluorescent beads atop of CMTs, we calculated the time to reach peak force (A), time to reach 50% relaxation (B) and time to complete a contraction (C). Additionally, we measured the ratio of time to 50% relaxation over time to peak force. Bars represent average of maximum power over 3-5 twitches across multiple tissues. Student's t-test was used to compare between day0 and day1; * denotes $p<0.05$.

2.3.7 *Power of contraction and relaxation measurements after 24 hours of hypertrophic agonist treatment*

Twitch power, which is the product of the instantaneous twitch force and twitch velocity, has a similar temporal trend as twitch velocity. Prior to contraction the power is zero. In the contraction phase, the twitch power reaches a maximum value, and then reduces back down to zero. A relaxation phase follows, during which the twitch power reaches a minimum (maximum negative) value of power, before it rises back up to zero. We found that maximum power was exerted after the time at which maximum velocity is reached, where force tends to be fairly low and before the time peak force is exerted, as at that point velocity equals 0 at that instant. We found that ET-1 [($P_{max\ day0}$ =160.33±42.81 vs. $P_{max\ day1}$ =363.48±84.32 $p<0.005$),($P_{max\ day0}$ =135.12±42.92 vs. $P_{max\ day1}$ =313.60±77.80)] and the Cocktail [($P_{max\ day0}$ =152.05±30.90 vs. $P_{max\ day1}$ =429.30±21.04),($P_{max\ day0}$ =125.16±33.59 vs. $P_{max\ day1}$ =433.98±46.35)] had statistically significant increases in generation of power of contraction and power of relaxation (Figure 14A-B). However, for the other treatments we did not identify any statistically significant changes in power generation.

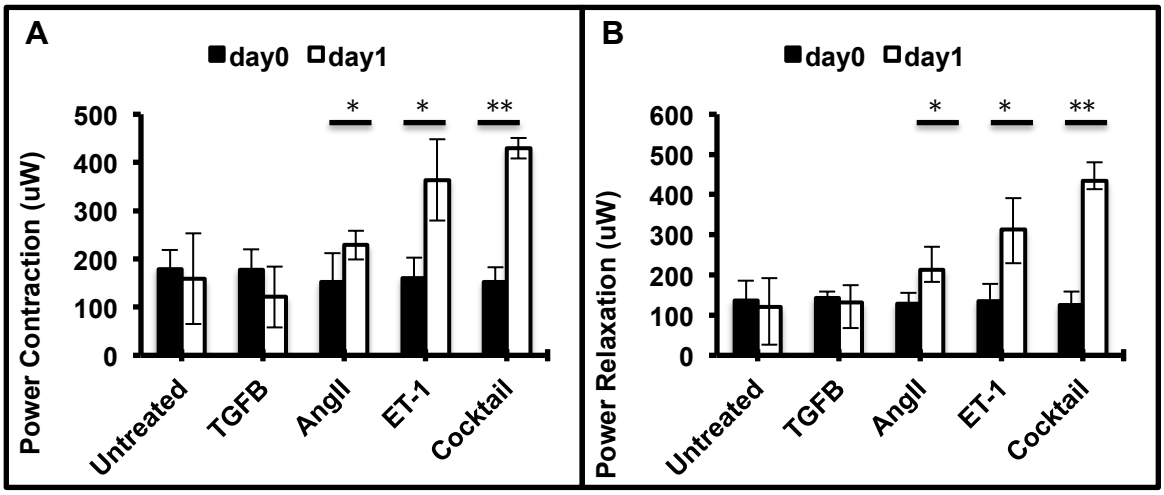

Figure 14. Power of contraction and relaxation after 24 hours of hypertrophic agonist treatment. Using a high-speed camera, we tracked the displacement of fluorescent beads atop of CMTs, and calculated kinetics of contractility. Bars represent average of maximum power over 3-5 twitches across multiple tissues. Measurements of maximum power of contraction (A), maximum power of relaxation (B) were obtained. Student's t-test was used to compare between day0 and day1; * denotes $p<0.05$ and ** denotes $p<0.005$.

2.3.8 *Relationship between forces, velocities and sarcomere length in individual tissues after ET-1 treatment for 24 hours*

To further evaluate the relationship amongst forces, velocities, and sarcomere length, we tracked the force generated per tissue in Untreated and ET-1 –treated arrays, and plotted against each tissue's average resting sarcomere length (Figure 15A-B). We observed that sarcomere length was longer in tissues that generated higher twitch force, in both the Untreated and ET-1 samples. Additionally we found that longer sarcomere lengths seem to be associated with higher V_{max} and V_{avg} values for both contraction and relaxation (Figure 15C-D). Therefore, in our model of auxotonic contractility we observe a relationship between sarcomere length and twitch force generation as well as velocities of relaxation and contraction.

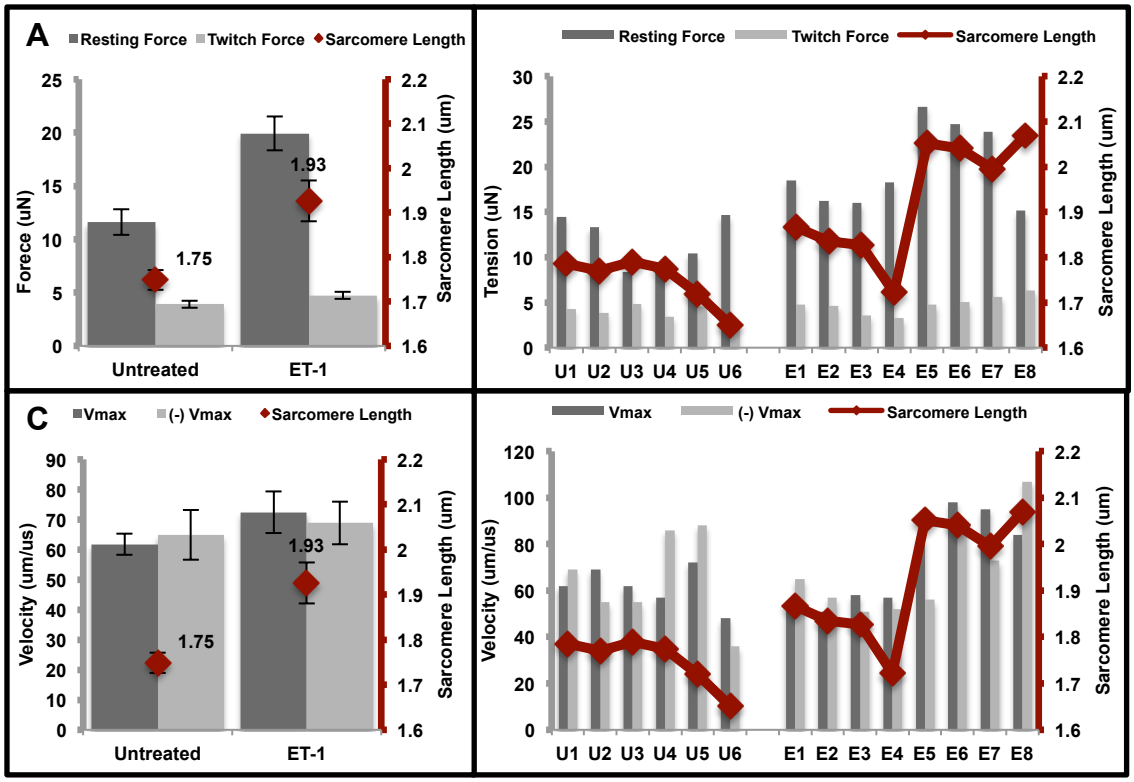

Figure 15. Paired force, velocity and sarcomere length measurements after 24 hours of ET-1 treatment. We repeated measurements for force velocity and sarcomere length as described above. In this experiment however, we plotted the average values on the left hand side and the paired values for each tissue's force (A), kinetics (B) and sarcomere length (C) measurements to compare the relationship between these variables.

2.4 Discussion

In this chapter, we demonstrate the ability of our system to identify contractile profiles in response to different agonists implicated in cardiac hypertrophy by simultaneously measuring the contractile force, velocity, and power produced by auxotonically-loaded CMTs. Additionally, we examined how tissue length and sarcomere length are associated to these changes in contractility.

Our results indicate that ET-1 elicits a larger positive inotropic effect in auxotonic twitch force and resting force generation as compared to Ang II and TGF-β. While Ang II, TGF-β, and ET-1 are known to play important roles in the promotion of hypertrophic remodeling, the specific contributions of each factor have remained unclear. Much attention has been paid to Ang II as a potent modulator of cardiac hypertrophy (Sadoshima J et al. 1993, Dasgupta C et al. 2011, Gray MO et al. 1998). However, studies have shown that ET-1 acts downstream of AngII and TGF-β, and thus the effects of these factors are in part mediated by ET-1. Given that ET-1 had the most significant effect in contractility, this could indicate that ET-1 may be a key player in mechanical remodeling in the heart. Nonetheless, model differences used in other studies should be taken into considerations (such as isometric vs. auxotonic preparations, flat culture vs. 3D tissue preparations, in vitro vs. in vivo). Previous studies using engineered tissue models conflict on whether ET-1 has a positive or negative inotropic effect. In the study that showed that ET-1 had a negative inotropic effect, ET-1 was added over 5 days in millimeter-length tissues, and in conjunction with thyroid hormone triiodothyronine (T_3). T_3 has been implicated in physiological hypertrophy, in increased release of TGF-β, and in significant increases in sarcomere lengths of cardiac cells (Yang X et al. 2014). In another study by the same group, using engineered tissues in an isometric preparation,

the authors identified that ET-1 treatment of engineered tissues, yielded positive inotropic response. However, sarcomere length was not discussed in these studies. Furthermore, the higher rates of tissue breakage in the AngII, ET-1 and Cocktail samples may lead to an underestimation of the maximum twitch force generated by the microtissues, as those with the highest resting force are the most likely to break. Further refinement of the model may allow the preservation of tissues that produce higher twitch forces.

The sarcomere is the fundamental structural unit involved in force generation within cardiomyocytes. We measured resting sarcomere length after 24 hours of hypertrophic agonist treatment and observed that upon treatment of microtissues with ET-1, resting sarcomere length increased. With TGF-β treatment, the resting sarcomere length decreased. Interestingly, we observed that decreases in tissue length (or increases in resting force), were in part correlated with increases in twitch force generation for ET-1 and the Cocktail of three factors. Furthermore, increases in sarcomere length, were positively correlated with increased twitch force generation while negatively correlated to tissue length. The discrepancy between tissue length and sarcomere length is counter-intuitive compared with purposeful stretching of isolated muscle, where increases in tissue length are positively correlated with sarcomere length and increased twitch force generation. However, we know that hypertrophic agonists lead to differentiation of fibroblasts to myofibroblasts, increasing the resting force generated by fibroblasts and myocardial tissue, in part by increased expression of alpha smooth muscle myosin as well as expression of extracellular proteins, which lead to increases in tissue stiffness. While the relationship of sarcomere length in myocytes and myofibroblast stiffness is not fully understood, previous studies have looked at the effect of stiffness on sarcomere length of myocytes. The authors found that with increasing

stiffness, myocyte sarcomere length increases (Rodriguez AG et al. 2011, Torre I et al. 2014). Further evaluation of our system's nonmyocyte effects in the tissue is needed to better understand this relationship. Moreover, upon treatment with Ang II, no significant changes in sarcomere length were observed. These results concur with a previous study using engineered multicellular constructs, which have revealed no change in sarcomere length upon Ang II treatment (Horton RE et al. 2016). Additionally, these results could suggest that the resting sarcomere length increases upon hypertrophic factor exposure in vivo, and may potentially be related to a transition to pathophysiological changes in contractility of the heart. However, these changes are not observed when the length is controlled in isometric preparations. Further experiments evaluating dynamic sarcomere length changes in real time in response to these hypertrophic factors should be explored.

To further our understanding of myocardial kinetics with force and sarcomere changes in auxotonically loaded microtissues, we measured maximum and average contraction and relaxation velocities, time to reach peak twitch force and 50% relaxation as well as maximum power of contraction and relaxation. We detected distinct kinetic responses among the different hypertrophic agonists. For example, microtissues treated with ET-1 reduced time to reach peak force, while the time to reach 50% relaxation increased. Despite the fact that the Cocktail treatment led to similar changes in resting and twitch force responses as ET-1, the kinetics were different. Cocktail treatment led to a shorter time to reach peak force as well as 50% relaxation, leading to an overall faster contraction.

To further understand the relationship between all of these parameters, we carried out paired experiments, where were able to trace a specific sarcomere length of cells in a tissue with the force and kinetics generated by the tissue. This study revealed

that sarcomere length was associated not only with higher twitch force generation, but also higher velocities of contraction and relaxation. While kinetic responses varied in for different treatments, we observed maintenance of the ratios of velocities of contraction and relaxation as well as the ratio of time to peak and time to reach 50% relaxation, a quality characteristic of myocardial tissue. Under physiological conditions, these effects on contractile function are likely to play an important role in adapting cardiac function to achieve optimal cardiac performance under the appropriate conditions of heart rate, loading and inotropic state (Janssen PML, 2010). A better understanding of the mechanisms of sarcomere length and contractility in health and disease may allow the development of novel therapeutic approaches for improving cardiac contractile function.

2.5 Limitations

Engineered heart tissue with auxotonic shortening, this technique has the potential to serve as a powerful tool to evaluate heart mechanics under different biochemical settings, and gained insights into the heterogeneity of microtissue contractile responses, that could not be captured by other methods. However, it is not without its limitations. To further examine the role of ET-1 in Ang II and TGF-β, co-treatment of these factors with an ET-1 inhibitor could be performed. Understanding the signals involved in transducing the hypertrophic actions of ET-1 to pathological mechanical remodeling in the heart will allow us to design selective therapies to prevent adverse cardiac remodeling. Another possible limitation is the fixation-related effects on sarcomere length. However, all samples were treated at the same time using the same fixation protocol. In its current configuration, this system does not allow for real-time measurements of sarcomere length. Sorting out the dynamic sarcomere changes that occur in vivo and in vitro (measuring changes live, for example with laser diffraction

techniques) could provide additional insight into these changes. Additionally, because force is dependent on many factors such as calcium concentration, myofilament calcium sensitivity, etc., additional studies should evaluate additional factors that contribute to changes in force. Furthermore, refinements of our model should allow for comparisons of force and kinetics after agonist treatments under different loading condition. Finally, given that this technique relies upon optically tracking the location of posts over time, the temporal resolution of the measurements is limited by the speed of the camera used to acquire them. Therefore, future research efforts should focus on addressing these shortcomings.

CHAPTER 3: COMBINATORIAL SCREEN OF MECHANICAL AND SOLUBLE FACTORS

3.1 Rationale

Cardiac remodeling is defined as changes in the size, shape and function of the heart, caused most commonly by hypertension-induced left ventricular (LV) hypertrophy and myocardial infarction (MI). The classical model to study cardiac hypertrophy *in vivo* has been aortic banding (AOB) in which the afterload of hearts is increased by banding of the thoracic or the abdominal aorta. Previous studies have showed that rat hearts exposed to AOB leads to activation of cardiac Ang II and ET-1, which occurred differentially during the period of transition from left ventricular hypertrophy to congestive heart failure (Piuhola J et al. 2003, Iwanaga Y et al. 2001). However, the study was limited by the presence of renin-angiotensin, ET-1, and TGF-β systems, which are present in nearly all tissues of the body, making the distinguishing load-induced effects from local and systemic responses difficult.

In vitro 2D models of cardiac hypertrophy have allowed rigorous mechanistic studies of cardiac cell-specific responses (avoiding systemic effects) to hypertrophy, however, there are still some limitations. For example, in a rigid 2D culture substrate, cardiac myocyte hypertrophy is amplified due to the stiffness of the culture substrates, while fibroblasts expand, differentiate to myofibroblasts and release TGF-β, ET-1, and Ang II, all of which function in an autocrine and paracrine manner (Ottaciano FG et al. 2011, Drwnel FM et al. 2015,). Thus, discerning between the effects of substrate stiffness and soluble factor-mediated responses is difficult to achieve. Culturing cells in silicon membranes that can be exposed to static stretch has overcome some of these limitations, however static stretch more closely mimics increase in preload rather than afterload, which is more closely associated with the development of cardiac hypertrophy.

Tissue engineering provides an opportunity to study cardiac cells in 3D, which more closely mimics physiological conditions and allow the opportunity to stimulate cells with load that is more similar to physiological conditions. As mentioned above, our system has the ability to stimulate microtissues with varied levels of the auxotonic load, which mimics afterload, by changing the PDMS concentration. To evaluate the role of increased load, cells were seeded in devices with a 10:1 PDMS-to-curing base concentration that yielded cantilevers with spring constants of [k=0.45 N/m]. Additionally, we aimed to determine the inotropic and kinetic effects of these hypertrophic agonists in auxotonic loading conditions and subsequently determine how the sarcomere length is associated with these responses. Investigating how myocytes respond to different mechanical environments remains crucial for understanding both normal development and disease progression. We hypothesized that co-application of inotropic hypertrophic factors and mechanical load leads to a synergistic effect in mechanical response, tissue and cellular morphology, and downstream pathway activation.

3.2 Materials and Methods

3.2.1 *Cell isolation and microtissue seeding*

Briefly, cardiac cells were isolated from 1 to 2 day neonatal Sprague-Dawley rats and seeded into the μTUGs as previously described in Section 2.2.1. The μTUG devices were made using a PDMS to cross-linker ratio of 10:1, which yields a stiffness of [k=0.45 μN/ μm]. Cell culture medium was changed daily, and hypertrophic agent stimulation was provided with the same timeline as described in section 2.2.4. Mechanical and kinetic measurements, as well as sarcomere length measurements were performed as described in section 2.2.3 and 2.2.5, respectively.

3.2.1 *Cell size measurements*

To measure the size of cells, the plasma membrane of cells within the microtissues was stained with Cell Mask Orange (Life Technologies) dye. According to the manufacturers recommendations, microtissues were washed with sterile 1X PBS and quickly submerged in a 1000X staining solution in cell culture media. Microtissues were quickly incubated for 7 minutes at 37 degrees. Microtissues were left intact in the microtissue device covered with PBS and a slide. Microtissues were imaged live immediately (within 20mins of staining). Fixation of microtissues was not possible, as the fixation caused disruption of the staining pattern in microtissues. Samples were imaged in a Leica TCS SP8 Confocal using a HC FLUOTAR L 25x/0.95 W VISIR, WD 2.50mm objective.

3.2.2 *Tissue volume estimation*

Tissue volume was calculated using the equation of an elliptical cylinder $V = \pi WLH/4$, where W is the long diameter of the cross-section of the ellipse at the center of the tissue, which is measured by taking a picture of the tissue at the middle; while H is the short diameter of the ellipse (or height of the tissue) which is acquired with a Z-stack acquired with a confocal microscope. Length of the tissue (L) was measured as the distance between the pillars.

3.2.3 *RNA isolation and RT-PCR*

Total RNA was extracted using the RNeasy micro kit (Qiagen), used in the high-capacity cDNA reverse transcription kit (Applied Biosystems), and cDNA amplified using TaqMan gene expression assays in an ABI 7,300 system (Applied BioSystems). The RNA isolation protocol improvement included using stainless steel beads to improve

RNA yield, 1-Bromo-3-chloropropane (*BCP*) instead of chloroform, and an RNA buffer for elution instead of water yielded tight cycle threshold values within technical replicates.

3.3 Results

3.3.1 *Effect of hypertrophic factors on auxotonic contractility of microtissues exposed to hypertrophic factors for 24 hours and 48 hours tethered to stiff cantilevers*

To determine early contractile responses of different hypertrophic agonists on engineered tissues, we treated tissues for 24 hours and 48 hours with 10ng TGF-β, 1μg AngII, or 500ng ET-1 in arrays of cantilevers with a spring constant of k=0.45 μN/μm. Additionally, we tested whether co-application of hypertrophic factors resulted in a synergistic effect on mechanical response. Single hypertrophic factor treatment as well as the cocktail of the three hypertrophic factors induced increases in resting force. A two-way multivariate analysis of variance was run to determine the effect of hypertrophic factors (Untreated, AngII, TGF-β and ET-1 and a Cocktail) on change in resting force in cardiac microtissues tethered to stiff pillars. Data are mean ± SEM (in μN) unless otherwise stated. Values of change in resting force were normally distributed, as assessed by Shapiro-Wilk's test ($p > 0.05$), and there were no outliers in the data, as assessed by Grubbs' test. The effect of the agonists on both resting force and developed force were assessed after 24 and 48 hours, as shown in Figure 14. To correct for differences in baseline measurements, we measured the change in resting force produced by each tissue, After the first 24 hours of treatment, ET-1 (ΔF_R 6.15±1.60 μN), Cocktail (ΔF_R 4.17±1.03 μN), and AngII (ΔF_R 4.01±1.09 μN) had the greatest change in resting force, while TGF-β (ΔF_R 1.32±0.77 μN) exhibited a similar change in resting force as the Untreated sample (ΔF_R 1.37±1.83 μN). In the second day of

hypertrophic factor treatment, the increase in resting force of all hypertrophic sample treatments (Cocktail: Δ F_R 1.24±1.42 μN; TGF-β: Δ F_R 0.87±1.76 μN; AngII: Δ F_R 1.30±3.11 μN; ET-1: Δ F_R 1.46±2.26 μN) was similar to the Untreated (Δ F_R 1.40±3.01 μN) sample (Figure 14B). The differences between the hypertrophic factors on the change in resting force was statistically significant, $F(8, 272) = 5.715$, $p < 0.001$. Follow-up univariate ANOVA shows that treatment after 24hours ($F(8, 54) = 4.947$, $p = 0.011$) was statistically significant between hypertrophic factors, but not after 48 hours ($F(2, 54) = 2.115$, $p = 0.131$). Statistical significance of a simple two-way interaction was accepted at a Bonferroni-adjusted alpha level of .025. Games-Howell post-hoc tests showed that for 24hour treatment, microtissues from AngII, ET-1 and Cocktail had statistically significantly higher mean change in resting force than Untreated ($p<0.05$). AngII, ET-1 and Cocktail were also statistically higher than TGF-β. However, there was no statistical significant between Ang II, ET-1 and Cocktail.

We measured twitch force generated after 24 and 48 hours of hypertrophic factor treatment (Figure 14C). Twitch force was recorded while microtissues were being electrically paced at 1hz using field electrodes as described in Chapter 2. We measured the change in force produced by each tissue, as described for resting force. The twitch force generated by these tissues was much smaller than the resting force. AngII and the Cocktail (Ang II: Δ F_R 1.52±0.50 μN, Cocktail: Δ F_R 1.81±0.46 μN) had the highest change in twitch force after 24hours of treatment for microtissues tethered to stiff pillars, while TGF-β had the lowest change (TGF-β: Δ F_R -1.75±0.35 μN). Tissues treated with ET-1, (Δ F_R 1.05±0.86 μN) were similar to Untreated sample (Δ F_R 1.01±0.49 μN). A second day of hypertrophic treatment, yielded a small change in twitch force among the samples compared to the first 24hours of treatment (Untreated: Δ F_R 0.06±1.55 μN; Cocktail: Δ F_R 0.16±0.57 μN; TGF-β: Δ F_R 0.35±1.04 μN; AngII: Δ F_R -0.20±2.02 μN;

ET-1: Δ F_R 0.25±1.31 μN). A one-way univariate ANOVA was conducted to compare the effect of hypertrophic factor treatment on twitch force of CMTs in TGF-β, AngII, ET-1 and Cocktail conditions after 24 and 48 hours of treatments. There was a significant effect of hypertrophic factor treatment on CMT contractility ($F(8, 224) = 7.618$ $p < 0.0001$,). Treatment after 24hours ($F(4, 112) = 18.376$, $p < 0.0005$) was statistically significant between hypertrophic factors, but not after 48 hours ($F(4, 112) = 0.499$, $p = 0.737$). Statistical significance of a simple two-way interaction was accepted at a Bonferroni-adjusted alpha level of p=0.025. Games-Howell post-hoc tests showed that for 24hour treatment, microtissues treated with Ang II (p=0.030) and Cocktail (p=0.022) had statistically significantly higher mean change in twitch force, while those treated with TGF-β (p=0.013) had statistically significant lower mean change in twitch force compared to the Untreated ($p<0.05$) samples. ET-1 treatment did not lead to significantly different twitch force changes compared to the Untreated (p=0.344), Ang II (p=0.483) and Cocktail (p=0.379).

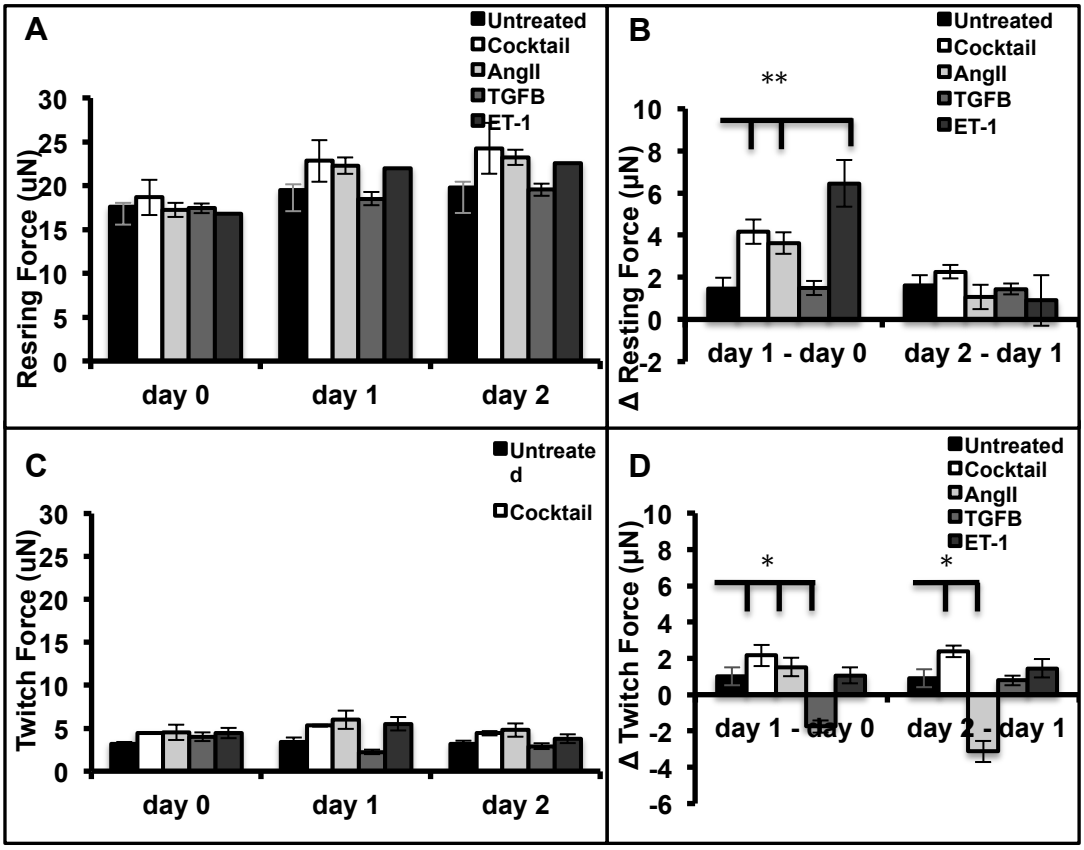

Figure 16. Resting and Twitch Force produced by CMTs after 24 and 48 hours of hypertrophic agonist treatment. After CMTs were formed and synchronously beating, baseline force measurements at day 0 were acquired. Brightfield images were used to calculate the resting force (A). To account for baseline force differences, we computed the change in resting force per tissue after 24 and 48 hours of treatment, and the average across multiple tissues (N=25) is represented by the bar graph above (B). Using a high-speed camera, we collected data of the displacement of the cantilevers over multiple contractions. The bar graph above represents the average peak twitch force for 3-5 contractions across multiple tissues (N=25) (C). Similarly to resting force, we computed the change in twitch force after 24 and 48 hours (D).

We performed a multivariate analysis to determine whether there was an interaction effect in the contractile response of cardiac microtissues to hypertrophic factors (AngII, TGF-β, ET-1, Cocktail) x Stiffness (0.20 μN/μm, 0.45 μN/μm) x length of treatment (24hours, 48hrs). We used the contractility data described in Chapter 2 on microtissues cultured in soft pillars. To calculate the expected additive response of load and hypertrophic factor for each condition, we used the difference between Untreated samples in soft and stiff ($\Delta F_{stiff-soft}$) as the value of contribution of load. We calculated the contribution of hypertrophic factor as the values of Force generated by the addition of a hypertrophic factor minus the baseline (force generated by the Untreated sample). We then added the effect of adding a hypertrophic factor from soft pillars to the "load factor". We performed a three-way mixed ANOVA to determine if there was an interaction effect among *stiffness x hypertrophic factor x time* in the resulting change in resting and twitch force (Data shown in Appendix 1A). Post-hoc pairwise comparisons revealed that stiff pillars in addition to the of the ET-1 ($p<0.0001$) and AngII ($p=0.003$) treatments resulted in a statistically significant response in change in resting force after the first 24 hours, but not after 48 hours of treatment as compared to the soft pillars. Furthermore our analysis revealed that addition of TGF-β ($p<0.0001$) or AngII ($p=0.007$) resulted in a synergistic response in the change in twitch force after the first 24 hours compared to soft pillars. (Further details are presented in Appendix 1A).

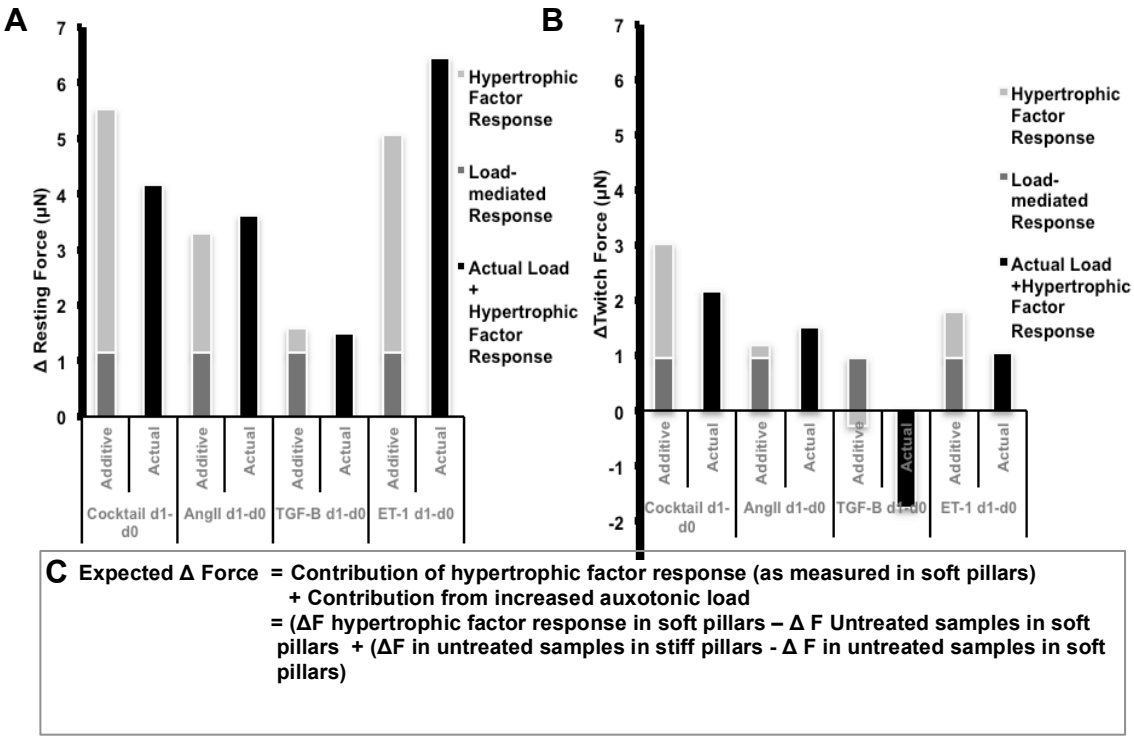

Figure 17. Calculation of expected additive response of load and hypertrophic factor effects. We estimated the expected additive response of hypertrophic factor treatment in change in resting (A) and twitch force (B), by first calculating the contribution of load (Untreated samples : load contribution = $\Delta F_{stiff\ -soft)}$. We calculated the contribution of hypertrophic factor as the values of Force generated by the addition of a hypertrophic factor minus the baseline (force generated by the Untreated sample). We added these two factors to get to the expected additive response (C).

3.3.2 *Effects of ET-1, TGF-β, Ang II alone and in combination, in contractile kinetics*

While the strength contraction of cardiac tissue is important, the kinetics of the contraction and relaxation are also an essential determinant of cardiac performance. As described in Section 2.3.5 we looked at the following metrics: V_{max} Contraction V_{max} Relaxation, and ratio of V_{max}Relaxation /V_{max} Contraction. As we observed the greater changes in force in the 24 hours of hypertrophic agonist treatment, we further evaluated the kinetic contractile profile in these first 24 hours. We observed that the V_{max} Contraction of the Ang II ($V_{maxday0}$= 48.66 ±7.89μm/s vs. $V_{maxday1}$= 58.16±8.88 μm/s, p<0.005), ET-1($V_{max\ day0}$= 47.95±4.38 μm/s vs. $V_{max\ day1}$= 68.41±5.68.11μm/s, p<0.005) and Cocktail ($V_{maxday0}$ = 44.55±1.55μm/s vs. $V_{maxday1}$ = 57.74±1.52μm/s, p<0.005) treatments were significantly increased after 24 hours (Figure 16A). However, for the Untreated ($V_{max\ day0}$ = 49.20±7.62 μm/s vs. $V_{max\ day1}$= 44.56± 7.62μm/s) and TGF-β ($V_{maxday0}$ = 46.82±3.29μm/s vs. $V_{maxday1}$= 32.44±2.14μm/s) the V_{max} Contraction decreased, but was not statistically significant (Figure 18A).

Similarly, for V_{max} Relaxation of the Ang II ($V_{max\ day0}$ 35.77±8.46 μm/s vs. $V_{max\ day1}$ = 42.12±3.56 μm/s p<0.005), ET-1 ($V_{max\ day0}$ 32.52±1.75 μm/s vs. $V_{max\ day1}$ = 44.96± 3.81 μm/s p<0.005), and Cocktail ($V_{max\ day0}$ 35.29±1.43μm/s vs. $V_{max\ day1}$ = 48.45±1.44 μm/s p<0.005) treatments were significantly increased, while Untreated ($V_{max\ day0}$ 34.90±4.85 μm/s vs. $V_{maxday1}$ = 31.26±4.83μm/s) and TGF-β ($V_{maxday0}$ 32.43±3.37μm/s vs. $V_{max\ day1}$ = 23.48±1.49μm/s) did not show statistical significant differences when comparing to the values before hypertrophic agonist treatment.

Similar to the results in the soft pillars that we discussed in the Chapter 2, we observed no statistically significant changes between the ratio of V_{max}Relaxation /V_{max} Contraction in the Untreated sample and in samples that were treated with hypertrophic agonists for 24 hours. Furthermore, the ratios of V_{max}Relaxation /V_{max} Contraction were

similar across all samples. We did not observe any statistically significant change in this ratio, indicating, that the equilibrium between contraction and relaxation is maintained. Further statistical analysis is provided in Appendix 1.

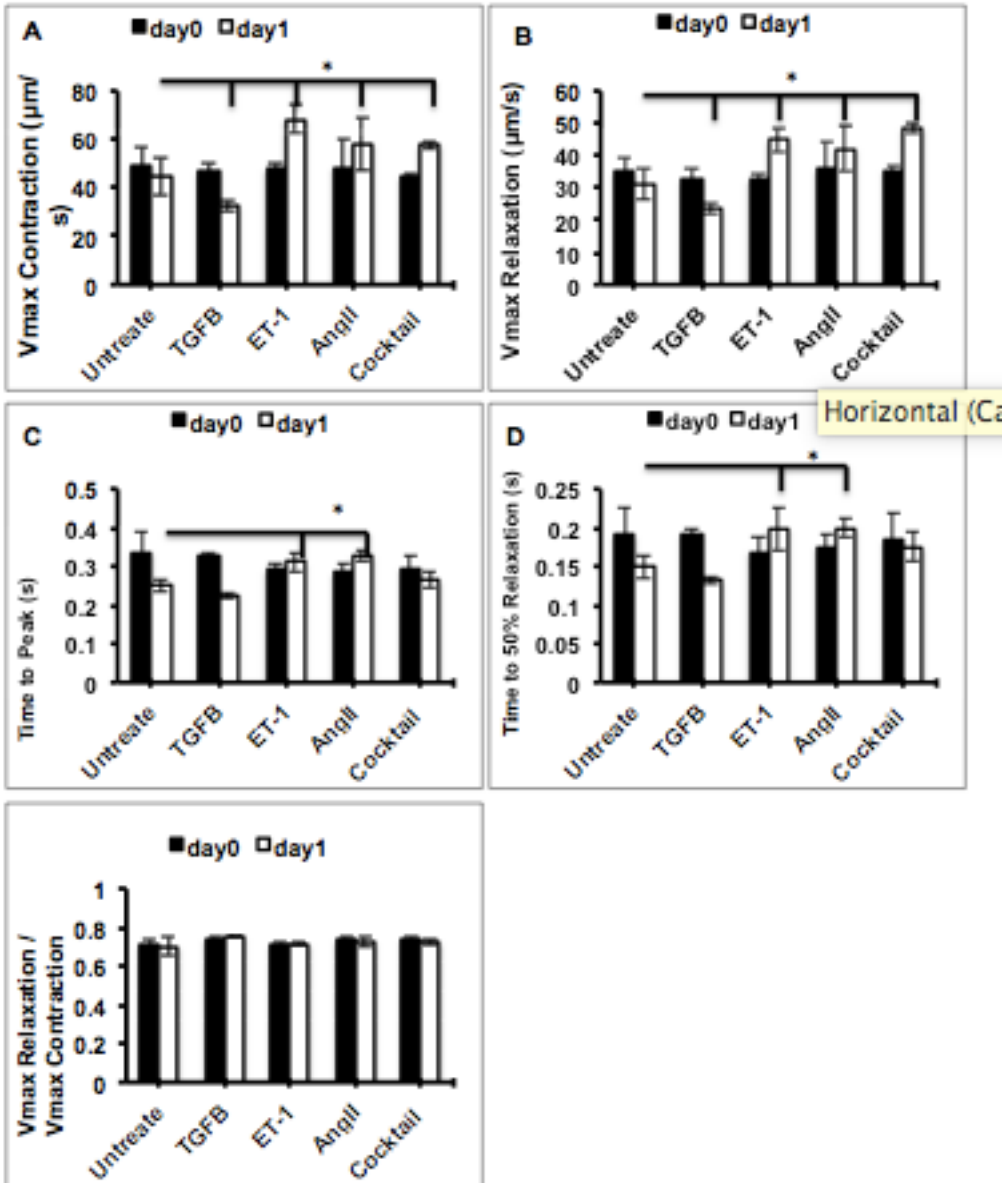

Figure 18. Contractile kinetics profile in CMTs after 24 hours of hypertrophic agonist treatments. Using a high-speed camera, we tracked the displacement of fluorescent beads atop of CMTs, and calculated kinetics of contractility. Bars represent the average of individual tissues velocities over 3-5 twitches. Maximum velocity of contraction (V_{max} Contraction) (A), V_{max} Relaxation (B), V_{avg} Contraction (C), V_{avg} Relaxation (D), V_{max}Relaxation /V_{max} Contraction (E) were calculated from the data. ANOVA was used to determine differences between groups at day 0 and at day 1; * denotes $p<0.05$.

3.3.3 *Power of contraction and relaxation measurements after 24 hours of hypertrophic agonist treatment*

Twitch power is calculated as previously described in Chapter 2. Briefly, we refer to Pmax of Contraction as the maximum value of the twitch power in the contraction phase, before it reduces back down to zero. Pmax of Relaxation is the twitch power reaches a minimum (maximum negative) value of power, before it rises back up to zero. We found that maximum power was exerted after the time at which maximum velocity is reached, where force tends to be fairly low and before the time peak force is exerted, as at that point velocity equals 0 at that instant. As shown in Figure 19A, we found that the tissues in the Untreated sample generated $P_{max\ day0}$ =183.95 vs. $P_{max\ day1}$ =166.82 however, tissues treated with ET-1 generated statistically significant increases in power after 24 hours of treatment ($P_{max\ day0}$ =201.74±42.81 vs. $P_{max\ day1}$ =431.19±84.32, $p<0.005$). Cocktail,($P_{max\ day0}$ =192.13±30.90 vs. $P_{max\ day1}$ =269.40±21.04, $p=0.023$), and Ang II (($P_{max\ day0}$ =203.76±33.59 vs. $P_{max\ day1}$ =238.26±46.35, $p=0.048$) had more moderate, but still significant increases in power after 24 hours of treatment. TGF-β on the other hand, caused a decrease in power generation in microtissues after 24 hours of treatment ($P_{max\ day0}$ =197.19±42.92 vs. $P_{max\ day1}$ =61.64±77.80).

Furthermore, we measured the generation of power of relaxation upon hypertrophic treatments (Figure 19B). The Untreated samples generated a moderate, but not significant increase in power generation ($P_{max\ day0}$ =76.61 vs. $P_{max\ day1}$ =82.90) while ET-1($P_{max\ day0}$ 77.52 vs. $P_{max\ day1}$ =246.67, $p<0.0001$) generated the largest and statistically significant increase in power generation. Ang-II ($P_{max\ day0}$ 76.41 vs. $P_{max\ day1}$ =106.82, $p=0.040$) and the Cocktail ($P_{max\ day0}$ 82.96 vs. $P_{max\ day1}$ =134.97, $p=0.033$)

generated more moderate increases in power of relaxation after 24 hours of treatment. Similarly, to the generation of power of contraction, treatment of TGF-β ($P_{max\ day0}$ 77.08 vs. $P_{max\ day1}$ =26.96) also led to a decrease in power of relaxation.

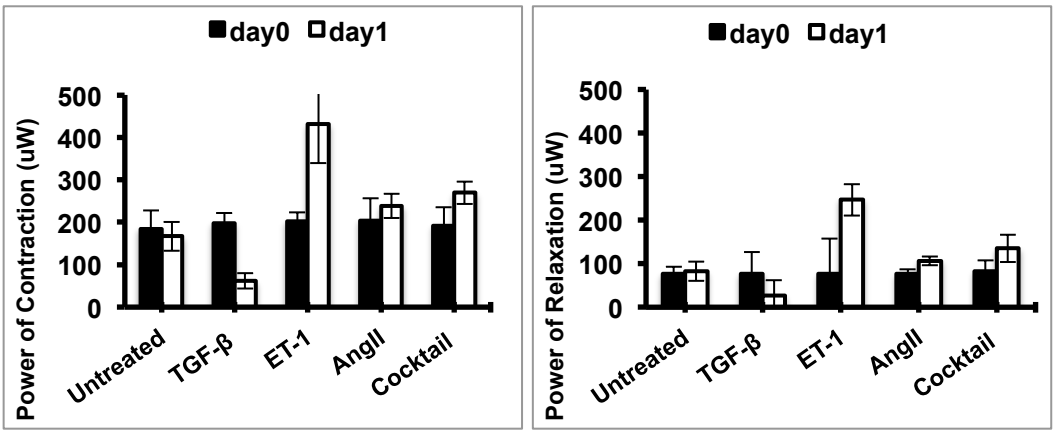

Figure 19. Power of contraction and relaxation after 24 hours of hypertrophic agonist treatment. Using a high-speed camera, we tracked the displacement of fluorescent beads atop of CMTs, and calculated kinetics of contractility. Bars represent average of maximum power over 3-5 twitches across multiple tissues. Measurements of maximum power of contraction (A), maximum power of relaxation (B) were obtained. Student's t-test was used to compare between day0 and day1; * denotes $p<0.05$ and ** denotes $p<0.005$.

3.3.4 *Effects of AngII, ET-1 and TGF-β alone and in combination, in sarcomere length*

To understand how sarcomere length correlated with microtissue force and velocity in our auxotonic preparation, we fixed the samples after 24 hours of stimulation and stained with α-actinin (ABCAM) as described in Section 2.2.8. We only included sarcomere lengths with variance less than 0.2μm. As shown in Figure 20, we found that the resting length of the sarcomere for the ET-1 and AngII treatments after 24 hours resulted in significant differences in sarcomere length 1.85 ± 0.03μm $p<0.05$ and 1.86 ±

0.03μm ($p<0.0001$) respectively, compared to 1.74 ± 0.02μm in the Untreated sample. The TGF-β treatment resulted in a decrease in sarcomere length, resulting in sarcomere length of 1.69 ± 0.02μm $p<0.05$. The Cocktail treatment however, did not exhibit significant differences as compared to the Untreated (1.79 ± 0.02μm vs. 1.74 ± 0.02μm).

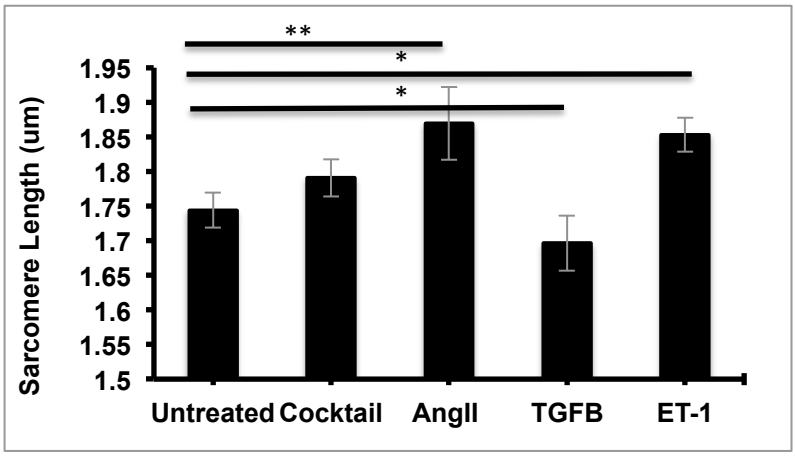

Figure 20. Resting sarcomere length in microtissues tethered to stiff pillars. Immunofluorescent images of microtissues attached to cantilevers stained with a-actinin were used to detect sarcomeres and measure sarcomere length (as described in 2.3.4). Our results show that sarcomere length is lower in stiff pillars than in soft pillars. Microtissues treated with AngII and ET-1 had statistically significant increases in sarcomere length, while those treated with TGF-β had statistically significant reduction in sarcomere length. Student's t-test was used to compare between an agonist treatment and the Untreated sample; * denotes $p<0.05$ and ** denotes $p<0.005$

3.3.5 *Effects of AngII, ET-1 and TGF-β alone and in combination, in cell and tissue size*

Hypertrophic remodeling in the heart is characterized by morphological changes including cell and tissue enlargement. To examine the effects of hypertrophic agonists on cell size within the microtissues, we compared the effect of both hypertrophic growth factor and afterload enhancement (microtissues tethered to stiff pillars) on cell size. We stained the plasma membrane of cells and measurements were performed as described in Figure 21A-B. For microtissues tethered to soft cantilevers, post -hoc

analysis using Games-Howell revealed that there were no statistically significant changes (Figure 21C) in cell size with hypertrophic factors (Cocktail: A_{C20}= 194.94± 11.93μm^2, p=0.152; Ang II: A_{A20}= 189.82 ± 8.32μm^2,p=0.102; TGF-β: A_{T20}=175.46 ± 15.02μm^2, p=0.894; ET-1; A_{E20}=181.34 ±13.55μm^2), p=0.097) compared with the Untreated sample (Untreated: A_{U20}=177.67 ± 12.62μm^2). For microtissues tethered to stiff cantilevers, AngII, Cocktail and ET-1 (A_{C10}=226.67± 7.53μm^2, p=0.020; A_{A10}=245.22± 9.55μm^2, p<0.0001; A_{E10}=231.95± 8.94μm^2, p=0.020) each significantly increased cell size compared the Untreated microtissues (A_{10T}=214.47± 14.54μm^2). TGF-β had no statistically significant change in cell size compared to the, Untreated microtissues p=0.250). However, we carried out a Two-Way ANOVA and found no synergistic interaction between factor and stiffness.

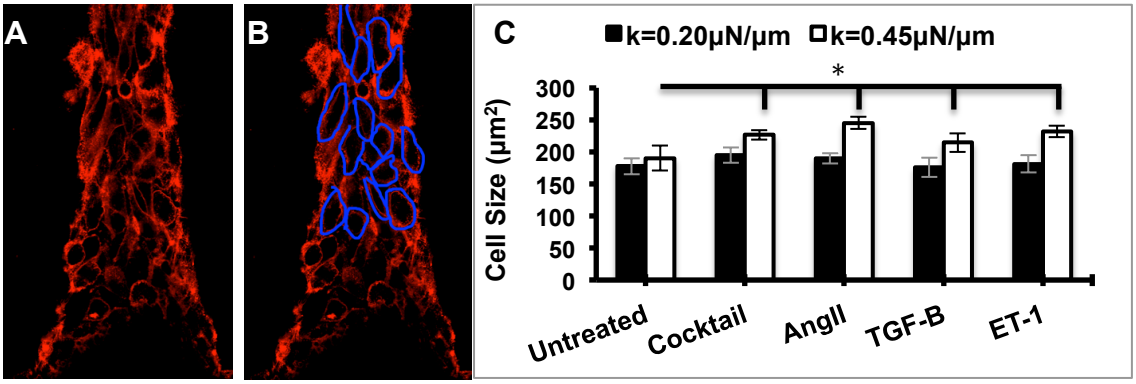

Figure 21. Cell membrane staining in situ, and assessment of average cardiomyocyte size in CMTs. Flourescent image of cell membrane staining with (Cell Mask Orange) (A). Deliniation of cell membrane to calculate areas of cells embedded in the microtissues (B). Assessment of cross-sectional areas of cells within CMTs after hypertrophic interventions in soft and stiff pillars (C). Scale bar indicates 50 μm.

Additionally, we measured tissue volume by estimating it to be a cylindrical ellipse using the equation V = πW*L*H/4 (Figure 21 A-C). We measured the cross-sectional area of each tissue and multiplied by the length of the tissue (Figure 21 D). In soft pillars, We observed 2.45x increase in volume in the microtissues treated with the Cocktail (V_{C20}= 1.20 ±0.36 x10^{-3} mm^3, p= p<0.0001) (Figure 21E), 2x smaller with AngII, (V_{A20}= -0.83±0.63 x10^{-3} mm^3, p=0.004), with TGF-β**,** 4x smaller (V_{T20}= -1.98±0.22 x10^{-3} mm^3, p=0.001), 1.5x increase (V_{E20}= 0.72 ±0.34x10^{-3} mm^3, p<0.0001) compared to the Untreated (V_{U20}= -0.49±0.24 x10^{-3} mm^3). In the stiff pillars, AngII treatment resulted in 0.20x larger (V_{A10}=-0.64± 0.21 x10^{-3} mm^3, p=0.043); TGF-β , 3.4x smaller (V_{T10}=-2.67±0.27 x10^{-3} mm^3, p<0.001), ET-1, .25x larger (V_{E10}=-0.59±0.54 x10^{-3} mm^3, p=0.001), the Cocktail, 3.42x larger (V_{C10}=1.11±0.46 x 10^{-3} mm^3, p=0.028) compared to the Untreated (V_{U10}=-0.78±0.30x10^{-3} mm^3).

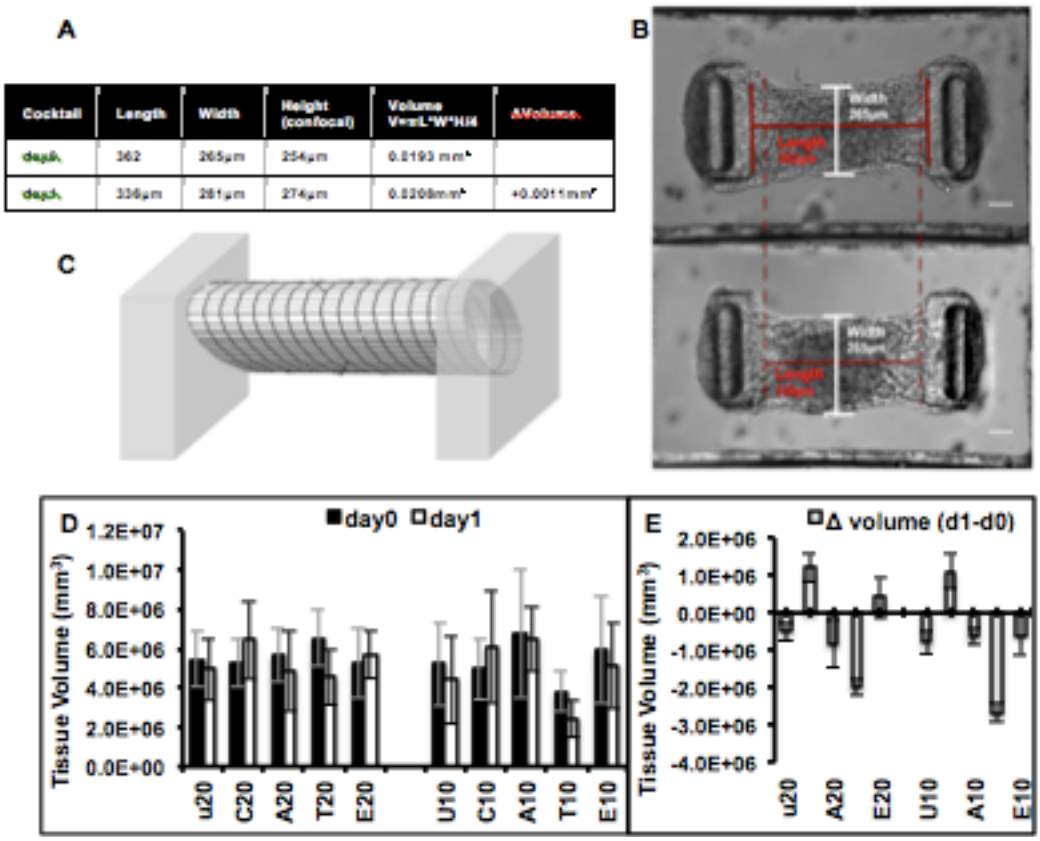

Figure 22. Microtissue volume after 24 hours of hypertrophic factors treatment in microtissue tethered in soft and stiff pillars. Data table shows an example of the measurements and calculations of microtissue volume (A) for a microtissue treated with the Cocktail treatment, as shown in (B). Diagram shows model used to estimate microtissue volume from Brightfield images (C). Baseline and 24 hour treatment measurements of microtissue volume (D). Change in microtissue volume after 24 hours of hypertrophic factor treatment (E). Scale bar indicates 50μm.

3.3.6 Effects of AngII, ET-1 and TGF-β alone and in combination, in gene expression

The changes in contractility upon hypertrophic factor stimulation led us to investigate gene expression associated with cardiac remodeling. Fibrosis is a hallmark of pathological cardiac remodeling. Fibrosis signals including collagen-1, collagen-3 expression in fibroblasts are augmented during pathological cardiac remodeling. In CMTs, transcript concentration of the collagen-1 was increased by all treatments compared to the Untreated samples (referred to as '20N' in the graph below) in soft cantilevers (our control), but particularly by ET-1 (20E: 2.6x) and Cocktail (20C: 2.5x). For collagen-3, the Untreated (10N: 3x) and Ang II (10A: 2.25x) samples of microtissues tethered to stiff cantilevers resulted in the highest fold change. Additionally, α-Smooth Muscle (α-SMA) is a characteristic marker of fibroblasts-to-myofibroblast transition in the fibrotic heart. We see increases in α-SMA expression for all treatments compared to the Untreated sample tethered to soft pillars (20N). In particular the (3.5x) Cocktail (20C) and (3.1x) ET-1 treatment (20E) in the soft cantilevers as well as the Ang II and Cocktail in stiff cantilevers, result in large increases in α-SMA. Furthermore, in myocardial hypertrophy, the re-expression of fetal actin isoforms, including the sarcomeric skeletal actin (SKA). Increased SKA expression represents a well-accepted marker for cardiac hypertrophy in different animal species and humans, during hemodynamic overload, passive stretch and TGF-β stimulation (Schaub et al., 1997; van Bilsen and Chien, 1993, Eppenberger-Eberhardt et al., 1990).. Our results show that SKA is upregulated upon treatment of hypertrophic factors, particularly when the microtissues are tethered to stiff cantilevers (10N: 1.71x , 10C: 1.89x, 10T: 1.37x, 10A:1.74x, 10E:1.66x) compared to our control.

We measured βMHC and αMHC expression, and the ratio of the two. We observed an increase in power generated by microtisssues. A higher

ratio of αMHC to βMHC, which correlates with what is observed in initial adaptive responses to hypertrophic factors, where the α-MHC (fast isoform) is actually higher than the β-MHC (slow isoform) isoform. In terms of mechanical power, which is a product of the developed force and the velocity of shortening, it has been previously shown that higher expression of α-MHC correlated to higher power produced by microtissues (Gupta MP 2007, Herron TJ and McDonald KS 2002). Our results show (Figure 19A-B) that all of our treatments were correlated with higher α-MHC expression than β-MHC leading to a higher *α-MHC* /β-MHC ratio. However, the highest ratio of *α-MHC* /β-MHC was observed in samples were microtissues tethered to soft pillars were treated with ET-1 (2.70x).

Lastly, we measured the expression of atrial natriuretic protein (ANP) gene, a classical marker of hypertrophy. Similar to above, all of our samples resulted in increases of ANP expression, however, Ang II (20A: 3.25x) in soft pillars as well as the Cocktail (10C:3.75x) and ET-1 (10E: 4x) in stiff pillars, resulted in the highest expression of ANP.

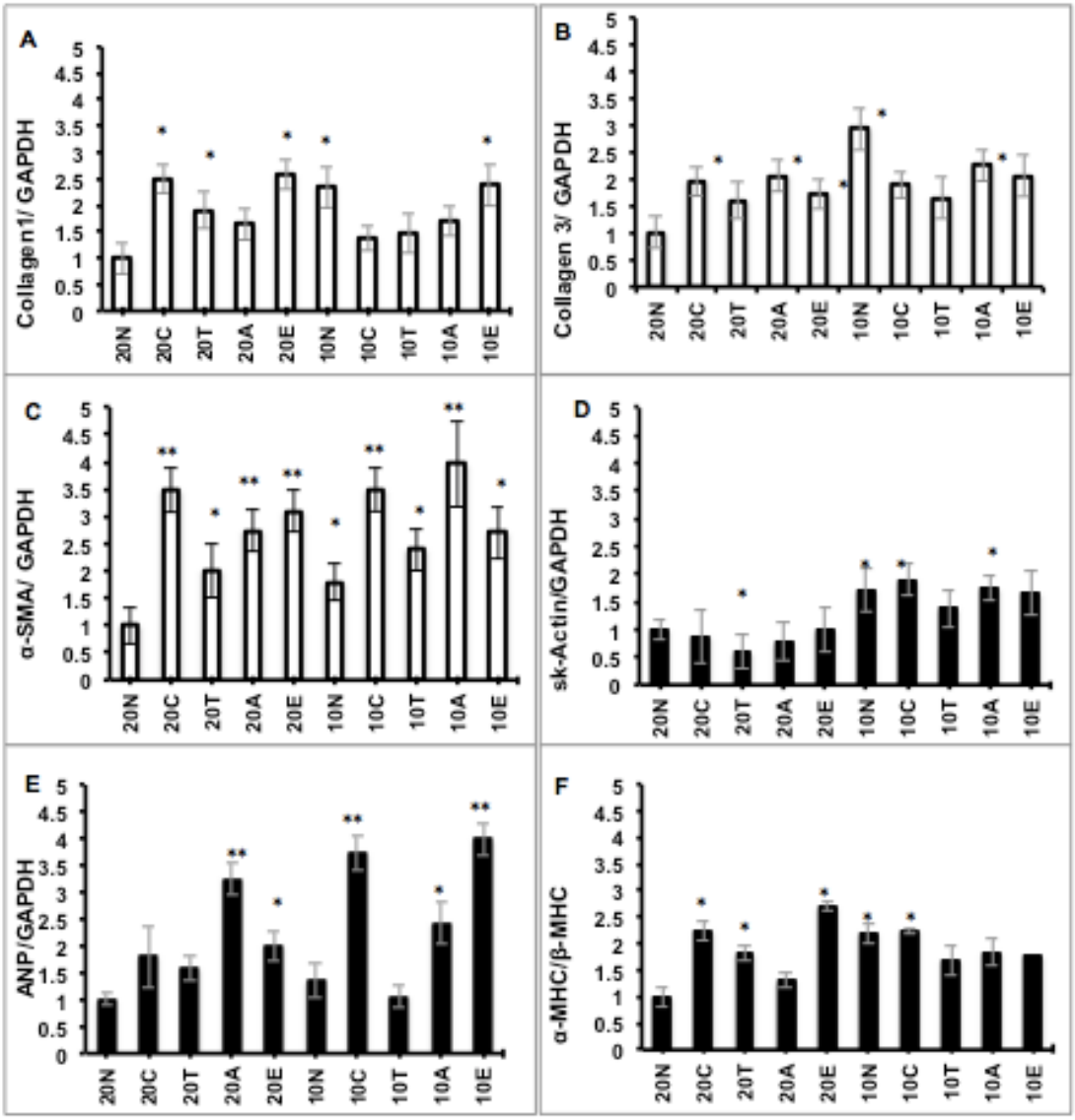

Figure 23. Gene expression responses to hypertrophic factors relative to the Untreated sample in soft cantilevers. In the graphs above, treatments are denotes as the following: Cocktail as 'C', TGF-β as 'T', AngII 'A' and ET-1 as 'E', stiffness is denoted by PDMS concentration, namely '20' for soft pillars made with 20-1 PDMS-to-curing base concentration, and '10' for stiff cantilevers made with 10-1 PDMS-to-curing base concentration. collagen 1 (A), collagen 3 (B), alpha smooth muscle actin (αSMA) (C), skeletal actin (D) ANP (E), and ratio of α-MHC to β-MHC (F), expression were measured in all microtissue samples. * denotes $p<0.05$ and ** denotes $p<0.005$

3.4 Discussion

This study provides a multivariate assessment of the effects of hypertrophic agonists AngII, TGF-β, and ET-1 alone and in combination, with length of treatment and stiffness on forcefulness and kinetics of contractility, sarcomere length, cell size, tissue width, and hypertrophic gene expression in engineered cardiac microtissues. Our studies revealed that the stiffness, hypertrophic factor stimulation and length of exposure has an effect in both resting and twitch force, as well as on kinetic parameters, such as V_{max} contraction, V_{max} relaxation, Time to peak and Time to reach 50% relaxation. Additionally, hypertrophic treatment led to structural changes in microtissues. Lastly, gene expression associated with hypertrophy and fibrosis was increased upon stimulation of hypertrophic factors.

Further analysis into the effect between stiffness, hypertrophic factor stimulation and length of exposure in resting force revealed a statistically significant effect of ET-1, AngII and Cocktail treatments after 24 hours. Multivariate analysis revealed that AngII and TGF-β, in particular, have a statistically significant interaction with stiffness on their effect on twitch force generation. Previous work revealed a relationship between AngII and stiffness in the form of stretch in *in vitro* studies and pressure overload models in *in vivo* studies. However, it wasn't clear if stiffness could provide a synergistic response. The increase in contractility could potentially be related to load-mediated activation of angiotensin type 1a receptor (AT1aR), which consequently leads to an enhanced AngII effect upon addition of this hypertrophic factor (Horton RE et al. 2016). Further investigation of AT1aR expression in our tissue model could provide additional insights into the mechanism of this synergy in our model system. Additionally, AngII resulted in a statistically significant increase in forcefulness of contraction, which is a characteristic of the initial adaptive response in load-mediated hypertrophy models (Emdad L et al.

2001). Further work could identify mechanical effectors downstream of this synergistic response and provide insights into the mechanisms of this response on the synergistic effect in forcefulness of contraction, which could prove useful for therapeutic studies.

We also observed diminished contractile kinetics, in particular reduced V_{max} of Contraction and Relaxation. While inherent variation of isolated neonatal rat ventricular myocytes could lead to variations in kinetic parameters, we carried out paired contractile analysis in stiff and soft arrays of tissues engineered from cells from the same isolation. A slower velocity generation has been characterized in tissues that are able to produce a larger force to pull on the stiffer pillars in previous studies (Edmund Sonnenblick 1982). Other work in single cells has shown that the rate of contraction is largest in the absence of any applied stress, monotonically decreases with increasing tensile stress, and eventually vanishes when the applied stress equals the stall stress. This was recently observed in cardiac microtissues, where microtissues contracted with smaller speeds when subject to increasing force (Wang H et al. 2013).

Furthermore, we studied the interaction of hypertrophic factor and increased afterload in sarcomere length. Sarcomere lengths of myocytes in microtissues tethered to stiff pillars were lower than in the sarcomere lengths of myocytes in softer pillars. Shorter sarcomere lengths have been associated with increased afterload in response to increased sarcomereogenesis. A recent study demonstrated that sarcomerogenesis is upregulated in myocytes cultured on stiff gels (McCain ML et al. 2014). However other reports have suggested that sarcomere structures are optimized on gels with physiological elasticity (Jacot JG 2008). Another factor to consider is the fibroblast effects on sarcomere length myocyte. Mechanical load has been known to be associated with fibroblast proliferation and differentiation to myofibroblasts. It is possible that upon increased load stimulation, myofibroblast population increases and leads to a

diminishing effect on contractility. Further work, looking at myofibroblast quantitation and increased matrix levels as well as matrix stiffness could provide insights into the effect of these factors on contractility. Further studies looking at sarcomereogenesis and fibroblast number and interaction with myocytes in microtissues exposed to higher afterloads would provide insights to further understand changes in sarcomere length.

Morphological changes after hypertrophic treatment of AngII, Cocktail and ET-1 demonstrated statistically significant increases in cell size in stiff pillars, but not in soft pillars. Studies performed *in vitro* in 2D cell culture systems have previously shown that myocytes increase in size in response to these factors, irrespective of mechanical load (static stretch). One challenge with these cell culture substrates is that cells are exposed to the stiffness of the plate, and thus makes it harder to distinguish between the load-mediated effects and the hypertrophic factor effects. A recent study using engineered tissues that were not exposed to load reported no cell size or tissue thickness difference in response to Ang II (Horton RE et al. 2016), while observing changes in contractility. Therefore it is possible that cell area changes observed in 2D culture systems are due to the increased load. Auxotonically-loaded engineered tissues model overcomes challenges related to dimensionality and culture substrate stiffness that confound traditional cell culture systems.

Interestingly, while cells in microtissues resulted in increased cell area, microtissue changes in volume were reduced in microtissues exposed to increased afterloads. In a recent report (Wang H et al. 2013) looking at microtissue morphology when exposed to higher loads, it was reported that increased load led to increased remodeling and compaction of the matrix by the cells and a steady reduction of construct size (Wang H et al. 2013). Therefore it is possible that while we do not observe larger changes in tissue width as in soft pillars, AngII, ET-1 and the Cocktail leads to a

reduction of the inherent thinning that is observed in microtissues tethered to stiff pillars. Additionally, the authors report that thinning occurs as part of an elastic deformation that is volume-conserving. In other words, while changes in length, height and width of microtissues occur result in a null change in volume. On the other hand, our results suggest that hypertrophic growth factor could lead to inelastic volume deformations in our microtissues. A limitation of these comparisons is that Wang et al. estimated volume changes using a dumbbell model to estimate tissue volume, and report that when the tissue gets thinner in the middle while areas around the posts get larger (hence forming a dumbbell shape). Furthermore, it is possible that there is a cell dropout that contributes to larger cell size without increasing tissue volume. Our results, as we can see in Figure 19B, did not lead to enlargement of tissues around the areas of the posts. Further studies with direct volume measurements should provide insights on whether changes in microtissue volume that we are elastic or inelastic.

In addition to contractile and morphological changes in response to load and hypertrophic factors, we observed increased expression of genes associated with cardiac remodeling, such as ANP, Collagens 1 and 3, skeletal actin and alpha smooth muscle actin. Afterload enhancement in our microtissues results in increased expression of skeletal actin and alpha smooth muscle actin. Interestingly, we did not observe the myosin heavy chain switching that is typically observed upon exposure to hypertrophic stimulants, such as load and hypertrophic factors. It has been reported that early after hypertrophic stimulation, an initial adaptive enhancement of contractile function is observed, and upon persistent activation of hypertrophic factors decrease in cardiac contractility ensues (Mann DL et al. 2005). Because we focus on the first 24 hours of treatment, we may be observing this enhanced contractile output, which is related to higher αMHC levels than βMHC. Higher αMHC values and lower βMHC values

are correlated with higher power generation by cardiac tissue (Gupta MP 2007, Herron TJ and McDonald KS 2002), which we observed in our model. Further studies evaluating longer exposures to hypertrophic factor treatment as well as increased afterload, could provide more information regarding whether our tissue can undergo that isoform switch that occurs in hypertrophic models in vivo as well as in passive stretch 2D models in vitro.

Changes in mechanical load lead to structural and functional phenotype changes in our microtissue model. Our results demonstrate that engineered cardiac constructs could provide a platform for studying *in vitro* effects of complex stimuli, including biochemical and load enhancement, that occur *in vivo*. Our data shows that we are able to de-couple and couple biochemical, in other words, hypertrophic factor stimulation and increased auxotonic load. We observed an increase in cell size occurred only in the presence of load and hypertrophic factor. In standard 2D flat culture in plastic substrates, the hypertrophic factor-mediated effects are hard to distinguish from the load-mediated effects. . Further refinements to our model should include the ability to increase load post tissue formation, as well as evaluated a graded effect of loading. These constructs can serve as a model system to improve our basic understanding of cardiac mechanical remodeling and identify underlying mechanisms that can potentially be exploited to improve mechanical remodeling in the heart.

3.5 Limitations

A limitation of this study was that the sarcomere measurements of myocytes in tissues tethered to soft and stiff cantilevers were not done in parallel, though the same procedure and reagents were used in both analyses. Furthermore, paired measurements of microtissue contractility and sarcomere length were not performed. Further work should be conducted in parallel to avoid potential confounders of experimental variability.

Additionally, we did not observe large enhancement on twitch force with the addition of load to the stimulation with different hypertrophic factors. Further work should explore whether large resting forces affect the twitch force generation. Incrementally dosing the load would also be valuable to determine if there is a graded effect in loading, going beyond the maximum value of load added in our experiments.

Furthermore, it is possible that enhanced load leads to activation of other factors in the sample, complicating the interpretation of the effects of each factor. It is also possible that some factors are more sensitive to load than others. Studies are needed that neutralize the effects of the factors not being studied, such as with neutralizing antibodies for the receptors of the hypertrophic factors, to isolate the effects of each factor being studied. Increased load effects can also be better studied this way.

While our studies focused on short-term responses of hypertrophic factors and load, it is possible that the effects of load take a longer time to manifest themselves. Longer studies may provide additional insights on the effects of hypertrophic factors long term, which are difficult to extrapolate from our data. AngII resulted in a statistically significant increase in forcefulness of contraction, which is a characteristic of the initial adaptive response in load-mediated hypertrophy models (Sadoshima J et al. 1993). However, TGF-β led to a diminished contractile response. Previous studies have shown

that TGF-β mediates the AngII transition (Schultz J et al. 2002) from adaptive enhanced to a subsequent caontractile dysfunction step in cardiac hypertrophic remodeling. However, our experiments were performed over 48 hours, therefore longer experiments are needed to determine if these changes are also reflective of the pathophysiological changes that occur weeks, months, or years down the road. Previous work demonstrated that TGF-β, (1) acts downstream of AngII, and (2) mediates AngII hypertrophic effects. Further work could identify mechanical effectors downstream of this synergistic response and provide insights into the mechanisms of this response on the synergistic effect in forcefulness of contraction, which could prove useful for therapeutic studies.

Additionally we measured tissue volume indirectly, by measuring the center of the tissue. Future studies should consider measuring volume directly by measuring widths throughout the length of the tissue. Cell dropout, which contributes to larger cell size without correspondingly greater tissue volume (Anversa P et al. 1986), also needs to be evaluated. This phenomenon could also explain disproportionate increases in resting force compared with twitch force.

CHAPTER 4: CELL-SPECIFIC CONTRIBUTIONS TO AUXOTONIC CONTRACTILITY IN CMTs

4.1 Rationale

Engineered cardiac microtissues (CMTs) provide a model for mechanistic studies with the potential to better understand of the interplay of cardiac cells in cardiac remodeling. Determining how nonmyocytes contribute to myocardial mechanical responses has proven difficult. In vivo, fibroblasts (CF) are buried within densely packed myocytes (CMs) making a direct investigation and quantification *in situ* extremely difficult. As the associated clinical picture of fibrosis represents a serious challenge in medical treatment, garnering a deeper understanding of the interplay between nonmyocytes and cardiomyocytes is pivotal to improve therapeutic methods for patients with myocardial infarction. Previous studies have demonstrated that engineered tissues made with a native heart cell population compared to myocyte-enriched (or nonmyocyte depleted) cell populations generated improved resting (diastolic) and twitch (systolic) force. (Nichol JW et al. 2012). Assessment of native neonatal heart cell populations has revealed that myocytes usually account for 45-55% of the cells while nonmyocytes account for 50-65% (Chlopcíková S et al.2011). Of the nonmyocyte population, studies have shown that more ~70% of the nonmyocyte population is made up of fibroblasts (Chlopcíková S et al.2011) While the native heart population may display higher contractile forces than the myocyte-enriched tissues, the ability to create tissues with different cell populations offers an opportunity to determine cell-specific responses in engineered tissues.

Our previous work using the native heart cell mix demonstrated that ET-1 resulted in increased twitch force, increased resting force (shorter tissue length) and longer resting sarcomere lengths compared to other hypertrophic factors such as TGF-β

and Ang II (Chapter 2). Interestingly, the sarcomere length of myocytes in shorter tissues with higher twitch force was longer than in longer, less active tissues. In other words, there was the expected positive correlation between sarcomere length and twitch force generation irrespective of the overall length of the engineered tissue. This led us to speculate that the resting force and thus, length of microtissues, is regulated by nonmyocytes in auxotonically-loaded microtissues engineered with a native heart cell population. We hypothesized that depleting nonmyocytes from microtissues to create myocyte-enriched microtissues, would produce lower resting force and increased tissue length. We first sought to understand the role of nonmyocytes in contractile responses, including resting and twitch force generation, kinetics and sarcomere length. We generated tissues with the native heart mix population (Chapter 2) ~50%CMs:50%CFs, tissues with intermediate ,myocyte enrichment with ~83%CM:17%CF, and tissues that contained mostly myocytes 93%CM:7%CF. Furthermore we investigated how myocyte-enriched tissues responded to ET-1 treatment. Building microtissues with varying proportions of cardiac cells is critical to understanding the role of myocytes and nonmyocytes in the contractility profile, including resting force and twitch forces, kinetics and sarcomere length, length-tension relationship, of CMTs in 3D.

4.2 Materials and Methods

4.2.1 *Cell isolation and contractility measurements*

Briefly, neonatal rat ventricular cells (NVRC) were isolated from 1 to 2 day-old neonatal Sprague-Dawley rats as previously described in Section 2.1. The μTUG devices were made using a PDMS to cross-linker ratio of 20:1, which yields a stiffness of [0.20μN/μm]. Cell culture medium was changed daily. Mechanical and kinetic measurements, as well as sarcomere length measurements were performed as

described in section 2.2.3 and 2.2.5, respectively.

4.2.2 *Flow Cytometry methods for sorting cardiac cells*

The cells were pre-plated onto multiple T-75 flasks for 1 hour to allow fibroblasts to attach to the dishes. Cardiomyocytes still suspended in the media were retained and seeded onto a T-75 flask coated with fibronectin. Cells were washed using 1x PBS and growth media was changed the next day at least three hours prior to the staining protocol. After cells were incubated for at least 3 hours with fresh media, 500ng/ml of Tetramethylrhodamine methyl ester perchlorate (TMRM) (ThermoFisher) in DMEM 3:1 M199, 1%HEPES, 1%Glutamax, 1%insulin, 1%Antibiotic-antimycotic was added and incubated at 37°C for 30 minutes. After incubation, cells were washed with 1X PBS and dissociated with a 500ng/ml TMRM in 0.05% trypsin solution for 3 minutes. Trypsin was deactivated with DTI and cells were spun down for 5 minutes at 1000 rpm. The cells were re-suspended in 1%BSA DMEM and DAPI to get 5-8x10^6 cells/ml. Cell solution was filtered (40μm filter) and added to a tube with 5 ml of media. Cells were sorted using the BD FACS Aria II SORP.

After excluding cell fragments and aggregates (Figure 24A) along with dead cells (DAPI+) (Figure 24B) gating was based on TMRM fluorescence (Figure 24C), employed to identify the myocyte enriched population based on mitochondrial size as previously described (Hattori F et al. 2010, Nguyen PD et al. 2012, Rachel Truitt, unpublished data). The TMRM- population was considered to be mostly nonmyocytes. Myocyte number in the TMRM+ population was confirmed with Troponin staining, which yielded 93% ± 3% Troponin+ cells (Figure 24D). The viability of the cells was assessed using Trypan blue dye that revealed 93% viability in the TMRM+ population (Figure 24D).

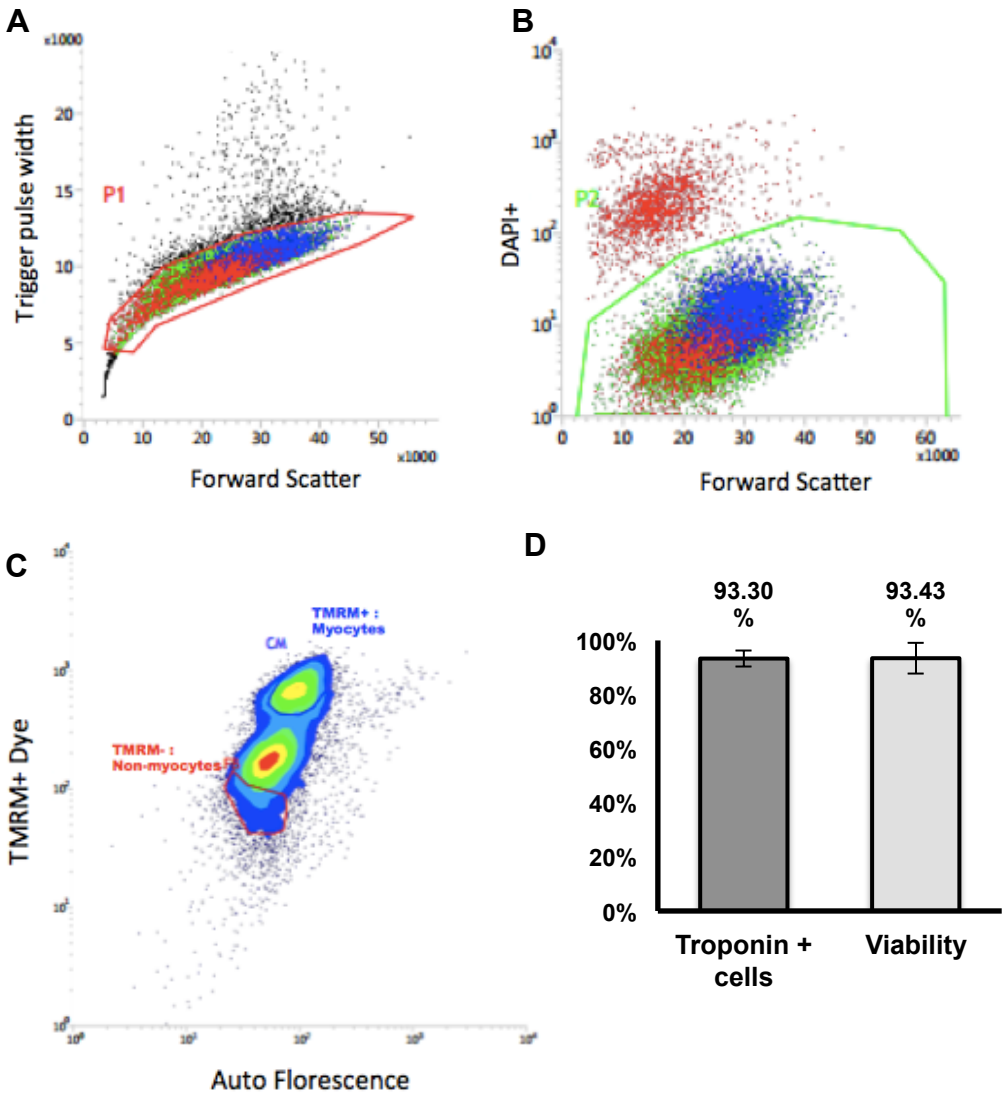

Figure 24. Serial Gating to sort viable TMRM+ myocytes from an NVRC isolation. The sample was serially gated to isolate the population of viable myocytes. Large aggregates were excluded (A). DAPI+ cells were excluded as dead (B). TMRM positivity was used to isolate myocytes from the native neonatal heart population. Further antibodies staining revealed a high myocyte purity and viability in the TMRM+ sample. Data from a representative native heart cell population is shown in this figure.

4.2.3 Microtissue seeding of sorted cells

Three different cell populations were created with the same number of cells. The native heart cell population, which we call Native (~50%CM: 50%CF) was generated as described previously in section 2.2.1. Tissues were made with intermediate number of fibroblasts, which we call CM+ samples (~83%CM: 17%NM). Basically, 10% of the cell population was added from the TMRM-1 (sorted as described above in 4.2.2), and 90% of the TMRM+ CM++ population (93%CM: 7%NM). Lastly, we created a myocyte-enriched population, which we call CM++ that contained the TMRM+ population that we sorted as described above in 4.2.2. (93%CM:7%CF). All of the experiments were performed paired, with cardiac cells from the same cell isolation to account for potential variations in contractility between isolations.

Contractile measurements on the tissues were performed on the same day for all arrays. However, because different proportions of fibroblasts lead to different length of time of tissue formation (i.e. the higher the fibroblast concentration the faster the tissue formed), we adjusted the surfactant (Pluronic 127) (Legant et al. 2009) concentration with which we coated the PDMS surface of the microtissue arrays to provide more surfactant with less sticking to the PDMS substrates for slower-forming tissues. For example, arrays used for the CM++ population were coated with 1% Pluronic F127 overnight (without spinning down). The arrays for the CM+ cell population were treated with 0.1% and Native population 0.01%.. In all cases, the Pluronic 127 is spun down the next day and left for 30 minutes to prevent PDMS and cell-extracellular matrix interactions. Two washes with 1X PBS were made to remove the excess Pluronic F127.

4.3 Results

4.3.1 *Characterization of resting and twitch force generation with different concentration of fibroblasts*

To determine contractile responses of different concentration of fibroblasts on engineered tissues, we used flow cytometry to separate nonmyocytes and CMs from the neonatal rat hearts and engineer tissues with different concentrations in arrays of cantilevers with a spring constant of [k=0.20 μN/μm]. The samples were prepared as described in 4.2.3. We carried out a one-way multivariate analysis of variance to determine the effect of hypertrophic factors on change in resting force in cardiac microtissues tethered. Data are mean ± SEM unless otherwise stated. Values of change in resting force (Figure 22) were normally distributed, as assessed by Shapiro-Wilk's test ($p > .05$), and there were no outliers in the data, as assessed by Grubbs' test. There were statistical significant differences in resting force between tissue types. At day 0, the resting force of the Native tissues was $F_{day0} = 9.95 \pm 3.00$ which is 21% higher than CM+ tissues ($F_{day0} = 8.24 \pm 0.78$, $p<0.01$) and 119% larger than in the CM++ tissues ($F_{day0} = 4.55 \pm 1.89$, $p<0.0001$). The resting force in the CM+ tissues was 81% higher than in the CM++ tissues ($p<0.001$). Within each group of tissues, there was no statistically significant difference in the change in resting force between day 0 and day 1 (Native: $F_{day0} = 9.95 \pm 3.00$ vs. $F_{day1} = 11.8 \pm 3.24$; CM+: $F_{day0} = 8.24 \pm 0.78$ vs. $F_{day1} = 7.72 \pm 1.50$; CM++: $F_{day0} = 4.55 \pm 1.89$ vs. $F_{day1} = 3.9 \pm 1.53$), though time-dependent increases tended to occur in the Native tissues while time-dependent decreases were observed in the CM+ and CM++ tissues. As a result, the intergroup differences in resting force were even more pronounced at day 1.

We also measured the twitch force generated by the microtissues with different proportions of nonmyocytes. At day 0, the twitch force of the Native tissues was

F_{day0} = F_{day0} = 3.23±0.48, which is 13% higher than CM+(F_{day0} = 2.85 ±0.59, p=0.05) and 48% larger than in the CM++ sample (F_{day0} = 2.18±0.56, p=0.005). Similar to resting tension, within each group of tissues, there was no statistically significant difference between the twitch force produced from day 0 and day 1 (Native: F_{day0} = 3.23±0.48 vs. F_{day1} = 2.60±0.64; CM+: F_{day0} = 2.85 ±0.59 vs. F_{day1} = 2.88±0.43; CM++: F_{day0} = 2.18±0.56 vs. F_{day1} = 2.09 ±0.77). Pairwise analysis revealed statistically significant differences across samples. At day 1, the twitch force developed by microtissues with the Native population of cells (F_{day1} = 2.60±0.64) was 10% less than that of CM+ (F_{day1} = 2.88±0.43, p=0.045) and 24% greater than that of CM++ (F_{day1} = 2.09 ±0.77, p=0.011). At day 1, the twitch force for CM+ tissues was 38% greater than in CM++ tissues (p<0.01). Therefore, an increasing proportion of fibroblasts has significant, but quantitatively smaller, effects on twitch force than on resting force.

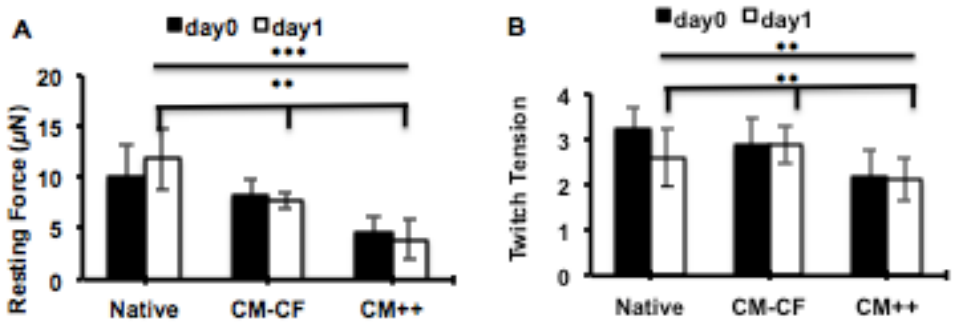

Figure 25. Resting and Twitch force generation in CMTs engineered with different number of fibroblasts. After CMTs were formed and synchronously beating, baseline force measurements at day 0 were acquired. Brightfield images were used to calculate the resting force (A). Using a high-speed camera, we collected data of the displacement of the cantilevers over multiple contractions (B). We observed that depletion of fibroblasts leads to lower resting forces and tends to lower twitch forces. The bar graph above represents the average peak force for 3-5 contractions across multiple tissues (n=15) (B).

4.3.2 *Contractile kinetics profile in CMTs after 24 hours of hypertrophic agonist treatments*

We also explored how contractile kinetics would respond to different amounts of fibroblasts. There was no difference in change in Vmax from day 0 and day 1 for all of the samples, however, there were differences among the different groups. At day 0 and day1, the maximal velocity of contraction increased was highest for the Native ($Vmax_{C\ day0}$ = 85.47 ±5.51 vs. $Vmax_{C\ day1}$ = 86.63 ±2.70) than the maximal velocity for CM+ ($Vmax_{C\ day0}$ = 70.49 ±4.11 vs. $Vmax_{C\ day1}$ = 74.20 ±3.73) and the CM++ CMTs (CM++: $Vmax_{C\ day0}$ = 52.35 ±3.64 vs. $Vmax_{C\ day1}$ = 60.59 ±2.43). To determine differences of maxima velocity, we performed a One-way ANOVA, to compare values of maximal velocity at day 1. There was a statistically significant difference between the Native and

CM+ (p=0.004) as well as CM++ (p<0.001). There was also a statistically significant difference betweem CM++ and the CM+ microtissues (p=0.003).

For maximal relaxation velocity , There was no difference in change in Vmax from day 0 and day 1 for all of the samples, however, there were differences among the different groups. At day 0 and day1, the maximal velocity of contraction increased was highest for the Native ($Vmax_{R\ day0}$ = 75.37 ±5.03 vs. $Vmax_{R\ day1}$ = 78.72±7.73), as compared to CM+ ($Vmax_{R\ day0}$ = 55.47±4.38 vs. $Vmax_{R\ day1}$ = 61.10 ±8.11) and the CM++ ($Vmax_{R\ day0}$ = 44.92±6.80 vs. $Vmax_{R\ day1}$ = 49.96 ±6.85). There was a statistically significant difference between the Native and CM+ (p<0.001) as well as CM++ (p<0.001). There was also a statistically significant difference betweem CM++ and the CM+ microtissues (p=0.02).

Similar to the results with native heart cell population described in the Chapter 2, we observed no statistically significant changes between the ratio of V_{max}Relaxation /V_{max} Contraction in the Untreated sample and ET-1 treated with hypertrophic agonists for 24 hours. Furthermore, the ratios of V_{max}Relaxation /V_{max} Contraction were similar across all samples. We did not observe any statistically significant change in this ratio, indicating, that the equilibrium between contraction and relaxation are maintained.

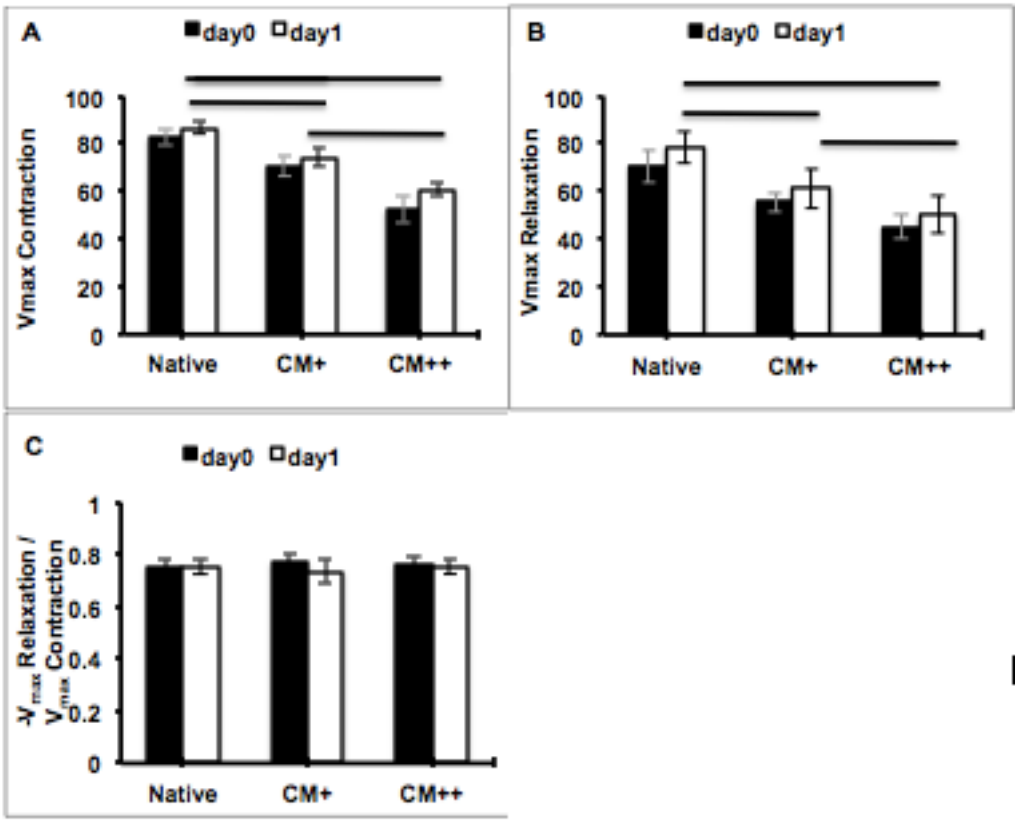

Figure 26. Contractile kinetics profile in CMTs with different number of fibroblasts. Using a high-speed camera, we tracked the displacement of fluorescent beads atop of CMTs, and calculated kinetics of contractility. Bars represent the average of individual tissues velocities over 3-5 twitches. V_{max} Contraction (A),V_{max} Relaxation (B), V_{max}Relaxation /V_{max} Contraction (C), were calculated from the data. Our results show that increasing the number of fibroblasts leads to increases in maximal velocities of contraction and relaxation. Student's t-test was used to compare between day0 and day1; * denotes $p<0.05$ and ** denotes $p<0.005$.

4.3.3 *Resting sarcomere length in microtissues engineered with different number of nonmyocytes*

To determine the effect of nonmyocytes in sarcomere length, we measured sarcomere length by fixing the samples as described in 2.2.5. As presented in Figure 24, At day 1, the resting sarcomere length by microtissues with the native population of cells (SL=1.76±0.02) was statistically significantly longer than that of CM+ (SL =1.71±0.02, p=0.057) and CM++ (SL = 1.66±0.01, p<0.0001). CM+ samples difference with CM++ was p=0.045.

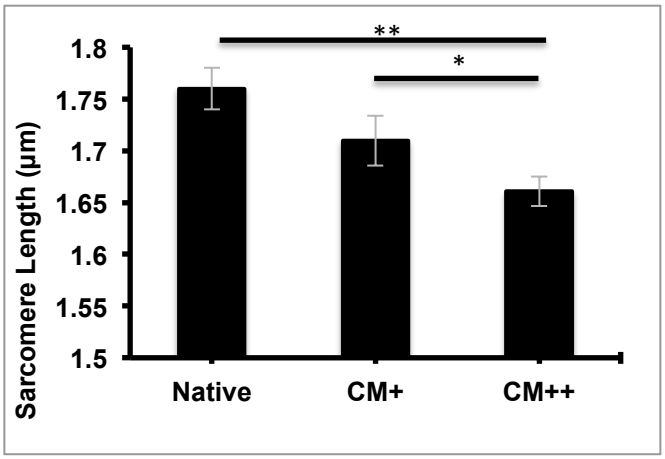

Figure 27: Resting sarcomere length in microtissues engineered with different number of fibroblasts. Immunofluorescent images of microtissues attached to cantilevers stained with a-actinin were used to detect sarcomeres and measure sarcomere length (as described in 2.3.4). Our results show that increasing fibroblast number in the tissues leads to increases in sarcomere length. Student's t-test was used to compare between an agonist treatment and the Untreated sample; * denotes p<0.05 and ** denotes p<0.005

4.3.4 *ET-1 response in myocyte-enriched tissues*

As described in Chapter 2, ET-1 induced the greatest resting and twitch forces in microtissues compared to other hypertrophic growth factors. We also observed and increase in sarcomere length that corresponded to the ET-1 treatment. By performing these experiments in myocyte-enriched preparations, we sought to investigate the role of fibroblasts in the responses observed during ET-1 exposure. In myocyte-enriched tissues, we observed negligible changes in resting force after ET-1 treatment compared to untreated tissues (Fig. 28A). However, we observed significant changes in twitch force after ET-1 addition (Fig. 28B). Interestingly, this ET-1 induced increase in twitch force was associated with a substantial increase in sarcomere length (Fig. 28C). This change in sarcomere length after ET-1 exposure in myocyte-enriched tissues was quantitatively greater than that observed after exposure to ET-1 in native tissues (Native: $SL_{Untreated}$ =1.89 ± 0.03 and SL_{ET-1} =2.02 ± 0.07 vs. CM-enriched: $SL_{Untreated}$ =1.64 ± 0.03 and SL_{ET-1}=1.91± 0.11, p-value for intergroup difference in the change with ET-1 p= 0.001).

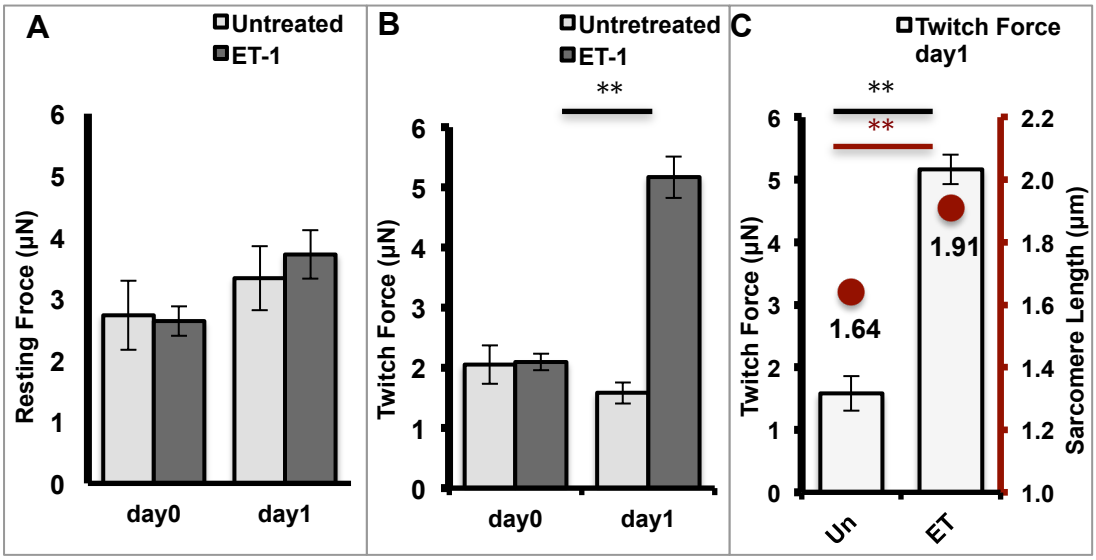

Figure 28. Resting and twitch force, and Sarcomere length measurements after 24 hours of ET-1 treatment in myocyte-enriched tissues (CM++). As described previously, baseline force measurements at day 0 were acquired after all tissues were synchronously beating. Brightfield images were used to calculate the resting force (A). Using a high-speed camera, we collected data of the displacement of the cantilevers over multiple contractions (B). Our data shows that ET-1 does not lead to a statistically significant effect in resting force (A), however it does lead to a statistically significant effect in twitch force in myocyte enriched tissues (CM++). Sarcomere length was increased upon stimulation of ET-1 for 24 hours.

4.3.4 *Length-tension relationship in CM-enriched microtissues*

We next evaluated how the resting length of the tissue correlated with twitch force generation in ET-1-treated and Untreated myocyte-enriched microtissues. The Untreated tissues exhibited a weak but positive length-tension relationship R^2=0.30 p=0.012, the longer the tissue the higher the twitch force generated (Figure 29A). On the other hand, the ET-1 treated samples exhibited a negative length-tension relationship, with longer tissues having *lower* twitch force R^2=0.74, p=0.001 (Figure 29B). These data indicate that while ET-1 treatment does not induce a significant change in average resting force (Figure 29A), the final resting length observed in individual microtissues is strongly and inversely correlated with the twitch force generated, such that the shortest tissues generate the highest twitch forces in myocyte enriched preparations.

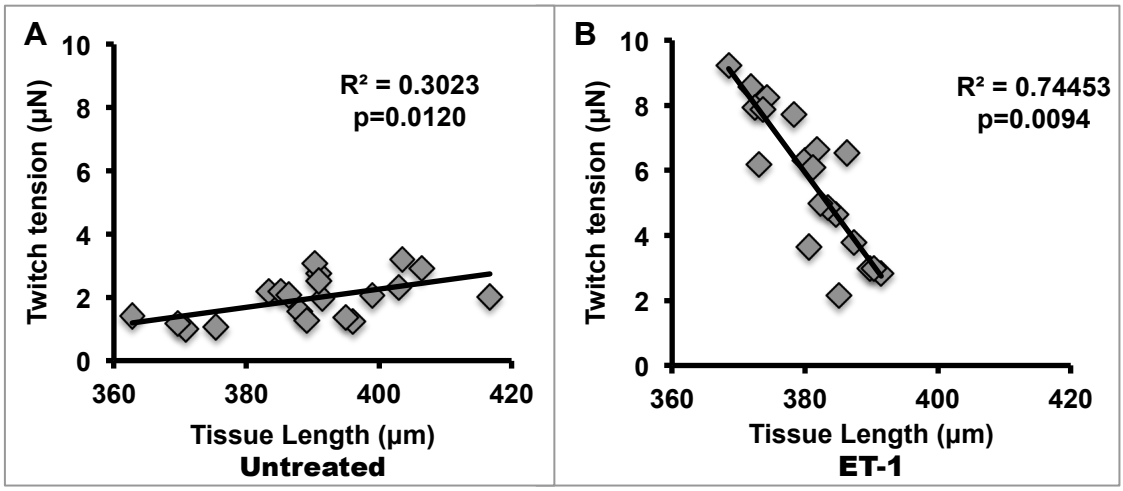

Figure 29. Correlation of the tissue length and twitch force at 1 day after ET-1 treatment in myocyte-enriched tissues (CM++). The twitch force and tissue length after 24 hours of ET-1 were plotted against each other. A linear regression analysis and a correlation coefficient R^2 were determined. In the Untreated sample (N=20), 30% of the variance in twitch force generation was related to the tissue length at day 1. In the ET-1 sample (N=20) we observed that 74% of the variance in twitch force generation was related to the tissue length at day 1.

4.3.5 *Kinetics of ET-1 treated myocyte enriched microtissues*

We also assessed how contractile kinetics were impacted by the addition of ET-1 over 24 hours, as illustrated in Figure 27. The Untreated sample started at $Vmax_{C\ day0}$ = 77.53±3.0, changed minimally the following 24 hours, reaching $Vmax_{C\ day1}$ = 72.73±2.49, which was not statistically significant. Meanwhile, while ET-1 $Vmax_{C\ day0}$ = 78.87±6.04, the maximal velocity of contraction increased by twofold upon the addition of ET-1 over 24 hours to $Vmax_{C\ day1}$ = 144.38±7.65 ($p<0.0001$)

Relaxation Velocity also increased significantly upon the application of ET-1 over 24 hours. There wasn't a statistically significant difference in the baseline relaxation Vmax at day 0 across samples (Untreated: $Vmax_{R\ day0}$ = 60.72±2.11 vs ET-1: $Vmax_{R\ day0}$ = 65.79±6.44). The Untreated sample did not change significantly in the next 24 hours ($Vmax_{R\ day1}$ = 50.77±2.22), while the exposure of ET-1 for 24 hours increased the relaxation velocity by 91% (ET-1: $Vmax_{R\ day1}$ = 115.91±5.78, $p<0.001$).

Similar to the results with native heart cell population described in the Chapter 2, we observed no statistically significant changes between the ratio of V_{max}Relaxation /V_{max} Contraction in the Untreated sample and ET-1 treated with hypertrophic agonists for 24 hours. Furthermore, the ratios of V_{max}Relaxation /V_{max} Contraction were similar across all samples. We did not observe any statistically significant change in this ratio, indicating, that the equilibrium between contraction and relaxation are maintained.

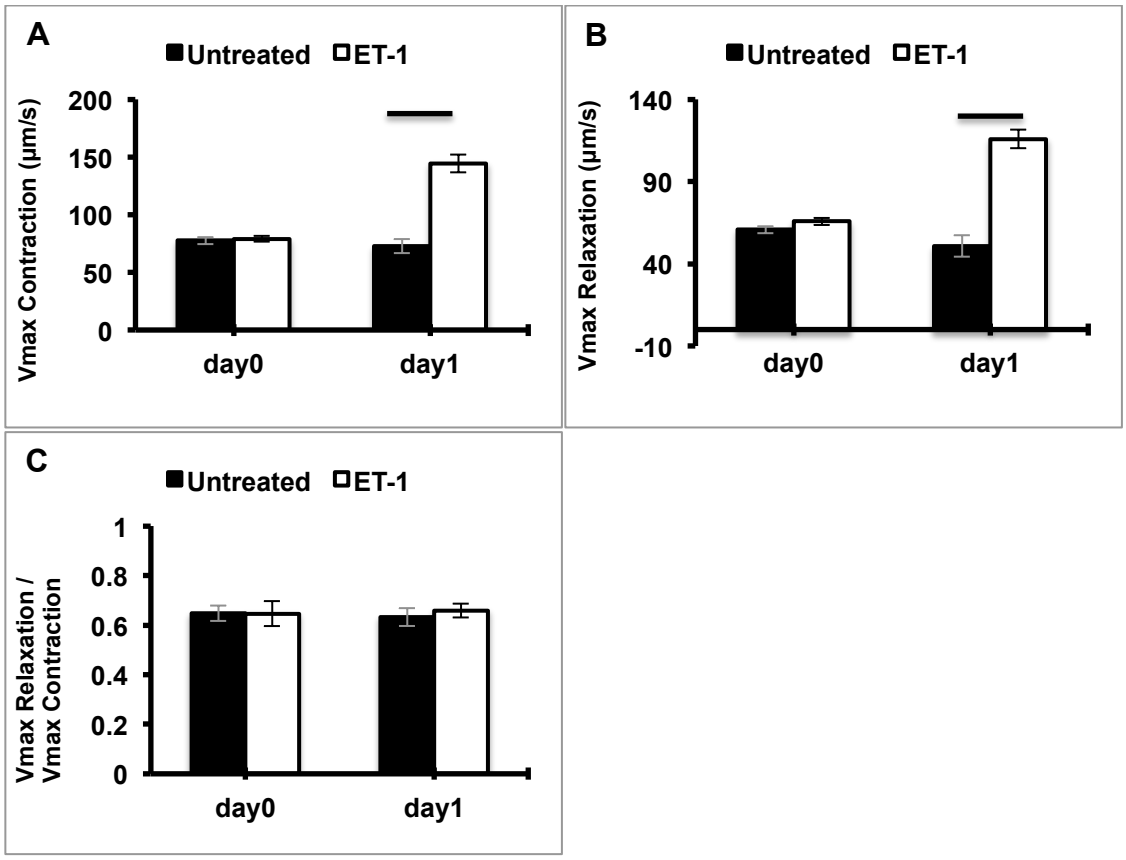

Figure 30. Contractile kinetics profile in CMTs after 24 hours of hypertrophic agonist treatments. Using a high-speed camera, we tracked the displacement of fluorescent beads atop of CMTs, and calculated kinetics of contractility. Bars represent the average of individual tissues velocities over 3-5 twitches. Maximum velocity of contraction (V_{max} Contraction) (A),Vmax Relaxation (B), Vavg Contraction (C), Vavg Relaxation (D), V_{max}Relaxation /V_{max} Contraction (E) were calculated from the data. Our results show a statistically significant increase in maximal velocities of contraction and relaxation after ET-1 treatment. Student's t-test was used to compare between day0 and day1; * denotes $p<0.05$ and ** denotes $p<0.005$.

4.4 Discussion

In this chapter, we examined the impact of differences in the proportions of cardiac myocytes on the contractility of engineered auxotonically-loaded CMTs. Additionally, we examined the effect of ET-1 in myocyte-enriched tissues and determined how tissue length and sarcomere length are associated to these changes in contractility.

Our results indicate that microtissues engineered with the native heart cell population with roughly 50% cardiac myocytes have enhanced contractile properties with higher tissue compliance than the microtissues engineered with moderately reduced fibroblast content (CM+) and highly myocyte-enriched (CM++) cell populations. The enhanced contractile performance of the tissues was determined by higher resting and twitch force generation as well as longer sarcomere lengths. Our results concur with previous studies that have described a superior contractile profile for engineered tissues generated from the native heart cell population (Radisic M et al. 2008, Asnes CF et al. 2006). The microtissues created with an intermediate fibroblast concentration, revealed contractile performance that was in between the native heart cell population and the myocyte-enriched population, indicating that there is a an association between increasing number of nonmyocytes and increasing resting and twitch force, as well as maximal contraction and relaxation velocities. Similarly, the sarcomere length measurements indicate that increasing the number of nonmyocytes in the microtissues leads to longer resting sarcomere lengths. These results underscore the importance of quantifying nonmyocytes in cardiac tissues, particularly when measuring forces in auxotonically loaded engineered tissues.

Our understanding of the length-tension relationships in heart tissue has been limited by the inability to control the cell content in the tissue, and understand how nonmyocytes contribute to contractile responses. The experimental loading conditions of isolated tissue strip systems have mainly been limited to isotonic (constant force), and isometric (constant length) setups, where the tissue length or sarcomere length are set to a specific value. Under the isometric conditions typically utilized (often at the tissue length associated with maximal twitch force, Lmax) the potential impact of how the nonmyocyte population dynamically affects the resting sarcomere length of myocytes, and thus their contractility, is not taken into consideration. Our previous work (Chapter 2) revealed a negative length - twitch force response in microtissues engineered with the native heart cell population, a relationship that was further exacerbated by the treatment of hypertrophic factors (Figure 5). These results led us to believe that the shorter resting length (or higher resting force) was possibly governed by activated nonmyocytes. In this chapter, we demonstrate that depleting nonmyocytes in microtissues (myocyte-enriched microtissues), yields a statistically significant positive length-tension relationship in Untreated samples. While the overall compliance of the tissue is reduced with the depletion of nonmyocytes, this experimental setup allow us to discern myocyte-governed contractile responses in auxotonically-loaded tissues, where longer lengths are correlated with higher twitch force generation. Consequently, auxotonic loading conditions in microtissues, which characterize cardiac tissue behavior in physiological conditions, reveals an interesting nonmyocyte governed behavior of tissue length – sarcomere length – twitch force generation.

Interestingly, after treating the microtissues with ET-1, we see a negative length –tension relationship. While our enrichment methods yields higher myocyte purities than previously described for pre-plating methods, (75%-90% purity, Chlopcíková S et

al.2011 , Brown MA et al. 2009) the nonmyocyte depletion is not absolute. This leads us to consider the possibility that ET-1 activates the nominal nonmyocyte population in the myocyte-enriched tissues. While this effect does not yield statistically significant changes in resting force, it does reveal that nominal differences in tissue length among the different microtissues in the array, that strongly influence twitch force generation. Based on previous work we know that ET-1 activation in nonmyocytes leads to proliferation and myofibroblast differentiation (Rodriguez-Pascual F et al. 2014), a cell population that is characterized by having muscle-like properties, including higher force-generating capabilities compared to inactivated fibroblasts. This contractile "phenotype" of the fibroblasts leads to more elongation of the myocytes as previously described (Nichol et al. JW 2008), and thus, as we observe here, a longer sarcomere length. Previous studies have suggested that the fibroblast can affect on myocytes contractility by direct interaction with myocytes as well as by the release of paracrine factors (Nichol et al. JW 2008, Pedrotty DM et al. 2009). Additionally, we also observed a low R^2 value in the length-tension relationship in the Untreated sample in the myocyte-enriched microtissues. Given that fibroblasts govern the resting force, it is possible that small differences in number of fibroblasts as well as levels of activation (due to the forces applied during isolation and sheer stress during flow cytometry) lead to variations in tissue length and thus a lower R^2 value in the positive length-tension relationship. Further work looking at the mechanism of the fibroblast effects on myoctes should be considered.

It is also possible that ET-1 affects cytoskeletal organization and myofilament properties directly. A Kruger at al. showed that Angiotensin II triggers a transition of titin isoform switch from N2A to the stiffer isoform N2B (expected to cause smaller sarcomere lengths) (Kruger M et al. 2008). Interestingly, ET-1 does not promote the

transition to the stiffer N2B isoform, and may potentially block the isoform switch. This would suggest that ET-1 might favor the more distensible N2BA isoform, and hence produce longer sarcomere lengths in our model.

Further work, using auxotonically-loaded single cells or an entirely pure myocyte engineered tissue, could reveal additional insights into the direct effect on ET-1 on myocyte cytoskeletal properties.

Based on our knowledge of fibrosis and pathological cardiac remodeling that lead to cardiac dysfunction, it is possible that the positive effect of nonmyocyte number on sarcomere length reaches a plateau, and becomes negative in the presence of a high nonmyocyte population.

In summary, this study reveals novel insights regarding the effect of nonmyocytes in the contractile profile of auxotonically-loaded microtissues. Our work reveals an interesting relationship between decreasing number of nonmyocytes and resulting decreases in resting force, twitch force, maximal contraction and relaxation velocities as well as sarcomere length. Particularly, it provides data demonstrating potential distinctions between sarcomere length and overall tissue length in auxotonically-loaded microtissues engineered with varying proportions of heart cell subtypes. These studies also highlight how differences in cell proportions can alter agonist-mediated responses in engineered hearts tissues. Further studies generating microtissues with different proportions of myocytes to nonmyocytes should reveal interesting insights about the effects of the different cells in the contractility of cardiac tissue and reveal new insights about the mechanisms associated with different cell-type contributions.

4.5 Limitations

It is important to highlight some limitations of these studies. Firstly, paired measurement of sarcomere length and contractile parameters, was not performed in these studies. Future studies should be performed such that each tissue's contractile properties are paired with its myocytes' sarcomere length. Additionally, it is important to note that sarcomere length was measured in fixed tissues, therefore it is possible that the fixation may have altered the absolute sarcomere length. However, the differences between groups should be consistent, as we performed sarcomere length measurements in parallel, and using the same fixation reagents and protocols.

Additionally, it is possible that there are variations in the number of nonmyocytes in each tissue sample, and variations in the level of fibroblast-to-myofibroblast differentiation. Further assessments of the nonmyocyte population in the tissues should reveal interesting insights about the effects of the different cells in the contractility of cardiac tissue and reveal new insights about the mechanisms associated with different cell-type contributions.

Moreover, the cells from native heart mix population were not exposed to the effects of sorting. While previous work in our lab revealed little damage to cells after exposure to cytometry sorting, this damage can be assessed by creating tissues with a 50:50 proportion of myocytes to nonmyocytes reconstituted the same way as the isolated cells. Furthermore, engineering tissues that have a larger nonmyocyte population than the myocyte population (myocyte depletion) resembling a fibrotic heart tissue, would provide novel insights as to the effect of number of nonmyocytes in contractility and sarcomere length.

CHAPTER 5. CONCLUSIONS AND FUTURE DIRECTIONS

5.1 Conclusions

The purpose of these investigations was to evaluate the differential effects of hypertrophic factor stimulation on cardiac contractility using an *in vitro* culture method that recapitulates the 3D in vivo organization of the myocytes and nonmyocytes to identify mechanisms by which these factors influence myocardial structure and function *in vivo*. We demonstrated the ability of our system to dissect differential contractile profiles in response to agents implicated in cardiac hypertrophy, namely, Ang II, ET-1, and TGF-β, as well as increased load by simultaneously measuring the contractile force, velocity, and power produced by auxotonically-loaded CMTs. Additionally, we examined how tissue length and sarcomere length are associated with these changes in contractility.

While the effects of these hypertrophic factors have been studied in *in vivo* (Souders CA et al. 2012, Bujak M and Frangogiannis NG 2007) and i*n vitro models*, both in flat culture (Schaub MC et al. 1997, Sadoshima J et al. 1993) and in 3D culture (Horton RE et al. 2016, McCain ML et al. 2013, Hirt MN et al. 2012) less is known about how engineered tissues in auxotonic preparations can recapitulate these changes in contractility. Furthermore, we realized that little is known about how sarcomere length and length-tension relationships play a role in contractile performance in cardiac engineered tissue studies using auxotonic preparations. Yet, the sarcomere is the fundamental structural unit involved in force generation within cardiomyocytes, and resting sarcomere length is major determinant of both resting and twitch force in cardiac myocytes and the intact myocardium. Accordingly, assessment of sarcomere

length is essential for determining how pro-hypertrophic factors are affecting contractile performance. For example one group, published a positive inotropic response in engineered tissues in an isometric preparation, and a negative inotropic response for millimeter-length tissues in an auxotonic preparation. However, there were key differences in the culture conditions. For example, in the second study, thyroid hormone triiodothyronine (T3), a physiological hypertrophic factor implicated in increases in sarcomere lengths of cardiac cells (Rodriguez AG et al. 2011, Yang X et al. 2011), was used to substitute for serum in the culture conditions, and could have contributed to the differences in inotropic responses. However, the myocyte sarcomere length was not noted. Our results indicate that for microtissues engineered with a native heart cell mix, ET-1 elicits a larger positive inotropic effect in auxotonic twitch force and resting force generation compared to Ang II. TGF-β, in contrast, produced a negative inotropic response. In other words, ET-1 produced the largest change in force, while AngII produced a moderate increase and TGF-β resulted in a decrease in twitch force generation. Interestingly, we observed that the sarcomere length of myocytes in tissues treated with ET-1 was longer than those in the Untreated, Ang II and TGF-β (shorter than in the Untreated), suggesting that at least some of the effects on contractility could be attributed to changes in sarcomere length induced by the hypertrophic factor. Furthermore, while the correlation of sarcomere length and twitch force generation goes hand in hand with what is expected from the Frank-Starling relationship (Konhilas JP et al. 2002), we observed a counter-intuitive correlation between sarcomere length and tissue length. The longer the sarcomere length, the shorter the tissue, and the higher the resting force. Sarcomere length and tissue length are usually positively controlled variables in isolated muscle preparations obtained from mature hearts. Changes in sarcomere length in myocytes within relatively immature engineered heart tissues had

not been previously noted.

The finding that myocytes exhibiting longer sarcomere length while the overall tissue length was shorter led us to speculate that the tissue length, or resting force, could be regulated by nonmyocytes in our auxotonically-loaded engineered microtissues system. The importance of nonmyocyte in engineering cardiac tissues has been previously noted (Radisic M et al. 2008, Nichol JW et al. 2008). Nonmyocytes have been shown to enhance resting and twitch force generation in engineered cardiac tissues (Asnes CF et al. 2006), elongated cells (Nichol JW et al. 2008), greater inotropic response (Naito H et al. 2008). However, how the number of nonmyocytes plays a role in sarcomere length in myocytes has not been previously studied. We developed engineered tissues with increasing number of myocytes (and decreasing number of nonmyocytes). Namely we engineered three types of tissues: Native heart cell mix (CM: 50% - NM: 50%), Cm+ (CM:83% - NM:17%), and CM++ (CM:93% - NM:7%). Our results suggest that microtissues engineered with the native heart cell population with roughly 50% cardiac myocytes have enhanced contractile properties than the microtissues engineered with moderately reduced fibroblast content (CM+) and highly myocyte-enriched (CM++) cell populations. The enhanced contractile performance of the tissues was determined by higher resting and twitch force generation in association with longer sarcomere length.

Moreover, we observed a moderate positive length-tension response in Untreated microtissues composed of mostly myocytes (CM++), but upon stimulation of ET-1, we observed a small and non-statistically significant increase in resting force in tissues treated with ET-1. However, when we looked at each tissue individually, we observed that small differences in length correlated with differences in twitch force generated. In particular, we observed that the shorter the tissue, the higher the twitch

force generated. It is possible that the small amount of (~7% nonmyocytes) nonmyocytes present in the tissue were enough contribute to the resting force and tissue length–tension relationship. However, this does not preclude whether other unidentified direct effects on myocytes are also involved (discussed below, in Future Directions section).

To further understand the contractilility of microtissues in response of hypertrophic effectors, we evaluated the effect of increased auxotonic load or afterload of the cantilevers by 2.25x. Increasing mechanical load led to structural and functional phenotype changes in our microtissue model, demonstrating the potential of engineered cardiac constructs as a platform for studying *in vitro* effects of complex stimuli, including the combination of biochemical and load enhancement, that occur *in vivo*. Treatment with AngII, ET-1 and the cocktail of hypertrophic factors induced significant increases in cell size in stiff pillars, but not in soft pillars. Studies performed *in vitro* in 2D cell culture systems have previously shown that myocytes increase in size in response to these hypertrophic factors, irrespective of mechanical load (static stretch) (Sadoshima J et al. 1993). One challenge with these flat cell culture substrates is that cells are exposed to the stiffness of the plate, making it harder to distinguish between the load-mediated effects and the hypertrophic factor effects.

Taken together, these studies have provided insights into the mechanisms by which hypertrophic effectors modulate contractility in auxotonically-loaded engineered tissues.

5.2 Future Directions

Future experiments will extend our understanding of how mechanical, soluble and cell interaction cues regulate myocyte contractility. Particularly,

further studies should focus on the mechanisms by which nonmyocytes, and hypertrophic factors affect the sarcomere length of tissues. Further refinements of the model, such as inhibitor studies, enhancements in loading conditions as well as live sarcomere imaging could prove useful for future studies.

5.2.1 Nonmyocyte effect on auxotonic contractility and sarcomere length

In our study, increasing fibroblast number in microtissues increased contractility and sarcomere length, so we suspect that nonmyocytes mediate the changes in sarcomere length in Untreated and ET-1 treated tissues. While previous studies showed that increased stiffness led to increased sarcomere length of myocytes (Rodriguez AG et al. 2011, Torre I et al. 2014), the basis for this relationship is not clear. It is possible that the presence of fibroblasts increase the stiffness of the tissue and thus affect sarcomere length via ECM modulation or higher resting force. Measuring stiffness of the tissue using a nanoindentator and over a series of tissue lengths could reveal whether the presence of nonmyocytes affects the overall stiffness of the tissue. Furthermore, fibroblasts induce ECM changes, such as increases in collagen and fibronectin in response to hypertrophic factors, such as Ang II (Gray MO et al. 1998, Sadoshima J et al. 1993, Sarkar S et al. 2004). These changes in ECM can induce changes in myocytes, as myocytes cultured on collagen display enhanced physical association between cytoskeletal components, for example myocyte surface integrins interact with to mediate cellular hypertrophy (Lal H et al. 2007, Lal H et al. 2009).

It is also possible that nonmycytes regulate sarcomere length in myocytes directly via cell-cell interactions, and thus may be pulling on and deforming the myocytes. Mechanical adherens junctions (cadherin) and electrical gap junctions (connexin) are heterocellular junctions that have been well studied in myocyte and

fibroblast interactions. For example, connexin 43 has been shown to dorm heterocellular junctions between nonmyocytes and myocytes. We could test the importance of these junctions in our system, by. Inhibiting these junctions using β-glycyrrhetinic acid (BGA). Additionally, previous studies showed that stimulating fibroblasts with TGF-β to induce a myofibroblast phenotype, leads to increase expression of N-cadherin junctions and a decrease in expression of connexin 43 junctions (Thompson SA et al. 2011), decreasing electrophysiological function, and induces an arrythmogenic effect. Using live cell imaging, they showed that myofibroblasts were capable of pulling on and deforming the myocyte cell membrane. This mechanical deformation is key to the cell aspect ratio of myocytes, which plays an important role in the contractility of myocytes (Bray MA et al. 2008). Furthermore, pre-treatment with blebbistatin or by using double knowckdown Rho fibroblasts to inhibit the contractility of nonmyocytes restored electrophysiological function. While this group did not see Cadherin 11 (OB-Cadherin) in heterocellular junctions, other groups have demonstrated the importance of Cadherin 11 to be the predominant cadherin in myofibroblasts alone or in combination myocytes both in vitro and in vivo (Bowen CJ et al. 2015, Borg TK and Baudino TA). Furthermore, investigating other possible junctions, such as integrins, other connexins, intercalating disks, desmosomes , tight junction proteins (Bowers SL 2012, Kakkar R and Lee RT 2010), which are mechanically anchored to the actin cytoskeleton could provide insights into whether these interactions can affect sarcomere length. The hypothesis that heterocellular junctions mediate the stretch of myocytes, as well increases in sarcomere length, can be addressed by blocking these heterocellular junctions with neutralizing antibodies or inhibiting the contractile properties of the nonmyocyte population. Therefore, further investigating the type of heterocellular junction that predominate in engineered tissues, and inhibiting

these interactions could lead to better understanding of how fibroblasts affect myocytes and sarcomere length in our tissues.

Other possible contributors to our findings are paracrine interactions. As we discussed in Chapter 1, there is intercellular paracrine communication that occurs upon stimulation of AngII, ET-1 and TGF-β in myocytes and nonmyocytes. Many factors are part of this autocrine/paracrine interaction, such as LIF, CT-1, MMP, TIMPs, etc. For example, a previous study showed that engineered cardiac tissues co-cultured with nonmyocytes led to myocyte elongation coupled with the expression of active MMP-2 protein (not present in CM-enriched constructs), increased pro-MMP-2, and reduced pro-MMP-9 expression (Nichol JW et al. 2008). Additionally, they showed that nonmyocytes led to a decrease in myocyte apoptosis, further confirming the importance of nonmyocytes in cardiac tissue. Interestingly, MMP inhibition studies suggested that MMP-1 is required for the cell elongation observed in the co-culture of nonmyocyte with myocytes in engineered tissues (Nichol JW et al. 2008). Furthermore, Radisic M et al. showed that pre-treating polymer scaffolds with cardiac fibroblasts before myocyte seeding, led to greater tissue contractility and myocyte alignment suggesting a paracrine effect from fibroblasts (Radisic M et al. 2008).

Further evaluation of our system's nonmyocyte effects in the tissue is needed to better understand the relationship of nonmyocyte number with sarcomere length and contractility. Better understanding of the interaction between myocytes and nonmyocytes in physiology and how they change in pathophysiology could provide novel insights of the importance of nonmyocytes in cardiac contractility.

5.2.2 ET-1 effect on sarcomere length

Our studies showed that ET-1 came out to be the largest modulator of

contractility and samples treated with ET-1 had the largest increases in sarcomere length. However, endothelin receptor antagonists have failed in clinical trials (Ertl G and Bauersachs J, 2004). Understanding the signals involved in transducing the hypertrophic actions of ET-1 to pathological mechanical remodeling in the heart will allow us to design selective therapies to prevent adverse cardiac remodeling.

ET-1 could also have a direct effect on myocytes that induces changes in sarcomere length and contractility rather than simply a main effect on fibroblasts. A previous study showed that AngII induced a transition from the isoform of titin to the stiffer N2B isoform of titin, with shorter sarcomere length in neonatal rat ventricular myocytes. However, ET-1 did not promote the transition to N2B, leading to longer sarcomere lengths. If this were observed in our microtissues, then ET-1 might favor the more distensible N2BA isoform and induce longer sarcomere lengths in our model. Therefore, follow up studies to examining N2B and N2A levels after ET-1 administration or manipulating N2B/N2A levels independent of ET-1 would help inform this speculation (Kruger M et al. 2008). Furthermore, results from another study suggested titin, and not ECM, is primarily responsible for the passive force (resting force) and sarcomere length in Lanfendorff perfused hearts. The role of titin in resting force was determined by degrading titin without affecting the ECM, using a relaxing solution that incorporated dithiothreitol (DTT). DTT however, has also been associated with inhibition of fibroblast spreading (Grinnell F and Feld MK, 1980). Therefore, further work is warranted to parse out role of titin, which modulates passive force in myocytes, and fibroblasts in resting force and myocyte sarcomere length in cardiac tissue. Interestingly, a recent study using microtissues engineered with iPS cells with Titin mutations, the authors did not observe any change in the tissue's resting force, while in vivo, titin mutations and isoforms have been linked to differences in resting force (passive/diastolic force) (Hinson JT et al.

2015). It is possible that the contributions of titin and nonmyocytes to the resting force of cardiac tissue vary from native tissue to engineered tissue. Understanding the signals involved in transducing the hypertrophic actions of ET-1 to pathological mechanical remodeling in the heart might allow design therapies to mitigate adverse cardiac remodeling.

5.2.3 Mechanisms of contractile changes and inhibitor studies

A limitation of this study is that the hypertrophic agonists have been known to affect each other. Ang II has been shown to increase the expression of ET-1 (Drawnel FM et al. 2013). Additionally, Ang II's hypertrophic effects have been previously attributed to the actions of TGF-β. These effects have been shown in a longer time scale. However, because of the nature of the micro-scale of our system where diffusion can occur within minutes, it is likely that these effects would occur in a shorter timescale. Future studies could address the potential of the hypertrophic factors inducing one another using selective antagonists and/or genetic manipulations of particular agonists or receptors. Additionally, extending our experiments beyond 48 hours could provide other insights of longer-term effects of these factors on the resting and twitch force changes.

5.2.4 Effect of loading conditions on contractility and sarcomere length

We observed that increased load led to shorter sarcomere lengths as well as a slower velocity generation described previous studies (Edmund Sonnenblick 1962). A limitation of our studies is that we only tested two loads. Further studies should consider a range of loads to parse out load dependent effects in contractility and sarcomere length. Additionally, given that the stiff arrays are already made at the time we add the

cells, the increased load not only affects the cells after the tissue is formed, but also during its formation. Further model refinements should consider utilizing materials that allow us to selectively modify load after tissue formation.

Moreover, different loading conditions (isometric, isovolumetric and auxotonic), have led to differences in inotropic responses (Layland J et al. 2004), therefore looking at how different conditions lead to changes in contractile responses would be valuable. While auxotonic load more closely resembles contractility of the heart in vivo, most studies in isolated papillary muscles have been done in isotonic and isometric preparations. Better understanding of how results of auxotonically-loaded tissues compare to previous studies is difficult with our current mode. Further refinements of our model should allow for comparisons of force and kinetics after agonist treatments under different loading conditions.

5.2.5 Live sarcomere length measurements

In its current configuration, this system does not allow for real-time measurements of sarcomere length in live tissues. Sorting out the dynamic sarcomere changes that occur *in vivo* and *in vitro* (measuring changes live, for example, with laser diffraction techniques) could provide additional insight into the sarcomere changes that we observed. Additionally, force is dependent sarcomere length-dependent changes in myofilament calcium sensitivity, as well as calcium concentration, additional studies should evaluate additional factors that contribute to changes in force.

These data reinforce the ability of engineered tissues to decouple different factors that contribute to cardiac remodeling. Future studies in this field will better describe how multiple factors, including mechanical, biochemical and cell-specific effects interact to produce a coordinated contractile output. Additionally, we highlight the

importance of sarcomere length, when determining inotropic contractile responses of cardiac tissue. Furthermore, our results suggest that nonmyocytes are required to engineer highly functional cardiac tissue their communication with neighboring myocytes are important to in the study of cardiac contractility and remodeling.

Arts T, Prinzen FW, Snoeckx LH, Rijcken JM, Reneman RS. Adaptation of cardiac structure by mechanical feedback in the environment of the cell: a model study. Biophys J. 1994 Apr;66(4):953-61.

Asnes CF, Marquez JP, Elson EL, Wakatsuki T. Reconstitution of the Frank-Starling Mechanism in Engineered Heart Tissues. Biophysical Journal. 2006;91(5):1800-1810.

Baar K, Birla R, Boluyt MO, Borschel GH, Arruda EM, Dennis RG. Self-organization of rat cardiac cells into contractile 3-D cardiac tissue. FASEB J. 2005 Feb;19(2):275-7.

Banerjee I, Fuseler JW, Price RL, Borg TK, Baudino TA. Determination of cell types and numbers during cardiac development in the neonatal and adult rat and mouse. Am J Physiol Heart Circ Physiol. 2007 Sep;293(3):H1883-91.

Baker BM, Chen CS. Deconstructing the third dimension: how 3D culture microenvironments alter cellular cues. J Cell Sci. 2012 Jul 1;125(Pt 13):3015-24.

Barker RJ, Price RL, Gourdie RG. Increased association of ZO-1 with connexin43 during remodeling of cardiac gap junctions. Circ Res. 2002 Feb 22;90(3):317-24

Baudino TA, McFadden A, Fix C, Hastings J, Price R, Borg TK. Cell patterning: interaction of cardiac myocytes and fibroblasts in three-dimensional culture. Microsc Microanal. 2008 Apr;14(2):117-25.

Blaauboer ME, Smit TH, Hanemaaijer R, Stoop R, Everts V. Cyclic mechanical stretch reduces myofibroblast differentiation of primary lung fibroblasts. Biochem Biophys Res Commun. 2011 Jan 7;404(1):23-7.

Boudou T, Legant WR, Mu A, Borochin MA, Thavandiran N, Radisic M, Zandstra PW, Epstein JA, Margulies KB, Chen CS. A microfabricated platform to measure and manipulate the mechanics of engineered cardiac microtissues. Tissue Eng Part A. 2012 May;18(9-10):910-9.

Bowers SL, Baudino TA. Laying the groundwork for growth: Cell-cell and cell-ECM interactions in cardiovascular development. Birth Defects Res C Embryo Today. 2010 Mar;90(1):1-7.

Bowers SL, Borg TK, Baudino TA. The dynamics of fibroblast-myocyte-capillary interactions in the heart. Ann N Y Acad Sci. 2010 Feb;1188:143-52

Bowers SL, McFadden WA, Borg TK, Baudino TA. Desmoplakin is important for proper cardiac cell-cell interactions. Microsc Microanal. 2012 Feb;18(1):107-14

Bowen, C J., J. Zhou, D C. Sung, J T Butcher. 2015. "Cadherin-11 coordinates cellular migration and extracellular matrix remodeling during aortic valve maturation". Developmental Biology 407 (1): 145-157.

Borg TK, Baudino TA. Dynamic interactions between the cellular components of the heart and the extracellular matrix. Pflugers Arch. 2011 Jul;462(1):69-74.

Bray MA, Sheehy SP, Parker KK. Sarcomere alignment is regulated by myocyte shape. Cell Motil Cytoskeleton. 2008 Aug;65(8):641-51.

Briasoulis A, Tousoulis D, Papageorgiou N, Kampoli AM, Androulakis E, Antoniades C, Tsiamis E, Latsios G, Stefanadis C. Novel therapeutic approaches targeting matrix metalloproteinases in cardiovascular disease. Curr Top Med Chem. 2012;12(10):1214-21.

Brown MA, Iyer RK, Radisic M. Pulsatile perfusion bioreactor for cardiac tissue engineering. Biotechnol Prog. 2008 Jul-Aug;24(4):907-20.

Bujak M, Frangogiannis NG. The role of TGF-beta signaling in myocardial infarction and cardiac remodeling. Cardiovasc Res. 2007 May 1;74(2):184-95.

Castanares C., Redondo-Horcajo M., Magan-Marchal N., ten Dijke P., Lamas S., Rodriguez-Pascual F. Signaling by ALK5 mediates TGF-beta-induced ET-1 expression in endothelial cells: a role for migration and proliferation. J. Cell Sci. 2007 120, 1256–126.

Chlopcíková S, Psotová J, Miketová P. Neonatal rat cardiomyocytes--a model for the study of morphological, biochemical and electrophysiological characteristics of the heart. Biomed Pap Med Fac Univ Palacky Olomouc Czech Repub. 2001 Dec;145(2):49-55.

Dasgupta C, Zhang L. Angiotensin II receptors and drug discovery in cardiovascular disease. Drug Discov Today. 2011 Jan;16(1-2):22-34.

de Haas HJ, van den Borne SW, Boersma HH, Slart RH, Fuster V, Narula J. Evolving role of molecular imaging for new understanding: targeting myofibroblasts to predict remodeling. Ann N Y Acad Sci. 2012 Apr;1254:33-41

de Lange WJ, Hegge LF, Grimes AC, Tong CW, Brost TM, Moss RL, Ralphe JC. Neonatal mouse-derived engineered cardiac tissue: a novel model system for studying genetic heart disease. Circ Res. 2011 Jun 24;109(1):8-19.

de Jonge HW, Dekkers DH, Houtsmuller AB, Sharma HS, Lamers JM. Differential Signaling and Hypertrophic Responses in Cyclically Stretched vs Endothelin-1 Stimulated Neonatal Rat Cardiomyocytes. Cell Biochem Biophys. 2007;47(1):21-32

Dasgupta C, Zhang L. Angiotensin II receptors and drug discovery in cardiovascular disease. Drug Discov Today. 2011 Jan;16(1-2):22-34

Diniz GP, Carneiro-Ramos MS, Barreto-Chaves ML. Thyroid Hormone Increases TGF-beta1 in Cardiomyocytes Cultures Independently of Angiotensin II Type 1 and Type 2 Receptors.Int J Endocrinol. 2010:384890.

Desroches BR, Zhang P, Choi BR, King ME, Maldonado AE, Li W, Rago A, Liu G, Nath N, Hartmann KM, Yang B, Koren G, Morgan JR, Mende U. Functional scaffold-free 3-D cardiac microtissues: a novel model for the investigation of heart cells. Am J Physiol Heart Circ Physiol. 2012 May 15;302(10):H2031-42.

Dodge SM, Beardslee MA, Darrow BJ, Green KG, Beyer EC, Saffitz JE. Effects of angiotensin II on expression of the gap junction channel protein connexin43 in neonatal rat ventricular myocytes. J Am Coll Cardiol. 1998 Sep;32(3):800-7.

Drawnel FM, Archer CR, Roderick HL. The role of the paracrine/autocrine mediator endothelin-1 in regulation of cardiac contractility and growth. Br J Pharmacol. 2013 Jan;168(2):296-317.

Emdad L, Uzzaman M, Takagishi Y, Honjo H, Uchida T, Severs N, Kodama I, Murata Y. Gap junction remodeling in hypertrophied left ventricles of aortic-banded rats: prevention by angiotensin II type 1 receptor blockade. J Mol Cell Cardiol. 2001 Feb;33(2):219-31.

Eschenhagen T. New tissue for failing hearts. Eur J Heart Fail. 2013 Jan;15(1):1-2.

Eschenhagen T, Eder A, Vollert I, Hansen A. Physiological aspects of cardiac tissue engineering. Am J Physiol Heart Circ Physiol. 2012 Jul 15;303(2):H133-43.

Eschenhagen T, Fink C, Remmers U, Scholz H, Wattchow J, Weil J, Zimmermann W, Dohmen HH, Schäfer H, Bishopric N, Wakatsuki T, Elson EL. Three-dimensional reconstitution of embryonic cardiomyocytes in a collagen matrix: a new heart muscle model system. FASEB J. 1997 Jul;11(8):683-94.

Feinberg AW, Alford PW, Jin H, Ripplinger CM, Werdich AA, Sheehy SP, Grosberg A, Parker KK. Controlling the contractile strength of engineered cardiac muscle by hierarchal tissue architecture. Biomaterials. 2012 Aug;33(23):5732-41

Fink C, Ergün S, Kralisch D, Remmers U, Weil J, Eschenhagen T. Chronic stretch of engineered heart tissue induces hypertrophy and functional improvement. FASEB J. 2000 Apr;14(5):669-79.

Fredj S, Bescond J, Louault C, Potreau D. Interactions between cardiac cells enhance cardiomyocyte hypertrophy and increase fibroblast proliferation. J Cell Physiol. 2005 Mar;202(3):891-9.

Fredj S, Bescond J, Louault C, Delwail A, Lecron JC, Potreau D. Role of interleukin-6 in cardiomyocyte/cardiac fibroblast interactions during myocyte hypertrophy and fibroblast proliferation. J Cell Physiol. 2005 Aug;204(2):428-36. .

Gaudesius G, Miragoli M, Thomas SP, Rohr S. Coupling of cardiac electrical activity over extended distances by fibroblasts of cardiac origin. Circ Res. 2003 Sep 5;93(5):421-8.

Gray MO, Long CS, Kalinyak JE, Li HT, Karliner JS. Angiotensin II stimulates cardiac myocyte hypertrophy via paracrine release of TGF-β_1 and endothelin-1 from fibroblasts. Cardiovascular Research Nov 1998, 40 (2) 352-363.

Guccione JM, Le Prell GS, de Tombe PP, Hunter WC. Measurements of active myocardial tension under a wide range of physiological loading conditions. J Biomech. 1997 Feb;30(2):189-92

Gupta MP. Factors controlling cardiac myosin-isoform shift during hypertrophy and heart failure. J Mol Cell Cardiol. 2007 Oct;43(4):388-403.

Hao J, Wang B, Jones SC, Jassal DS, Dixon IM. Interaction between angiotensin II and Smad proteins in fibroblasts in failing heart and in vitro. Am J Physiol

Heart Circ Physiol. 2000 Dec;279(6):H3020-30.

Hattori F, Chen H, Yamashita H, Tohyama S, Satoh Y, Yuasa S, Li W, Yamakawa H, Tanaka T, Onitsuka T, et al. Nongenetic method for purifying stem cell–derived cardiomyocytes. Nature Methods. 2010 Jan;7: 61 - 66

Herron TJ, McDonald KS. Small amounts of alpha-myosin heavy chain isoform expression significantly increase power output of rat cardiac myocyte fragments. Circ Res. 2002 Jun 14;90(11):1150-2.

Hinson JT, Chopra A, Nafissi N, Polacheck WJ, Benson CC, Swist S, Gorham J, Yang L, Schafer S, Sheng CC, Haghighi A, Homsy J, Hubner N, Church G, Cook SA, Linke WA, Chen CS, Seidman JG, Seidman CE. HEART DISEASE. Titin mutations in iPS cells define sarcomere insufficiency as a cause of dilated cardiomyopathy. Science. 2015 Aug 28;349(6251):982-6.

Hirt MN, Sörensen NA, Bartholdt LM, Boeddinghaus J, Schaaf S, Eder A, Vollert I, Stöhr A, Schulze T, Witten A, Stoll M, Hansen A, Eschenhagen T. Increased afterload induces pathological cardiac hypertrophy: a new in vitro model. Basic Res Cardiol. 2012 Nov;107(6):307.

Horton RE, Yadid M, McCain ML, Sheehy SP, Pasqualini FS, Park SJ, Cho A, Campbell P, Parker KK. Angiotensin II Induced Cardiac Dysfunction on a Chip. PLoS One. 2016 Jan 25; 11(1).

Iravanian S, Sovari AA, Lardin HA, Liu H, Xiao HD, Dolmatova E, Jiao Z, Harris BS, Witham EA, Gourdie RG, Duffy HS, Bernstein KE, Dudley SC Jr. Inhibition of renin-angiotensin system (RAS) reduces ventricular tachycardia risk by altering connexin43. J Mol Med (Berl).2011 Jul;89(7):677-87.

Iwanaga Y, Kihara Y, Inagaki K, Onozawa Y, Yoneda T, Kataoka K, Sasayama S. Differential effects of angiotensin II versus endothelin-1 inhibitions in hypertrophic left ventricular myocardium during transition to heart failure. Circulation. 2001 Jul 31;104(5):606-12.

Kakkar R, Lee RT. Intramyocardial fibroblast myocyte communication. Circ Res. 2010 Jan 8; 106(1):47-57.

Kellar RS, Shepherd BR, Larson DF, Naughton GK, Williams SK. Cardiac patch constructed from human fibroblasts attenuates reduction in cardiac function after acute infarct. Tissue Eng. 2005 Nov-Dec;11(11-12):1678-87.

Kohl P, Gourdie RG. Fibroblast-myocyte electrotonic coupling: does it occur in native cardiac tissue? J Mol Cell Cardiol. 2014 May;70:37-46.

Konhilas JP, Irving TC, De Tomb PP. Frank-Starling law of the heart and the cellular mechanisms of length-dependent activation. Pflugers Arch. 2002 445: 305–310

Koitabashi N, Danner T, Zaiman AL, Pinto YM, Rowell J, Mankowski J, Zhang D, Nakamura T, Takimoto E, Kass DA. Pivotal role of cardiomyocyte TGF-β signaling in the murine pathological response to sustained pressure overload. J Clin Invest. 2011 Jun;121(6):2301-12

Krüger M, Sachse C, Zimmermann WH, Eschenhagen T, Klede S, Linke WA. Thyroid hormone regulates developmental titin isoform transitions via the phosphatidylinositol-3-kinase/ AKT pathway. Circ Res. 2008 Feb 29;102(4):439-47.

Jacot JG, McCulloch AD, Omens JH. Substrate stiffness affects the functional maturation of neonatal rat ventricular myocytes. Biophys J. 2008 Oct;95(7):3479-87

Janssen PM. Kinetics of cardiac muscle contraction and relaxation are linked and determined by properties of the cardiac sarcomere. Am J Physiol Heart Circ Physiol. 2010 Oct;299(4):H1092-9.

Layland J, Grieve DJ, Cave AC, Sparks E, Solaro RJ, Shah AM. Essential role of troponin I in the positive inotropic response to isoprenaline in mouse hearts contracting auxotonically. J Physiol. 2004 May 1;556(Pt 3):835-47.

LaFramboise WA, Scalise D, Stoodley P, Graner SR, Guthrie RD, Magovern JA, Becich MJ. Cardiac fibroblasts influence cardiomyocyte phenotype in vitro. Am J Physiol Cell Physiol. 2007 May;292(5):C1799-808.

Lal H, Guleria RS, Foster DM, Lu G, Watson LE, Sanghi S, Smith M, Dostal DE. I Ontegrins: novel therapeutic targets for cardiovascular diseases. Cardiovasc Hematol Agents Med Chem. 2007 Apr;5(2):109-32.

Lal H, Verma SK, Foster DM, Golden HB, Reneau JC, Watson LE, Singh H, Dostal DE. I ntegrins and proximal signaling mechanisms in cardiovascular disease. Front Biosci. 2009 Jan 1;14:2307-34.

Laser M, Willey CD, Jiang W, Cooper Gt, Menick DR, Zile MR, Kuppuswamy D. Integrin activation and focal complex formation in cardiac hypertrophy. J Biol Chem.2000;275:35624–35630.

Legant WR, Pathak A, Yang MT, Deshpande VS, McMeeking RM, Chen CS. Microfabricated tissue gauges to measure and manipulate forces from 3D microtissues. Proc Natl Acad Sci U S A. 2009 Jun 23;106(25):10097-102. doi: 10.1073/pnas.0900174106.

LeWinter MM, Granzier HL. Titin is a major human disease gene. Circulation. 2013 Feb 26;127(8):938-44.

Li P, Sonnenblick EH, Anversa P, Capasso JM. Length-dependent modulation of ANG II inotropism in rat myocardium: effects of myocardial infarction. Am J Physiol. 1994 Feb;266(2 Pt 2):H779-86.

Li YY, Feldman AM, Sun Y, McTiernan CF. Differential expression of tissue inhibitors of metalloproteinases in the failing human heart. Circulation. 1998 Oct 27;98(17):1728-34.

MacGowan GA, Koretsky AP. Inotropic and energetic effects of altering the force-calcium relationship: mechanisms, experimental results, and potential molecular targets. J Card Fail. 2000 Jun;6(2):144-56. Review.

Malhotra R, Sadoshima J, Brosius FC 3rd, Izumo S. Mechanical stretch and angiotensin II differentially upregulate the renin-angiotensin system in cardiac myocytes In vitro. Circ Res. 1999 Jul 23;85(2):137-46.

Mann DL, Bristow MR. Mechanisms and models in heart failure: the biomechanical model and beyond. Circulation. 2005 May 31;111(21):2837-49.

Martin ML, Blaxall BC. Cardiac intercellular communication: are myocytes and fibroblasts fair-weather friends? J Cardiovasc Transl Res. 2012 Dec;5(6):768-82.

Matsusaka T, Katori H, Inagami T, Fogo A, Ichikawa I. Communication between myocytes and fibroblasts in cardiac remodeling in angiotensin chimeric mice. J Clin Invest. 1999 May 15;103(10):1451-8.

McCain ML, Sheehy SP, Grosberg A, Goss JA, Parker KK. Recapitulating maladaptive, multiscale remodeling of failing myocardium on a chip. Proc Natl Acad Sci U S A. 2013 Jun 11;110(24):9770-5.

McCain ML, Yuan H, Pasqualini FS, Campbell PH, Parker KK. Matrix elasticity regulates the optimal cardiac myocyte shape for contractility. Am J Physiol Heart Circ Physiol. 2014 Jun 1;306(11):H1525-39.

Mezzano V, Sheikh F. Cell-cell junction remodeling in the heart: possible role in cardiac conduction system function and arrhythmias?. Life Sci. 2012 Feb 27;90(9-10): 313-315.

Miragoli M, Gaudesius G, Rohr S. Electrotonic modulation of cardiac impulse conduction by myofibroblasts. Circ Res. 2006 Mar 31;98(6):801-10.

Naito H, Melnychenko I, Didié M, Schneiderbanger K, Schubert P, Rosenkranz S, Eschenhagen T, Zimmermann WH. Optimizing engineered heart tissue for therapeutic applications as surrogate heart muscle. Circulation. 2006 Jul 4;114(1 Suppl):I72-8.

Nichol JW, Engelmayr GC Jr, Cheng M, Freed LE. Co-culture induces alignment in engineered cardiac constructs via MMP-2 expression. Biochem Biophys Res Commun. 2008 Aug 29;373(3):360-5.

Nguyen PD, Hsiao ST, Sivakuaran P, Lim SY, Dilley RJ. Enrichment of neonatal rat cardiomyocytes in primary culture facilities long-term maintenance of contractility in vitro. Am J Physiol Cell Physiol. 2012 Aug 29:303:1220-1228

Olson ER, Shamhart PE, Naugle JE, Meszaros JG. Angiotensin II-induced extracellular signal-regulated kinase 1/2 activation is mediated by protein kinase C delta and intracellular calcium in adult rat cardiac fibroblasts. Hypertension. 2008 Mar;51(3):704-11.

Ongstad EL, Gourdie RG. Myocyte-fibroblast electrical coupling: the basis of a stable relationship? Cardiovasc Res. 2012 Feb 1;93(2):215-7.

Ongstad E, Kohl P. Fibroblast-myocyte coupling in the heart: Potential relevance for therapeutic interventions. J Mol Cell Cardiol. 2016 Feb;91:238-46.

Ongstad EL, O'Quinn MP, Ghatnekar GS, Yost MJ, Gourdie RG. A Connexin43 Mimetic Peptide Promotes Regenerative Healing and Improves Mechanical Properties in Skin and Heart. Adv Wound Care (New Rochelle). 2013 Mar;2(2):55-62.

Ottaviano FG, Yee KO. Communication signals between cardiac fibroblasts and cardiac myocytes. J Cardiovasc Pharmacol. 2011 May;57(5):513-21.

Piuhola J, Mäkinen M, Szokodi I, Ruskoaho H. Dual role of endothelin-1 via ETA and ETB receptors in regulation of cardiac contractile function in mice. Am J Physiol Heart Circ Physiol. 2003 Jul;285(1):H112-8.

Palomeque J, Sapia L, Hajjar RJ, Mattiazzi A, Petroff MV. Angiotensin II-induced negative inotropy in rat ventricular myocytes: role of reactive oxygen species and p38 MAPK. American Journal of Physiology - Heart and Circulatory Physiology Jan 2006, 290 (1) H96-H106;

Pedrotty DM, Klinger RY, Kirkton RD, Bursac N. Cardiac fibroblast paracrine factors alter impulse conduction and ion channel expression of neonatal rat cardiomyocytes. Cardiovasc Res. 2009 Sep 1;83(4):688-97.

Radisic, M., Euloth, M., Yang, L., Langer, R., Freed, L.E., and Vunjak-Novakovic, G. High-density seeding of myocyte cells for cardiac tissue engineering. Biotechnol Bioeng 82, 403, 2003.

Radisic M, Deen W, Langer R, Vunjak-Novakovic G. Mathematical model of oxygen distribution in engineered cardiac tissue with parallel channel array perfused with culture medium containing oxygen carriers. Am J Physiol Heart Circ Physiol. 2005 Mar;288(3):H1278-89.

Radisic M, Park H, Martens TP, Salazar-Lazaro JE, Geng W, Wang Y, Langer R, Freed LE, Vunjak-Novakovic G. Pre-treatment of synthetic elastomeric scaffolds by cardiac fibroblasts improves engineered heart tissue. J Biomed Mater Res A. 2008 Sep;86(3):713-24.

Radisic M, Park H, Shing H, Consi T, Schoen FJ, Langer R, Freed LE, Vunjak-Novakovic G. Functional assembly of engineered myocardium by electrical stimulation of cardiac myocytes cultured on scaffolds. Proc Natl Acad Sci U S A. 2004 Dec 28;101(52):18129-34.

Radisic M, Yang L, Boublik J, Cohen RJ, Langer R, Freed LE, Vunjak-Novakovic G. Medium perfusion enables engineering of compact and contractile cardiac tissue. Am J Physiol Heart Circ Physiol. 2004 Feb;286(2):H507-16.

Raman S, Kelley MA, Janssen PML. Effect of muscle dimensions on trabecular contractile performance under physiological conditions. Pflugers Arch – Eur J Physiol. 2005 Aug; 451: 625–630

Ravenscroft SM, Pointon A, Williams AW, Cross MJ, Sidaway JE. Cardiac Non-myocyte Cells Show Enhanced Pharmacological Function Suggestive of Contractile Maturity in Stem Cell Derived Cardiomyocyte Microtissues. Toxicol Sci. 2016 Jul;152(1):99-112.

Rivard K, Paradis P, Nemer M, Fiset C. Cardiac-specific overexpression of the human type 1 angiotensin II receptor causes delayed repolarization. Cardiovasc Res. 2008 Apr 1;78(1):53-62.

Rohr S. Cardiac fibroblasts in cell culture systems: myofibroblasts all along? J Cardiovasc Pharmacol. 2011 Apr;57(4):389-99.

Rosenkranz S, Flesch M, Amann K, Haeuseler C, Kilter H, Seeland U, Schlüter KD, Michael Böhm. Alterations of β-adrenergic signaling and cardiac hypertrophy in transgenic mice overexpressing TGF-β_1. American Journal of Physiology - Heart and Circulatory Physiology. 2002 Sep; 283 (3) H1253-H1262.

Rossman EI, Petre RE, Chaudhary KW, Piacentino V, Janssen PML, Gaughan JP, Houser SR, Margulies KB. Abnormal frequency-dependent responses represent the pathophysiologic signature of contractile failure in human myocardium. Journal of Molecular and Cellular Cardiology. 2003 Sep; 36: 33–42

Sadoshima J, Xu Y, Slayter HS, Izumo S. Autocrine release of angiotensin II mediates stretch-induced hypertrophy of cardiac myocytes in vitro. Cell. 1993 Dec 3;75(5):977-84.

Sadoshima J, Izumo S. Molecular characterization of angiotensin II--induced hypertrophy of cardiac myocytes and hyperplasia of cardiac fibroblasts. Critical role of the AT1 receptor subtype. Circ Res. 1993 Sep;73(3):413-23.

Schaefer KL, Porter JA. Angiotensin II receptor antagonists: the prototype losartan. Ann Pharmacother. 1996 Jun;30(6):625-36.

Schaub MC, Hefti MA, Harder BA, Eppenberger HM. Various hypertrophic stimuli induce distinct phenotypes in cardiomyocytes. J Mol Med (Berl). 1997 Nov-Dec;75(11-12):901-20.

Sarkar S, Vellaichamy E, Young D, Sen S. Influence of cytokines and growth factors in ANG II-mediated collagen upregulation by fibroblasts in rats: role of myocytes. Am J Physiol Heart Circ Physiol. 2004 Jul;287(1):H107-17.

Sadoshima J, Izumo S. Molecular characterization of angiotensin II--induced hypertrophy of cardiac myocytes and hyperplasia of cardiac fibroblasts. Critical role of the AT1 receptor subtype. Circ Res. 1993 Sep;73(3):413-23.

Schultz J, Witt SA, Glascock BJ, Nieman ML, Reiser PJ, Nix SL, Kimball TR, Doetschman T. TGF-beta1 mediates the hypertrophic cardiomyocyte growth induced by angiotensin II. J Clin Invest. 2002 Mar;109(6):787-96.

Stastna M, Van Eyk JE. Investigating the secretome: lessons about the cells that comprise the heart. Circ Cardiovasc Genet. 2012 Feb 1;5(1):o8-o18.

Schaaf S, Shibamiya A, Mewe M, Eder A, Stöhr A, Hirt MN, Rau T, Zimmermann WH, Conradi L, Eschenhagen T, Hansen A. Human engineered heart tissue as a versatile tool in basic research and preclinical toxicology. PLoS One. 2011;6(10):e26397.

Sil P, Sen S. Angiotensin II and myocyte growth: role of fibroblasts. Hypertension. 1997 Aug;30(2 Pt 1):209-16.

Rodriguez AG, Han SJ, Regnier M, Sniadecki NJ. Substrate Stiffness Increases Twitch Power of Neonatal Cardiomyocytes in Correlation with Changes in Myofibril Structure and Intracellular Calcium. Biophysical Journal. 2011;101(10):2455-2464.

Souders CA, Bowers SL, Baudino TA. Cardiac fibroblast: the renaissance cell. Circ Res. 2009 Dec 4;105(12):1164-76.

Souders CA, Borg TK, Banerjee I, Baudino TA. Pressure overload induces early morphological changes in the heart. Am J Pathol. 2012 Oct;181(4):1226-35.

Song H, Zandstra PW, Radisic M. Engineered heart tissue model of diabetic myocardium. Tissue Eng Part A. 2011 Jul;17(13-14):1869-78.

Stevens KR, Kreutziger KL, Dupras SK, Korte FS, Regnier M, Muskheli V, Nourse MB, Bendixen K, Reinecke H, Murry CE. Physiological function and transplantation of scaffold-free and vascularized human cardiac muscle tissue. Proc Natl Acad Sci U S A. 2009 Sep 29;106(39):16568-73.

Stevens KR, Pabon L, Muskheli V, Murry CE. Scaffold-free human cardiac tissue patch created from embryonic stem cells. Tissue Eng Part A. 2009 Jun;15(6):1211-22.

ter Keurs HE, Shinozaki T, Zhang YM, Zhang ML, Wakayama Y, Sugai Y, Kagaya Y, Miura M, Boyden PA, Stuyvers BD, Landesberg A. Sarcomere mechanics in uniform and non-uniform cardiac muscle: a link between pump function and arrhythmias.Prog Biophys Mol Biol. 2008 Jun-Jul;97(2-3):312-31.

Takeda N, Manabe I. Cellular Interplay between Cardiomyocytes and Nonmyocytes in Cardiac Remodeling. Int J Inflam. 2011;2011:535241.

Thompson SA, Copeland CR, Reich DH, Tung L. Mechanical coupling between myofibroblasts and cardiomyocytes slows electric conduction in fibrotic cell monolayers. Circulation. 2011 May 17;123(19):2083-93.

Thompson SA, Blazeski A,Copeland CR, Cohen DM, Chen CS, Reich DM, Tung L. Acute slowing of cardiac conduction in response to myofibroblast coupling to cardiomyocytes through N-cadherin. J Mol Cell Cardiol. 2014 Mar;68:29-37.

Torre I, González-Tendero A, García-Cañadilla P, Crispi F, García-García F, Bijnens B, Iruretagoyena I, Dopazo J, Amat-Roldán I, Gratacós E. Permanent cardiac sarcomere changes in a rabbit model of intrauterine growth restriction. PLoS One. 2014 Nov 17;9(11):e113067

Tulloch NL, Muskheli V, Razumova MV, Korte FS, Regnier M, Hauch KD, Pabon L, Reinecke H, Murry CE. Growth of engineered human myocardium with mechanical loading and vascular coculture. Circ Res. 2011 Jun 24;109(1):47-59.

Vasquez C, Benamer N, Morley GE. The cardiac fibroblast: functional and electrophysiological considerations in healthy and diseased hearts. J Cardiovasc Pharmacol. 2011 Apr;57(4):380-8.

Wang H, Svoronos AA, Boudou T, Sakar MS, Schell JY, Morgan JR, Chen CS, Shenoy VB. Necking and failure of constrained 3D microtissues induced by cellular tension. Proc Natl Acad Sci U S A. 2013 Dec 24;110(52):20923-8.

Wang J, Chen H, Seth A, McCulloch CA. Mechanical force regulation of myofibroblast differentiation in cardiac fibroblasts. Am J Physiol Heart Circ Physiol. 2003 Nov;285(5):H1871-81.

Xu J, Carretero OA, Lin CX, Cavasin MA, Shesely EG, Yang JJ, Reudelhuber TL, Yang XP. Role of cardiac overexpression of ANG II in the regulation of cardiac function and remodeling postmyocardial infarction. Am J Physiol Heart Circ Physiol. 2007 Sep;293(3):H1900-7.

Yang X, Rodriguez M, Pabon L, Fischer KA, Reinecke H, Regnier M, Sniadecki NJ, Ruohola-Baker H, Murry CE. Tri-iodo-l-thyronine promotes the maturation of human cardiomyocytes-derived from induced pluripotent stem cells. J Mol Cell Cardiol. 2014 Jul;72:296-304.

Zhang P, Su J, Mende U. Cross talk between cardiac myocytes and fibroblasts: from multiscale investigative approaches to mechanisms and functional consequences. Am J Physiol Heart Circ Physiol. 2012 Dec;303(12):H1385-96.

Zimmermann WH, Didié M, Döker S, Melnychenko I, Naito H, Rogge C, Tiburcy M, Eschenhagen T.Heart muscle engineering: an update on cardiac muscle replacement therapy. Cardiovasc Res. 2006 Aug 1;71(3):419-29. Epub 2006 Apr 7.

APPENDIX

STATISTICAL ANALYSIS

Variable Labels:

Stffness		Factor
0 (k=0.20uN/um)	Untreated	0
	Cocktail	1
	TGF-B	2
	Ang II	3
	ET-1	4
1 (k=0.45uN/um)	Untreated	0
	Cocktail	1
	TGF-B	2
	Ang II	3
	ET-1	4

A1.1 RESTING FORCE

Univariate Analysis of Variance

Between-Subjects Factors

		N
Stiffness	0	147
	1	141
Factor	0	63
	1	57
	2	63
	3	60
	4	55

Tests of Between-Subjects Effects

Dependent Variable: Delta1

Source	Type III Sum of Squares	df	Mean Square	F	Sig.
Corrected Model	1148.372[a]	9	127.597	23.269	.000
Intercept	2659.370	1	2659.370	484.979	.000
Stiffness	70.462	1	70.462	12.850	.000
Factor	834.540	4	208.635	38.048	.000
Stiffness * Factor	67.147	4	16.787	3.061	.017
Error	1853.414	338	5.483		
Total	5542.352	348			
Corrected Total	3001.786	347			

a. R Squared = .383 (Adjusted R Squared = .366)

Estimated Marginal Means

1. Stiffness * Factor

Estimates

Dependent Variable: Delta1

Stiffness	Factor	Mean	Std. Error	95% Confidence Interval	
				Lower Bound	Upper Bound
0	0	.603	.295	.023	1.183
	1	4.670	.375	3.933	5.408
	2	.808	.361	.097	1.518
	3	2.534	.396	1.756	3.313
	4	3.699	.443	2.828	4.569
1	0	1.368	.428	.527	2.209
	1	4.172	.552	3.086	5.258
	2	1.322	.511	.317	2.327
	3	4.088	.349	3.401	4.775
	4	6.152	.451	5.266	7.039

Pairwise Comparisons

Dependent Variable: Delta1

Factor	(I) Stiffness	(J) Stiffness	Mean Difference (I-J)	Std. Error	Sig.[b]	95% Confidence Interval for Difference[b] Lower Bound	Upper Bound
0	0	1	-.765	.519	.142	-1.787	.257
	1	0	.765	.519	.142	-.257	1.787
1	0	1	.498	.667	.456	-.814	1.811
	1	0	-.498	.667	.456	-1.811	.814
2	0	1	-.514	.626	.412	-1.745	.717
	1	0	.514	.626	.412	-.717	1.745
3	0	1	-1.554*	.528	.003	-2.592	-.516
	1	0	1.554*	.528	.003	.516	2.592
4	0	1	-2.453*	.632	.000	-3.696	-1.211
	1	0	2.453*	.632	.000	1.211	3.696

Based on estimated marginal means

*. The mean difference is significant at the .05 level.

b. Adjustment for multiple comparisons: Bonferroni.

Univariate Tests

Dependent Variable: Delta1

Factor		Sum of Squares	df	Mean Square	F	Sig.
0	Contrast	11.893	1	11.893	2.169	.142
	Error	1853.414	338	5.483		
1	Contrast	3.059	1	3.059	.558	.456
	Error	1853.414	338	5.483		
2	Contrast	3.703	1	3.703	.675	.412
	Error	1853.414	338	5.483		
3	Contrast	47.535	1	47.535	8.669	.003
	Error	1853.414	338	5.483		
4	Contrast	82.742	1	82.742	15.089	.000
	Error	1853.414	338	5.483		

Each F tests the simple effects of Stiffness within each level combination of the other effects shown. These tests are based on the linearly independent pairwise comparisons among the estimated marginal means.

2. Stiffness * Factor

Estimates

Dependent Variable: Delta1

Stiffness	Factor	Mean	Std. Error	95% Confidence Interval	
				Lower Bound	Upper Bound
0	0	.603	.295	.023	1.183
	1	4.670	.375	3.933	5.408
	2	.808	.361	.097	1.518
	3	2.534	.396	1.756	3.313
	4	3.699	.443	2.828	4.569
1	0	1.368	.428	.527	2.209
	1	4.172	.552	3.086	5.258
	2	1.322	.511	.317	2.327
	3	4.088	.349	3.401	4.775
	4	6.152	.451	5.266	7.039

Pairwise Comparisons

Dependent Variable: Delta1

Stiffness	(I) Factor	(J) Factor	Mean Difference (I-J)	Std. Error	Sig.[b]	95% Confidence Interval for Difference[b]	
						Lower Bound	Upper Bound
0	0	1	-4.068*	.477	.000	-5.416	-2.719
		2	-.205	.466	1.000	-1.523	1.113
		3	-1.931*	.494	.001	-3.326	-.536
		4	-3.096*	.532	.000	-4.599	-1.593
	1	0	4.068*	.477	.000	2.719	5.416
		2	3.863*	.521	.000	2.391	5.334
		3	2.136*	.545	.001	.596	3.677
		4	.972	.580	.948	-.667	2.611
	2	0	.205	.466	1.000	-1.113	1.523
		1	-3.863*	.521	.000	-5.334	-2.391
		3	-1.727*	.536	.014	-3.241	-.212
		4	-2.891*	.571	.000	-4.505	-1.277
	3	0	1.931*	.494	.001	.536	3.326
		1	-2.136*	.545	.001	-3.677	-.596

		2	1.727*	.536	.014	.212	3.241
		4	-1.165	.594	.506	-2.842	.513
	4	0	3.096*	.532	.000	1.593	4.599
		1	-.972	.580	.948	-2.611	.667
		2	2.891*	.571	.000	1.277	4.505
		3	1.165	.594	.506	-.513	2.842
1	0	1	-2.804*	.698	.001	-4.777	-.831
		2	.046	.666	1.000	-1.837	1.929
		3	-2.720*	.552	.000	-4.280	-1.161
		4	-4.784*	.621	.000	-6.539	-3.029
	1	0	2.804*	.698	.001	.831	4.777
		2	2.850*	.752	.002	.725	4.976
		3	.084	.653	1.000	-1.761	1.929
		4	-1.980	.713	.058	-3.993	.033
	2	0	-.046	.666	1.000	-1.929	1.837
		1	-2.850*	.752	.002	-4.976	-.725
		3	-2.766*	.619	.000	-4.515	-1.018
		4	-4.830*	.681	.000	-6.755	-2.905
	3	0	2.720*	.552	.000	1.161	4.280
		1	-.084	.653	1.000	-1.929	1.761
		2	2.766*	.619	.000	1.018	4.515
		4	-2.064*	.570	.003	-3.675	-.453
	4	0	4.784*	.621	.000	3.029	6.539
		1	1.980	.713	.058	-.033	3.993
		2	4.830*	.681	.000	2.905	6.755
		3	2.064*	.570	.003	.453	3.675

Based on estimated marginal means

*. The mean difference is significant at the .05 level.

b. Adjustment for multiple comparisons: Bonferroni.

Univariate Tests

Dependent Variable: Delta1

Stiffness		Sum of Squares	df	Mean Square	F	Sig.
0	Contrast	546.544	4	136.636	24.918	.000
	Error	1853.414	338	5.483		
1	Contrast	449.610	4	112.402	20.498	.000
	Error	1853.414	338	5.483		

Each F tests the simple effects of Factor within each level combination of the other effects shown. These tests are based on the linearly independent pairwise comparisons among the estimated marginal means.

Univariate Analysis of Variance

Between-Subjects Factors

		N
Stiffness	0	148
	1	141
Factor	0	64
	1	57
	2	63
	3	60
	4	55

Tests of Between-Subjects Effects

Dependent Variable: Delta2

Source	Type III Sum of Squares	df	Mean Square	F	Sig.
Corrected Model	105.084[a]	9	11.676	2.768	.004
Intercept	488.906	1	488.906	115.896	.000
Stiffness	.501	1	.501	.119	.731
Factor	48.335	4	12.084	2.864	.023
Stiffness * Factor	37.994	4	9.498	2.252	.063
Error	1430.066	339	4.218		
Total	2010.312	349			
Corrected Total	1535.151	348			

Estimated Marginal Means

1. Stiffness * Factor

Estimates

Dependent Variable: Delta2

Stiffness	Factor	Mean	Std. Error	95% Confidence Interval	
				Lower Bound	Upper Bound
0	0	.366	.257	-.139	.871
	1	1.643	.329	.996	2.290
	2	.991	.317	.368	1.615
	3	1.038	.347	.356	1.721
	4	2.467	.388	1.703	3.230
1	0	1.403	.375	.665	2.140
	1	1.243	.484	.291	2.195
	2	.875	.448	-.007	1.756
	3	1.118	.306	.516	1.721
	4	1.463	.395	.686	2.241

Pairwise Comparisons

Dependent Variable: Delta2

Factor	(I) Stiffness	(J) Stiffness	Mean Difference (I-J)	Std. Error	Sig.[b]	95% Confidence Interval for Difference[b]	
						Lower Bound	Upper Bound
0	0	1	-1.036*	.454	.023	-1.930	-.142
	1	0	1.036*	.454	.023	.142	1.930
1	0	1	.400	.585	.495	-.752	1.551
	1	0	-.400	.585	.495	-1.551	.752
2	0	1	.116	.549	.832	-.963	1.196
	1	0	-.116	.549	.832	-1.196	.963
3	0	1	-.080	.463	.863	-.990	.831
	1	0	.080	.463	.863	-.831	.990
4	0	1	1.004	.554	.071	-.086	2.093
	1	0	-1.004	.554	.071	-2.093	.086

Based on estimated marginal means

*. The mean difference is significant at the .05 level.

b. Adjustment for multiple comparisons: Bonferroni.

Univariate Tests

Dependent Variable: Delta2

Factor		Sum of Squares	df	Mean Square	F	Sig.
0	Contrast	21.937	1	21.937	5.200	.023
	Error	1430.066	339	4.218		
1	Contrast	1.967	1	1.967	.466	.495
	Error	1430.066	339	4.218		
2	Contrast	.190	1	.190	.045	.832
	Error	1430.066	339	4.218		
3	Contrast	.126	1	.126	.030	.863
	Error	1430.066	339	4.218		
4	Contrast	13.845	1	13.845	3.282	.071
	Error	1430.066	339	4.218		

Each F tests the simple effects of Stiffness within each level combination of the other effects shown. These tests are based on the linearly independent pairwise comparisons among the estimated marginal means.

2. Stiffness * Factor

Estimates

Dependent Variable: Delta2

				95% Confidence Interval	
Stiffness	Factor	Mean	Std. Error	Lower Bound	Upper Bound
0	0	.366	.257	-.139	.871
	1	1.643	.329	.996	2.290
	2	.991	.317	.368	1.615
	3	1.038	.347	.356	1.721
	4	2.467	.388	1.703	3.230
1	0	1.403	.375	.665	2.140
	1	1.243	.484	.291	2.195
	2	.875	.448	-.007	1.756
	3	1.118	.306	.516	1.721
	4	1.463	.395	.686	2.241

Pairwise Comparisons

Dependent Variable: Delta2

Stiffness	(I) Factor	(J) Factor	Mean Difference (I-J)	Std. Error	Sig.[b]	95% Confidence Interval for Difference[b]	
						Lower Bound	Upper Bound
0	0	1	-1.276*	.417	.024	-2.455	-.098
		2	-.625	.408	1.000	-1.777	.527
		3	-.672	.432	1.000	-1.892	.548
		4	-2.101*	.465	.000	-3.416	-.786
	1	0	1.276*	.417	.024	.098	2.455
		2	.651	.457	1.000	-.639	1.942
		3	.604	.478	1.000	-.747	1.955
		4	-.824	.509	1.000	-2.262	.613
	2	0	.625	.408	1.000	-.527	1.777
		1	-.651	.457	1.000	-1.942	.639
		3	-.047	.470	1.000	-1.375	1.281
		4	-1.476*	.501	.035	-2.891	-.060
	3	0	.672	.432	1.000	-.548	1.892
		1	-.604	.478	1.000	-1.955	.747
		2	.047	.470	1.000	-1.281	1.375
		4	-1.428	.521	.064	-2.900	.043
	4	0	2.101*	.465	.000	.786	3.416
		1	.824	.509	1.000	-.613	2.262
		2	1.476*	.501	.035	.060	2.891
		3	1.428	.521	.064	-.043	2.900
1	0	1	.160	.612	1.000	-1.571	1.890
		2	.528	.584	1.000	-1.123	2.179
		3	.284	.484	1.000	-1.084	1.652
		4	-.061	.545	1.000	-1.600	1.479
	1	0	-.160	.612	1.000	-1.890	1.571
		2	.368	.660	1.000	-1.496	2.232
		3	.125	.573	1.000	-1.494	1.743
		4	-.220	.625	1.000	-1.986	1.546
	2	0	-.528	.584	1.000	-2.179	1.123
		1	-.368	.660	1.000	-2.232	1.496
		3	-.244	.543	1.000	-1.777	1.290

		4	-.588	.598	1.000	-2.277	1.100
	3	0	-.284	.484	1.000	-1.652	1.084
		1	-.125	.573	1.000	-1.743	1.494
		2	.244	.543	1.000	-1.290	1.777
		4	-.345	.500	1.000	-1.758	1.068
	4	0	.061	.545	1.000	-1.479	1.600
		1	.220	.625	1.000	-1.546	1.986
		2	.588	.598	1.000	-1.100	2.277
		3	.345	.500	1.000	-1.068	1.758

Based on estimated marginal means

*. The mean difference is significant at the .05 level.

b. Adjustment for multiple comparisons: Bonferroni.

Univariate Tests

Dependent Variable: Delta2

Stiffness		Sum of Squares	df	Mean Square	F	Sig.
0	Contrast	98.725	4	24.681	5.851	.000
	Error	1430.066	339	4.218		
1	Contrast	5.571	4	1.393	.330	.858
	Error	1430.066	339	4.218		

Each F tests the simple effects of Factor within each level combination of the other effects shown. These tests are based on the linearly independent pairwise comparisons among the estimated marginal means.

A1.2 TWITCH FORCE

Between-Subjects Factors

		N
Stiffness	0	168
	1	170
Factor	0	69
	1	69
	2	70
	3	66
	4	64

Stffness	Factor	Mean	Std. Deviation	N
0	0	.027428568	.334036159	34
	1	1.355063523	.676761051	32
	2	-.214188235	.345381049	34
	3	.690377438	.560129429	33
	4	1.01427437	.804048889	30
	Total	.51417974	.808348989	168
1	0	.292331741	1.85785923	35
	1	.712532796	.529729433	35
	2	-1.028741593	1.012925404	33
	3	1.22886219	1.058981894	33
	4	.94952217	1.043201413	33
	Total	.480952935	1.388468168	170
Total	0	.115729626	1.100678987	69
	1	1.083995873	.692687516	67
	2	-.496149013	.756509807	67
	3	.921156618	.846310096	66
	4	.986879208	.903752674	63
	Total	.501357315	1.068016945	298

Tests of Between-Subjects Effects

Dependent Variable: Force

Source	Type III Sum of Squares	df	Mean Square	F	Sig.	Partial Eta Squared
Corrected Model	125.455[a]	9	13.939	18.819	.000	.370
Intercept	68.925	1	68.925	93.054	.000	.244
Stffness	1.408	1	1.408	1.900	.169	.007
Factor	107.234	4	26.809	36.194	.000	.335
Stffness * Factor	17.839	4	4.460	6.021	.000	.077
Error	213.321	288	.741			
Total	413.681	298				
Corrected Total	338.776	297				

a. R Squared = .370 (Adjusted R Squared = .351)

Estimates

Dependent Variable: Force

Stffness	Factor	Mean	Std. Error	95% Confidence Interval	
				Lower Bound	Upper Bound
0	0	.027	.117	-.203	.258
	1	1.355	.141	1.077	1.634
	2	-.214	.148	-.505	.076
	3	.690	.163	.370	1.011
	4	1.014	.157	.705	1.324
1	0	.292	.166	-.034	.618
	1	.713	.166	.387	1.039
	2	-1.029	.203	-1.428	-.629
	3	1.229	.188	.859	1.599
	4	.950	.183	.588	1.311

Stiffness	(I) Factor	(J) Factor	Mean Difference (I-J)	Std. Error	Sig.[b]	95% Confidence Interval for Difference[b]	
						Lower Bound	Upper Bound
0	0	1	1.328*	0.184	0	-1.847	-0.808
		2	0.242	0.188	1	-0.291	0.775
		3	-.663*	0.2	0.011	-1.23	-0.096
		4	-.987*	0.196	0	-1.541	-0.432
	1	0	1.328*	0.184	0	0.808	1.847
		2	1.569*	0.204	0	0.991	2.148
		3	.665*	0.216	0.022	0.055	1.275
		4	0.341	0.211	1	-0.257	0.939
	2	0	-0.242	0.188	1	-0.775	0.291
		1	-1.569*	0.204	0	-2.148	-0.991
		3	-.905*	0.22	0	-1.526	-0.283
		4	-1.228*	0.216	0	-1.838	-0.619
	3	0	.663*	0.2	0.011	0.096	1.23
		1	-.665*	0.216	0.022	-1.275	-0.055
		2	.905*	0.22	0	0.283	1.526
		4	-0.324	0.226	1	-0.964	0.316
	4	0	.987*	0.196	0	0.432	1.541
		1	-0.341	0.211	1	-0.939	0.257
		2	1.228*	0.216	0	0.619	1.838
		3	0.324	0.226	1	-0.316	0.964
1	0	1	-0.42	0.234	0.739	-1.083	0.242
		2	1.321*	0.262	0	0.58	2.062
		3	-.937*	0.25	0.002	-1.645	-0.228
		4	-0.657	0.247	0.033	-1.356	0.042
	1	0	0.42	0.234	0.739	-0.242	1.083
		2	1.741*	0.262	0	1	2.482
		3	-0.516	0.25	0.401	-1.225	0.192
		4	-0.237	0.247	1	-0.936	0.462
	2	0	-1.321*	0.262	0	-2.062	-0.58
		1	-1.741*	0.262	0	-2.482	-1
		3	-2.258*	0.276	0	-3.04	-1.476
		4	-1.978*	0.274	0	-2.752	-1.204
	3	0	.937*	0.25	0.002	0.228	1.645
		1	0.516	0.25	0.401	-0.192	1.225
		2	2.258*	0.276	0	1.476	3.04
		4	0.279	0.263	1	-0.463	1.022
	4	0	0.657	0.247	0.033	-0.042	1.356
		1	0.237	0.247	1	-0.462	0.936
		2	1.978*	0.274	0	1.204	2.752
		3	-0.279	0.263	1	-1.022	0.463

Based on estimated marginal means

*. The mean difference is significant at the .05 level.

b. Adjustment for multiple comparisons: Bonferroni.

Univariate Tests

Dependent Variable: Force

Stffness		Sum of Squares	df	Mean Square	F	Sig.	Partial Eta Squared
0	Contrast	65.366	4	16.342	22.062	.000	.235
	Error	213.321	288	.741			
1	Contrast	60.011	4	15.003	20.255	.000	.220
	Error	213.321	288	.741			

Each F tests the simple effects of Factor within each level combination of the other effects shown. These tests are based on the linearly independent pairwise comparisons among the estimated marginal means.

A1.3 Kinetics

A1.3.1 Vmax Contraction

Between-Subjects Factors

		N
Stiffness	0	168
	1	170
Factor	0	69
	1	69
	2	70
	3	66
	4	64

Tests of Between-Subjects Effects

Dependent Variable: day1

Source	Type III Sum of Squares	df	Mean Square	F	Sig.
Corrected Model	112367.309[a]	9	12485.257	29.795	.000
Intercept	1126362.432	1	1126362.432	2687.966	.000
Stiffness	17872.975	1	17872.975	42.652	.000
Factor	75252.106	4	18813.027	44.896	.000
Stiffness * Factor	13186.976	4	3296.744	7.867	.000
Error	137444.787	328	419.039		
Total	1496574.549	338			
Corrected Total	249812.096	337			

a. R Squared = .450 (Adjusted R Squared = .435)

Estimated Marginal Means

1. Stiffness * Factor

Estimates

Dependent Variable: day1

Stiffness	Factor	Mean	Std. Error	95% Confidence Interval	
				Lower Bound	Upper Bound
0	0	48.846	4.015	40.948	56.744
	1	94.705	3.237	88.338	101.072
	2	43.079	3.619	35.960	50.198
	3	73.903	3.940	66.153	81.653
	4	76.650	3.122	70.509	82.792
1	0	44.744	4.268	36.347	53.140
	1	57.267	2.924	51.514	63.020
	2	33.096	3.321	26.563	39.628
	3	58.220	3.278	51.772	64.669
	4	68.412	4.467	59.625	77.200

Pairwise Comparisons

Dependent Variable: day1

Factor	(I) Stiffness	(J) Stiffness	Mean Difference (I-J)	Std. Error	Sig.[b]	95% Confidence Interval for Difference[b]	
						Lower Bound	Upper Bound
0	0	1	4.102	5.860	.484	-7.425	15.630
	1	0	-4.102	5.860	.484	-15.630	7.425
1	0	1	37.438*	4.362	.000	28.857	46.019
	1	0	-37.438*	4.362	.000	-46.019	-28.857
2	0	1	9.983*	4.911	.043	.322	19.645
	1	0	-9.983*	4.911	.043	-19.645	-.322
3	0	1	15.683*	5.125	.002	5.601	25.765
	1	0	-15.683*	5.125	.002	-25.765	-5.601
4	0	1	8.238	5.450	.132	-2.483	18.959
	1	0	-8.238	5.450	.132	-18.959	2.483

Based on estimated marginal means

*. The mean difference is significant at the .05 level.

b. Adjustment for multiple comparisons: Bonferroni.

Univariate Tests

Dependent Variable: day1

Factor		Sum of Squares	df	Mean Square	F	Sig.
0	Contrast	205.383	1	205.383	.490	.484
	Error	137444.787	328	419.039		
1	Contrast	30866.917	1	30866.917	73.661	.000
	Error	137444.787	328	419.039		
2	Contrast	1731.412	1	1731.412	4.132	.043
	Error	137444.787	328	419.039		
3	Contrast	3924.143	1	3924.143	9.365	.002
	Error	137444.787	328	419.039		
4	Contrast	957.542	1	957.542	2.285	.132
	Error	137444.787	328	419.039		

Each F tests the simple effects of Stiffness within each level combination of the other effects shown. These tests are based on the linearly independent pairwise comparisons among the estimated marginal means.

2. Stiffness * Factor

Estimates

Dependent Variable: day1

Stiffness	Factor	Mean	Std. Error	95% Confidence Interval	
				Lower Bound	Upper Bound
0	0	48.846	4.015	40.948	56.744
	1	94.705	3.237	88.338	101.072
	2	43.079	3.619	35.960	50.198
	3	73.903	3.940	66.153	81.653
	4	76.650	3.122	70.509	82.792
1	0	44.744	4.268	36.347	53.140
	1	57.267	2.924	51.514	63.020
	2	33.096	3.321	26.563	39.628
	3	58.220	3.278	51.772	64.669
	4	68.412	4.467	59.625	77.200

Pairwise Comparisons

Dependent Variable: day1

Stiffness	(I) Factor	(J) Factor	Mean Difference (I-J)	Std. Error	Sig.[b]	95% Confidence Interval for Difference[b] Lower Bound	Upper Bound
0	0	1	-45.859*	5.157	.000	-60.433	-31.285
		2	5.767	5.405	1.000	-9.508	21.041
		3	-25.057*	5.625	.000	-40.954	-9.161
		4	-27.805*	5.085	.000	-42.177	-13.432
	1	0	45.859*	5.157	.000	31.285	60.433
		2	51.626*	4.855	.000	37.905	65.347
		3	20.802*	5.099	.001	6.392	35.211
		4	18.055*	4.497	.001	5.346	30.763
	2	0	-5.767	5.405	1.000	-21.041	9.508
		1	-51.626*	4.855	.000	-65.347	-37.905
		3	-30.824*	5.349	.000	-45.942	-15.706
		4	-33.571*	4.779	.000	-47.078	-20.065
	3	0	25.057*	5.625	.000	9.161	40.954
		1	-20.802*	5.099	.001	-35.211	-6.392
		2	30.824*	5.349	.000	15.706	45.942
		4	-2.747	5.026	1.000	-16.953	11.458
	4	0	27.805*	5.085	.000	13.432	42.177
		1	-18.055*	4.497	.001	-30.763	-5.346
		2	33.571*	4.779	.000	20.065	47.078
		3	2.747	5.026	1.000	-11.458	16.953
1	0	1	-12.523	5.174	.160	-27.146	2.099
		2	11.648	5.408	.320	-3.636	26.932
		3	-13.477	5.382	.128	-28.686	1.733
		4	-23.669*	6.178	.002	-41.130	-6.208
	1	0	12.523	5.174	.160	-2.099	27.146
		2	24.171*	4.425	.000	11.666	36.676
		3	-.953	4.393	1.000	-13.368	11.461
		4	-11.145	5.339	.376	-26.235	3.944
	2	0	-11.648	5.408	.320	-26.932	3.636
		1	-24.171*	4.425	.000	-36.676	-11.666

		3	-25.125*	4.666	.000	-38.311	-11.938
		4	-35.317*	5.566	.000	-51.047	-19.586
	3	0	13.477	5.382	.128	-1.733	28.686
		1	.953	4.393	1.000	-11.461	13.368
		2	25.125*	4.666	.000	11.938	38.311
		4	-10.192	5.541	.667	-25.851	5.467
	4	0	23.669*	6.178	.002	6.208	41.130
		1	11.145	5.339	.376	-3.944	26.235
		2	35.317*	5.566	.000	19.586	51.047
		3	10.192	5.541	.667	-5.467	25.851

Based on estimated marginal means

*. The mean difference is significant at the .05 level.

b. Adjustment for multiple comparisons: Bonferroni.

Univariate Tests

Dependent Variable: day1

Stiffness		Sum of Squares	df	Mean Square	F	Sig.
0	Contrast	61546.733	4	15386.683	36.719	.000
	Error	137444.787	328	419.039		
1	Contrast	23306.721	4	5826.680	13.905	.000
	Error	137444.787	328	419.039		

Each F tests the simple effects of Factor within each level combination of the other effects shown. These tests are based on the linearly independent pairwise comparisons among the estimated marginal means.

A1.3.2 Vmax 50% Relaxation

Between-Subjects Factors

		N
Stiffness	0	168
	1	170
Factor	0	69
	1	69
	2	70
	3	66
	4	64

Tests of Between-Subjects Effects

Dependent Variable: Vmax1

Source	Type III Sum of Squares	df	Mean Square	F	Sig.
Corrected Model	151365.230[a]	9	16818.359	55.716	.000
Intercept	1127392.979	1	1127392.979	3734.856	.000
stiffness	79255.041	1	79255.041	262.558	.000
factor	47705.083	4	11926.271	39.510	.000
stiffness * factor	7682.070	4	1920.518	6.362	.000
Error	147608.163	489	301.857		
Total	1713473.338	499			
Corrected Total	298973.392	498			

a. R Squared = .506 (Adjusted R Squared = .497)

Estimated Marginal Means

1. stiffness * factor

Estimates

Dependent Variable: Vmax1 day1

stiffness	factor	Mean	Std. Error	95% Confidence Interval	
				Lower Bound	Upper Bound
0	0	42.758	3.407	36.063	49.453
	1	80.828	2.896	75.139	86.518
	2	60.928	2.650	55.722	66.134
	3	70.599	3.344	64.029	77.168
	4	80.757	2.123	76.587	84.928
1	0	33.841	3.623	26.723	40.959
	1	48.838	1.792	45.317	52.359
	2	23.816	2.590	18.727	28.905
	3	43.040	2.534	38.061	48.020
	4	45.556	1.821	41.977	49.134

Pairwise Comparisons

Dependent Variable: Vmax1

factor	(I) stiffness	(J) stiffness	Mean Difference (I-J)	Std. Error	Sig.[b]	95% Confidence Interval for Difference[b]	
						Lower Bound	Upper Bound
0	0	1	8.917	4.973	.074	-.855	18.689
	1	0	-8.917	4.973	.074	-18.689	.855
1	0	1	31.990*	3.405	.000	25.300	38.681
	1	0	-31.990*	3.405	.000	-38.681	-25.300
2	0	1	37.112*	3.705	.000	29.832	44.392
	1	0	-37.112*	3.705	.000	-44.392	-29.832
3	0	1	27.558*	4.196	.000	19.315	35.802
	1	0	-27.558*	4.196	.000	-35.802	-19.315
4	0	1	35.201*	2.797	.000	29.706	40.696
	1	0	-35.201*	2.797	.000	-40.696	-29.706

Based on estimated marginal means

*. The mean difference is significant at the .05 level.

b. Adjustment for multiple comparisons: Bonferroni.

Univariate Tests

Dependent Variable: Vmax1

factor		Sum of Squares	df	Mean Square	F	Sig.
0	Contrast	970.425	1	970.425	3.215	.074
	Error	147608.163	489	301.857		
1	Contrast	26639.452	1	26639.452	88.252	.000
	Error	147608.163	489	301.857		
2	Contrast	30284.556	1	30284.556	100.327	.000
	Error	147608.163	489	301.857		
3	Contrast	13023.748	1	13023.748	43.145	.000
	Error	147608.163	489	301.857		
4	Contrast	47815.933	1	47815.933	158.406	.000
	Error	147608.163	489	301.857		

Each F tests the simple effects of stiffness within each level combination of the other effects shown. These tests are based on the linearly independent pairwise comparisons among the estimated marginal means.

2. stiffness * factor

Estimates

Dependent Variable: Vmax1

				95% Confidence Interval	
stiffness	factor	Mean	Std. Error	Lower Bound	Upper Bound
0	0	42.758	3.407	36.063	49.453
	1	80.828	2.896	75.139	86.518
	2	60.928	2.650	55.722	66.134
	3	70.599	3.344	64.029	77.168
	4	80.757	2.123	76.587	84.928
1	0	33.841	3.623	26.723	40.959
	1	48.838	1.792	45.317	52.359
	2	23.816	2.590	18.727	28.905
	3	43.040	2.534	38.061	48.020
	4	45.556	1.821	41.977	49.134

Pairwise Comparisons

Dependent Variable: Vmax1

stiffness	(I) factor	(J) factor	Mean Difference (I-J)	Std. Error	Sig.[b]	95% Confidence Interval for Difference[b]	
						Lower Bound	Upper Bound
0	0	1	-38.070*	4.472	.000	-50.679	-25.461
		2	-18.170*	4.316	.000	-30.341	-5.999
		3	-27.841*	4.774	.000	-41.302	-14.379
		4	-37.999*	4.014	.000	-49.319	-26.679
	1	0	38.070*	4.472	.000	25.461	50.679
		2	19.900*	3.925	.000	8.833	30.968
		3	10.230	4.423	.212	-2.243	22.702
		4	.071	3.590	1.000	-10.053	10.195
	2	0	18.170*	4.316	.000	5.999	30.341
		1	-19.900*	3.925	.000	-30.968	-8.833
		3	-9.671	4.266	.238	-21.701	2.359
		4	-19.829*	3.395	.000	-29.402	-10.256
	3	0	27.841*	4.774	.000	14.379	41.302
		1	-10.230	4.423	.212	-22.702	2.243
		2	9.671	4.266	.238	-2.359	21.701
		4	-10.159	3.960	.106	-21.326	1.009
	4	0	37.999*	4.014	.000	26.679	49.319
		1	-.071	3.590	1.000	-10.195	10.053
		2	19.829*	3.395	.000	10.256	29.402
		3	10.159	3.960	.106	-1.009	21.326
1	0	1	-14.997*	4.042	.002	-26.394	-3.600
		2	10.025	4.453	.248	-2.533	22.582
		3	-9.200	4.421	.380	-21.667	3.267
		4	-11.715*	4.055	.040	-23.149	-.281
	1	0	14.997*	4.042	.002	3.600	26.394
		2	25.022*	3.149	.000	16.141	33.903
		3	5.798	3.104	.624	-2.955	14.550
		4	3.282	2.555	1.000	-3.923	10.487
	2	0	-10.025	4.453	.248	-22.582	2.533
		1	-25.022*	3.149	.000	-33.903	-16.141
		3	-19.224*	3.624	.000	-29.442	-9.006
		4	-21.740*	3.166	.000	-30.668	-12.812

3	0	9.200	4.421	.380	-3.267	21.667
	1	-5.798	3.104	.624	-14.550	2.955
	2	19.224*	3.624	.000	9.006	29.442
	4	-2.516	3.121	1.000	-11.316	6.285
4	0	11.715*	4.055	.040	.281	23.149
	1	-3.282	2.555	1.000	-10.487	3.923
	2	21.740*	3.166	.000	12.812	30.668
	3	2.516	3.121	1.000	-6.285	11.316

Based on estimated marginal means

*. The mean difference is significant at the .05 level.

b. Adjustment for multiple comparisons: Bonferroni.

Univariate Tests

Dependent Variable: Vmax1

stiffness		Sum of Squares	df	Mean Square	F	Sig.
0	Contrast	34814.196	4	8703.549	28.833	.000
	Error	147608.163	489	301.857		
1	Contrast	22007.173	4	5501.793	18.226	.000
	Error	147608.163	489	301.857		

Each F tests the simple effects of factor within each level combination of the other effects shown. These tests are based on the linearly independent pairwise comparisons among the estimated marginal means.

A1.3.3 Time to Peak

Between-Subjects Factors

		N
Stiffness	0	168
	1	170
Factor	0	69
	1	69
	2	70
	3	66
	4	64

Tests of Between-Subjects Effects

Dependent Variable: timePeak1

Source	Type III Sum of Squares	df	Mean Square	F	Sig.
Corrected Model	.481[a]	8	.060	8.869	.000
Intercept	15.879	1	15.879	2341.922	.000
stiffness	.044	1	.044	6.486	.011
factor	.226	4	.057	8.344	.000
stiffness * factor	.231	3	.077	11.359	.000
Error	2.495	368	.007		
Total	29.083	377			
Corrected Total	2.976	376			

a. R Squared = .162 (Adjusted R Squared = .143)

Estimated Marginal Means

1. stiffness * factor

Estimates

Dependent Variable: timePeak1

				95% Confidence Interval	
stiffness	factor	Mean	Std. Error	Lower Bound	Upper Bound
0	0	.[a]	.	.	.
	1	.255	.019	.217	.293
	2	.187	.018	.153	.222
	3	.223	.021	.181	.265
	4	.311	.012	.288	.335
1	0	.256	.015	.228	.285
	1	.244	.009	.227	.261
	2	.245	.013	.219	.271
	3	.330	.013	.304	.355
	4	.266	.009	.247	.284

a. This level combination of factors is not observed, thus the corresponding population marginal mean is not estimable.

Pairwise Comparisons

Dependent Variable: timePeak1

factor	(I) stiffness	(J) stiffness	Mean Difference (I-J)	Std. Error	Sig.[d]	95% Confidence Interval for Difference[d] Lower Bound	Upper Bound
0	0	1	.[a]	.	.	.	.
	1	0	.[c]	.	.	.	.
1	0	1	.011	.021	.598	-.031	.053
	1	0	-.011	.021	.598	-.053	.031
2	0	1	-.058*	.022	.008	-.101	-.015
	1	0	.058*	.022	.008	.015	.101
3	0	1	-.107*	.025	.000	-.156	-.058
	1	0	.107*	.025	.000	.058	.156
4	0	1	.046*	.015	.003	.016	.076
	1	0	-.046*	.015	.003	-.076	-.016

Based on estimated marginal means

*. The mean difference is significant at the .05 level.

a. The level combination of factors in (I) is not observed.

c. The level combination of factors in (J) is not observed.

d. Adjustment for multiple comparisons: Bonferroni.

Univariate Tests

Dependent Variable: timePeak1

factor		Sum of Squares	df	Mean Square	F	Sig.
0	Contrast	.000	0	.	.	.
	Error	2.495	368	.007		
1	Contrast	.002	1	.002	.279	.598
	Error	2.495	368	.007		
2	Contrast	.047	1	.047	7.003	.008
	Error	2.495	368	.007		
3	Contrast	.124	1	.124	18.233	.000
	Error	2.495	368	.007		
4	Contrast	.061	1	.061	9.032	.003
	Error	2.495	368	.007		

Each F tests the simple effects of stiffness within each level combination of the other effects shown. These tests are based on the estimable linearly independent pairwise comparisons among the estimated marginal means.

2. stiffness * factor

Estimates

Dependent Variable: timePeak1

				95% Confidence Interval	
stiffness	factor	Mean	Std. Error	Lower Bound	Upper Bound
0	0	.[a]	.	.	.
	1	.255	.019	.217	.293
	2	.187	.018	.153	.222
	3	.223	.021	.181	.265
	4	.311	.012	.288	.335
1	0	.256	.015	.228	.285
	1	.244	.009	.227	.261
	2	.245	.013	.219	.271
	3	.330	.013	.304	.355
	4	.266	.009	.247	.284

a. This level combination of factors is not observed, thus the corresponding population marginal mean is not estimable.

Pairwise Comparisons

Dependent Variable: timePeak1

stiffness	(I) factor	(J) factor	Mean Difference (I-J)	Std. Error	Sig.[d]	95% Confidence Interval for Difference[d] Lower Bound	Upper Bound
0	0	1	.[a]	.	.	.	.
		2	.[a]	.	.	.	.
		3	.[a]	.	.	.	.
		4	.[a]	.	.	.	.
	1	0	.[b]	.	.	.	.
		2	.068	.026	.057	-.001	.138
		3	.032	.029	1.000	-.044	.109
		4	-.056	.023	.086	-.117	.004
	2	0	.[b]	.	.	.	.
		1	-.068	.026	.057	-.138	.001
		3	-.036	.028	1.000	-.109	.037
		4	-.124*	.021	.000	-.181	-.068
	3	0	.[b]	.	.	.	.
		1	-.032	.029	1.000	-.109	.044
		2	.036	.028	1.000	-.037	.109
		4	-.089*	.024	.002	-.153	-.024
	4	0	.[b]	.	.	.	.
		1	.056	.023	.086	-.004	.117
		2	.124*	.021	.000	.068	.181
		3	.089*	.024	.002	.024	.153
1	0	1	.012	.017	1.000	-.036	.060
		2	.011	.020	1.000	-.044	.067
		3	-.073*	.020	.002	-.129	-.018
		4	-.009	.017	1.000	-.058	.040
	1	0	-.012	.017	1.000	-.060	.036
		2	-.001	.016	1.000	-.046	.044
		3	-.086*	.016	.000	-.130	-.041
		4	-.022	.013	.941	-.058	.015
	2	0	-.011	.020	1.000	-.067	.044
		1	.001	.016	1.000	-.044	.046
		3	-.084*	.019	.000	-.137	-.032
		4	-.020	.016	1.000	-.066	.025

3	0	.073*	.020	.002	.018	.129
	1	.086*	.016	.000	.041	.130
	2	.084*	.019	.000	.032	.137
	4	.064*	.016	.001	.018	.110
4	0	.009	.017	1.000	-.040	.058
	1	.022	.013	.941	-.015	.058
	2	.020	.016	1.000	-.025	.066
	3	-.064*	.016	.001	-.110	-.018

Based on estimated marginal means

*. The mean difference is significant at the .05 level.

a. The level combination of factors in (I) is not observed.

b. The level combination of factors in (J) is not observed.

d. Adjustment for multiple comparisons: Bonferroni.

Univariate Tests

Dependent Variable: timePeak1

stiffness		Sum of Squares	df	Mean Square	F	Sig.
0	Contrast	.262	3	.087	12.876	.000
	Error	2.495	368	.007		
1	Contrast	.219	4	.055	8.068	.000
	Error	2.495	368	.007		

Each F tests the simple effects of factor within each level combination of the other effects shown. These tests are based on the estimable linearly independent pairwise comparisons among the estimated marginal means.

A1.3.4 Time to 50% Relaxation

Between-Subjects Factors

		N
Stiffness	0	168
	1	170
Factor	0	69
	1	69
	2	70
	3	66
	4	64

Tests of Between-Subjects Effects

Dependent Variable: TimeR1

Source	Type III Sum of Squares	df	Mean Square	F	Sig.
Corrected Model	.306[a]	9	.034	1.542	.131
Intercept	9.247	1	9.247	419.606	.000
Stiffness	.004	1	.004	.203	.653
Factor	.260	4	.065	2.952	.020
Stiffness * Factor	.077	4	.019	.878	.477
Error	9.520	432	.022		
Total	23.038	442			
Corrected Total	9.826	441			

a. R Squared = .031 (Adjusted R Squared = .011)

Estimated Marginal Means

1. Stiffness * Factor

Estimates

Dependent Variable: TimeR1

Stiffness	Factor	Mean	Std. Error	95% Confidence Interval	
				Lower Bound	Upper Bound
0	0	.188	.028	.134	.242
	1	.204	.035	.135	.273
	2	.117	.030	.057	.176
	3	.133	.035	.065	.202
	4	.214	.021	.173	.255
1	0	.148	.026	.097	.200
	1	.178	.016	.147	.208
	2	.135	.023	.090	.179
	3	.175	.020	.134	.215
	4	.184	.016	.152	.215

Pairwise Comparisons

Dependent Variable: TimeR1

Factor	(I) Stiffness	(J) Stiffness	Mean Difference (I-J)	Std. Error	Sig.[a]	95% Confidence Interval for Difference[a]	
						Lower Bound	Upper Bound
0	0	1	.040	.038	.297	-.035	.115
	1	0	-.040	.038	.297	-.115	.035
1	0	1	.026	.038	.494	-.049	.102
	1	0	-.026	.038	.494	-.102	.049
2	0	1	-.018	.038	.630	-.093	.056
	1	0	.018	.038	.630	-.056	.093
3	0	1	-.041	.040	.310	-.121	.038
	1	0	.041	.040	.310	-.038	.121
4	0	1	.030	.026	.252	-.022	.082
	1	0	-.030	.026	.252	-.082	.022

Based on estimated marginal means

a. Adjustment for multiple comparisons: Bonferroni.

Univariate Tests

Dependent Variable: TimeR1

Factor		Sum of Squares	df	Mean Square	F	Sig.
0	Contrast	.024	1	.024	1.092	.297
	Error	9.520	432	.022		
1	Contrast	.010	1	.010	.468	.494
	Error	9.520	432	.022		
2	Contrast	.005	1	.005	.232	.630
	Error	9.520	432	.022		
3	Contrast	.023	1	.023	1.035	.310
	Error	9.520	432	.022		
4	Contrast	.029	1	.029	1.314	.252
	Error	9.520	432	.022		

Each F tests the simple effects of Stiffness within each level combination of the other effects shown. These tests are based on the linearly independent pairwise comparisons among the estimated marginal means.

2. Stiffness * Factor

Estimates

Dependent Variable: TimeR1

				95% Confidence Interval	
Stiffness	Factor	Mean	Std. Error	Lower Bound	Upper Bound
0	0	.188	.028	.134	.242
	1	.204	.035	.135	.273
	2	.117	.030	.057	.176
	3	.133	.035	.065	.202
	4	.214	.021	.173	.255
1	0	.148	.026	.097	.200
	1	.178	.016	.147	.208
	2	.135	.023	.090	.179
	3	.175	.020	.134	.215
	4	.184	.016	.152	.215

Pairwise Comparisons

Dependent Variable: TimeR1

Stiffness	(I) Factor	(J) Factor	Mean Difference (I-J)	Std. Error	Sig.[a]	95% Confidence Interval for Difference[a]	
						Lower Bound	Upper Bound
0	0	1	-.016	.045	1.000	-.141	.110
		2	.072	.041	.814	-.044	.187
		3	.055	.045	1.000	-.071	.181
		4	-.026	.035	1.000	-.123	.072
	1	0	.016	.045	1.000	-.110	.141
		2	.087	.046	.606	-.044	.218
		3	.070	.049	1.000	-.069	.210
		4	-.010	.041	1.000	-.125	.105
	2	0	-.072	.041	.814	-.187	.044
		1	-.087	.046	.606	-.218	.044
		3	-.017	.046	1.000	-.147	.114
		4	-.097	.037	.086	-.201	.007
	3	0	-.055	.045	1.000	-.181	.071
		1	-.070	.049	1.000	-.210	.069
		2	.017	.046	1.000	-.114	.147
		4	-.080	.041	.489	-.195	.034
	4	0	.026	.035	1.000	-.072	.123
		1	.010	.041	1.000	-.105	.125
		2	.097	.037	.086	-.007	.201
		3	.080	.041	.489	-.034	.195
1	0	1	-.029	.031	1.000	-.115	.057
		2	.014	.035	1.000	-.084	.111
		3	-.026	.033	1.000	-.120	.068
		4	-.035	.031	1.000	-.122	.052
	1	0	.029	.031	1.000	-.057	.115
		2	.043	.028	1.000	-.035	.120
		3	.003	.026	1.000	-.070	.076
		4	-.006	.023	1.000	-.070	.058
	2	0	-.014	.035	1.000	-.111	.084
		1	-.043	.028	1.000	-.120	.035
		3	-.040	.030	1.000	-.126	.046

		4	-.049	.028	.813	-.127	.030
	3	0	.026	.033	1.000	-.068	.120
		1	-.003	.026	1.000	-.076	.070
		2	.040	.030	1.000	-.046	.126
		4	-.009	.026	1.000	-.082	.064
	4	0	.035	.031	1.000	-.052	.122
		1	.006	.023	1.000	-.058	.070
		2	.049	.028	.813	-.030	.127
		3	.009	.026	1.000	-.064	.082

Based on estimated marginal means

a. Adjustment for multiple comparisons: Bonferroni.

Univariate Tests

Dependent Variable: TimeR1

Stiffness		Sum of Squares	df	Mean Square	F	Sig.
0	Contrast	.206	4	.051	2.332	.055
	Error	9.520	432	.022		
1	Contrast	.089	4	.022	1.014	.400
	Error	9.520	432	.022		

Each F tests the simple effects of Factor within each level combination of the other effects shown. These tests are based on the linearly independent pairwise comparisons among the estimated marginal means.

A1.4 Cell Size

Univariate Analysis of Variance

Between-Subjects Factors

		N
Factor	0	46
	1	50
	2	46
	3	48
	4	48

Descriptive Statistics

Dependent Variable: CellSize

Factor	Mean	Std. Deviation	N
0	186.63361899	51.760458680	46
1	226.67364519	41.91141073	50
2	215.1709091	58.20572317	46
3	247.0990000	37.38510411	48
4	234.71367859	41.13840859	48
Total	224.39003079	49.04103548	238

Tests of Between-Subjects Effects

Dependent Variable: CellSize

Source	Type III Sum of Squares	df	Mean Square	F	Sig.	Partial Eta Squared
Corrected Model	49391.669[a]	4	12347.917	5.917	.000	.159
Intercept	6265218.240	1	6265218.240	3002.236	.000	.960
Factor	49391.669	4	12347.917	5.917	.000	.159
Error	260856.319	125	2086.851			
Total	6855863.156	130				
Corrected Total	310247.988	129				

a. R Squared = .159 (Adjusted R Squared = .132)

CellSize

	Factor	N	Subset 1	Subset 2
Tukey HSD[a,b,c]	0	21	186.6336189	
	2	22	215.1709091	215.1709091
	1	31		226.6736452
	4	28		234.7136786
	3	28		247.099000
	Sig.		.177	.099

Means for groups in homogeneous subsets are displayed.

a. Uses Harmonic Mean Sample Size = 25.412.

b. The group sizes are unequal. The harmonic mean of the group sizes is used. Type I

c. Alpha = .05.